



**Excitatory/inhibitory balance in iPSC-
derived glutamatergic/GABAergic neuronal
networks:
differential Cadherin-13 genotype effects**

**Exzitatorisch/inhibitorisches Gleichgewicht in iPSC-
abgeleiteten glutamaterg/GABAergen neuronalen
Netzwerken:
Differentielle Cadherin-13 Genotyp-Effekte**

Doctoral thesis for a doctoral degree
at the Graduate School of Life Sciences,
Julius-Maximilians-Universität Würzburg,
Section Neuroscience

submitted by
Maria Rosaria Vitale

from
London, United Kingdom

Würzburg 2022



Submitted on:

Office stamp

Members of the Thesis Committee

Chairperson: Prof. Dr. Matthias Gamer

Primary Supervisor: Prof. Dr. Klaus-Peter Lesch

Supervisor (Second): PD Dr. Frank Döring

Supervisor (Third): Prof. Dr. Esther Asan

Date of Public Defence:

Date of Receipt of Certificates:

Table of Contents

Abbreviations	vii
Abstract.....	ix
Zusammenfassung.....	xi
1. Introduction	13
1.1. Cadherins	13
1.2. Classical Cadherins	13
1.3. Cadherin-13.....	14
1.3.1. Domains, processing, and activation of <i>CDH13</i>	14
1.4. <i>CDH13</i> in neurodevelopmental and psychiatric disorders	17
1.5. <i>CDH13</i> signalling pathways	18
1.6. Effects of <i>CDH13</i> axonal migration and outgrowth.....	19
1.7. Induced pluripotent stem cells.....	19
1.8. Genetic engineering.....	20
1.8.1. CRISPR/Cas9.....	20
1.9. Excitatory/inhibitory balance.....	22
1.9.1. E/I balance: physiology	22
1.9.2. E/I balance: mode of action.....	24
1.9.3. <i>CDH13</i> involved in the E/I balance.....	25
2. Aims of the thesis	26
3. Methods	26
3.1. Cell culture methods	26
3.1.1. Cells.....	26
3.1.2. Culturing and passaging human induced pluripotent stem cells	26
3.1.3. Coating for human iPSC cultures	27
3.2. Genetic editing	28
3.2.1. Sequencing region of interest.....	28
3.2.2. Designing sgRNAs	28
3.2.3. pSpCas9(BB)-2A-Puro (PX459) V2.0 plasmid5 digestion and phosphorylation and annealing of sgRNA.....	29
3.2.4. Cloning of sgRNAs.....	29
3.2.5. Nucleofection of the plasmids	29
3.2.6. Colony selection.....	30
3.3. Validation of genetic modifications	30
3.3.1. Trilineage differentiation	30

3.3.2. PCR cloning for verification of biallelic modifications	30
3.3.3. Identification of potential CRISPR/Cas9 off target effects.....	31
3.4. iPSCs characterization.....	32
3.4.1. Germ layer differentiation.....	32
3.4.2. Pluripotency expression markers	32
3.4.3. Sendai transgene analysis	33
3.4.4. Karyotype analysis.....	33
3.4.5. Mycoplasma contamination detection	33
3.4.6. Short Tandem Repeat analysis	33
3.4.7. <i>CDH13</i> SNP rs2199430 genotype sequencing.....	34
3.5. Direct neuronal differentiation	34
3.5.1. Lentivirus generation and harvesting.....	34
3.5.2. Generation of rtTA/Ngn2- and rtTA/Ascl1-positive iPSCs.....	35
3.5.3. Confirmation of rtTA, Ngn2 and Ascl1 vector integration in iPSCs.....	35
3.5.4. Glutamatergic neuron differentiation	36
3.5.5. GABAergic neuron differentiation.....	36
3.5.6. Glutamatergic/GABAergic co-culturing differentiation.....	36
3.5.7. Astrocyte isolation for neuron differentiation support.....	36
3.5.7.1. Dissection of the brain from newborn mice.....	37
3.5.7.2. Removing the meninges.....	37
3.5.7.3. Astrocytes isolation	37
3.6. Molecular biology methods: RNA analysis	38
3.6.1. Complementary deoxyribonucleic acid (cDNA) synthesis.....	38
3.6.2. Quantitative real-time polymerase chain reaction.....	38
3.7. Molecular biology methods: Protein analysis.....	39
3.7.1. Western blot procedure.....	39
3.8. Immunocytochemistry	39
3.8.1. Immunocytochemistry procedure	39
3.8.2. Epifluorescence	40
3.9. Microelectrode array (MEA) recording and data analysis	40
3.9.1 Statistical analysis.....	40
4. Results	41
4.1 Generation of a <i>CDH13</i> knockout and heterozygotic iPSC line	41
4.1.1. Sequencing <i>CDH13</i> 's open reading frame	41
4.1.2. Nucleofection of plasmids and colony selection	41
4.1.3. Sequencing of CRISPRed clones.....	42
4.1.4. Single cell expansion of CRISPRed clones	43

4.1.5. Allelic separation using PCR cloning	44
4.1.6. Indel mutations in each CRISPRed clone.....	45
4.1.7. Confirmation of <i>CDH13</i> ^{-/-} at the protein level	46
4.2. Characterization of generated isogenic cell lines.....	47
4.2.1. iPSCs morphology	47
4.2.2. Germ layer differentiation and pluripotency characterization	47
4.2.3. Standard G-banding.....	48
4.2.4. Absence of Sendai virus transcripts	48
4.2.5. STR	49
4.2.6. Off-target effects	49
4.3. Generation of rtTA/Ngn2- and rtTA/Ascl1-positive hiPSCs to model excitatory/inhibitory network activity	50
4.3.1. Verification of <i>CDH13</i> SNP rs2199430 variants in iPSC lines	51
4.3.2. Generation of rtTa/Ngn2- and rtTa/Ascl1-positive iPSCs.....	52
4.3.3. Characterization of rtTa/Ngn2- and rtTa/Ascl1-positive iPSCs	55
4.4. Qualitative characterization of glutamatergic neurons	56
4.5. Qualitative characterization of GABAergic neurons.....	57
4.6. Qualitative characterization of co-cultures.....	59
4.7. Network activity measurement of co-cultures	61
5. Discussion.....	67
5.1. Generation of isogenic cell lines by using CRISPR/Cas9 with a gene dose-dependent deficiency of <i>CDH13</i> (<i>CDH13</i> ^{-/-} and <i>CDH13</i> ^{+/-})	68
5.2. Differentiation into glutamatergic and GABAergic neurons and their co-culture for excitatory/inhibitory network assessment.....	69
5.3. Neuronal network activity analysis	70
6. Conclusion and outlook	71
7. Supplementary files	73
7.1. Supplementary files: iPSC characterization of <i>CDH13</i> ^{ΔA} and <i>CDH13</i> ^{ΔG}	73
7.2. Supplementary files: Qualitative characterization of glutamatergic neurons	74
7.3. Supplementary files: Qualitative characterization of GABAergic neurons.....	75
7.4. Supplementary files: Qualitative characterization of co-culture neurons.....	76
7.5 Supplementary file: Network burst rate	78
7.6 Supplementary file: MEA statistics	78
7.7. Supplementary file: Cell lines	79
7.8. Supplementary file: Astrocyte isolation.....	82
7.9. Supplementary file: Schematic representation of spontaneous electric activity patterns measured on MEAs	83
8. Materials.....	84

8.1. Cell culture.....	84
8.1.1. Cell culture media	84
8.1.2. Cell culture reagents and supplements	84
8.1.3. Cell culture small molecules and growth factors.....	86
8.2. Lentivirus reagents.....	86
8.3. Genome editing using CRISPR/Cas9.....	87
8.3.1. Kits.....	87
8.4. Primary and secondary antibodies	87
8.4.1. Primary antibodies	87
8.4.2. Secondary antibodies.....	88
8.5. Technical equipment.....	89
8.6. Software.....	89
Appendix	89
1. List of tables	89
2. List of figures.....	90
3. List of supplementary figures.....	91
4. List of supplementary tables	91
References	92
Affidavit/Eidesstattliche Erklärung	104
List of publications	105
Acknowledgements.....	106
Curriculum Vitae	Error! Bookmark not defined.

Abbreviations

- ACTB
Actin beta, 40
- ADHD
Attention-
deficit/hyperactivity, 18
- AFP
alpha-1- fetoprotein, 32
- AKT
protein kinase B, 18
- ALAS
5'-Aminolevulinat Synthase
1, 40
- Ascl1
Achaete-scute homolog 1,
35
- ASD
autism spectrum disorder,
22
- BDNF
Brain Derived Neurotrophic
Factor, 18
- CDH13*
Cadherin-13, ix
- cDNA
complementary DNA, 39
- c-Myc*
avian myelocytomatosis
viral oncogene
homolog, 19
Myc gene, 33
- CNV
Copy number variant, 17
- CNVs
copy number variants, ix, xi
- Cq
quantification cycle, 40
- CRISPR/Cas9
Clustered Regulatory
Interspaced Short
Palindromic
Repeats/CRISPR-
associated protein 9, ix
- C-terminus
Carboxyl-terminal domain,
13
- DAPI
6-diamidino-2-phenylindole,
41
- DMSO
Dimethyl sulfoxide, 87
- dNTPs
desoxyribonucleotide
triphosphates, 39
- DSB
double-strand break, 20
- E/I
excitation-inhibition, 22
- EBs
embryonic bodies, 32
- EC
Ectodomain, 13
- EEG
electroencephalographic, 69
- EHS
Engelbreth-Holm-Swarm, 27
- Elfn1
Extracellular Leucine Rich
Repeat And Fibronectin
Type III Domain
Containing 1, 22
- Eppi
Eppendorf tubes, 35
- ER
endoplasmic reticulum, 15
- ESCs
embryonic stem cells, 19
- FLRT3
Fibronectin Leucine Rich
Transmembrane Protein
3, 22
- GABA
γ-aminobutyric acid, 22
- GABAA α 1
GABAA receptor α 1 subunit,
18
- GAPDH
Glyceraldehyde 3-
phosphate
dehydrogenase, 40
- GPI
glycosylphosphatidyl
inositol-anchored, 14
- GPI-AP
GPI-anchored protein, 15
- GTG
G-bands by trypsin using
Giemsa, 33
- GUSB
Glucuronidase Beta, 40
- GWAS
Genome-wide association
studies, 17
- HAV motif
Histidine-Alanine-Valine
motif, 14
- HDR
homology directed repair,
20
- HPRT1
Hypoxanthine
Phosphoribosyltransferas
e 1, 40
- IGF-1
Insulin-like growth factor 1,
18
- IgSF11
Immunoglobulin
Superfamily Member 11,
22
- iPSCs
Induced pluripotent stem
cells, ix
- ITG β 1
Integrin β 1, 18
- ITG β 3
Integrin β 3, 18
- Klf4*
Kruppel-like factor 4, 19,
33
- KOS
hKlf4, hOct3/4, hSox2, 33
- LRRTMs
Leucine-rich-repeat
transmembrane neuronal
proteins, 22
- LTRs
long terminal repeats, 35
- MDGA2
MAM Domain Containing
Glycosylphosphatidylinosi
tol Anchor 2, 22
- MEA
microelectrode array, ix
- mTOR
mammalian target of
rapamycin, 18
- NBD
network burst duration, x
- NBR
network burst rate, x
- NEAA

MEM non-essential amino acid solution (100x), 37

NGL-2
Netrin-G ligand-2, 22

Ngn2
Neurogenin 2, 35

NHEJ
non-homologous end joining, 20

NT3
Neurotrophin-Type 3, 37

N-terminus
Amino-terminal domain, 13

Oct3/4
octamer-binding transcription factor 3/4, 19

OD
optical density, 39

PAM
Protospacer Adjacent Motif, 20

PFA
paraformaldehyde, 41

PSD
postsynaptic density, 22

PV+
Parvalbumin-positive, 23

RhoA
Ras homolog family member A, 18

RI
Rock inhibitor, 27

ROCK
Rho-associated protein kinase, 18

RT-PCR
Reverse Transcription Polymerase Chain Reaction, 32

rtTA
Reverse tetracycline-controlled transactivator, 35

S.P.
Signalling Peptide, 14

SCID-I
Structured Clinical Interview for DSM-IV, 26

SeV
Sendai Virus, 33

sgRNA
single guide RNA, 20

SNP
single nucleotide polymorphism, ix

Sox2
SRY-box 2, 19

SpCas9
S. pyogenes Cas9, 20

STR
Short tandem repeat, 52

Short Tandem Repeat, 34

TBP
TATA-Box Binding Protein, 40

tDCS
transcranial direct current stimulation, 73

TE buffer
1x Tris-EDTA buffer, 39

TFRC
Transferrin Receptor, 40

TrkB
Tropomyosin-Related Kinase B, 18

UBC
Ubiquitin C, 40

VGATs
vesicular GABA transporters, 22

VGLUTs
vesicular glutamate transporters, 22

VSV-G
vesicular stomatitis G protein, 35

α -SMA
alpha-smooth muscle actin, 32

Abstract

While the healthy brain works through balanced synaptic communication between glutamatergic and GABAergic neurons to coordinate excitation (E) and inhibition (I), disruption of E/I balance interferes with synaptic communication, information processing, and ultimately cognition. Multiple line of evidence indicates that E/I imbalance represents the pathophysiological basis of a wide spectrum of mental disorders. Genetic screening approaches have identified Cadherin-13 (*CDH13*) as a risk gene across neurodevelopmental and mental disorders. *CDH13* regulates several cellular and synaptic processes in brain development and neuronal plasticity in adulthood. In addition to other functions, it is specifically localized at inhibitory synapses of parvalbumin- and somatostatin-expressing GABAergic neurons. In support of *CDH13*'s function in moderating E/I balance, electrophysiological recordings of hippocampal slices in a *CDH13*-deficient mouse model revealed an increase in basal inhibitory but not excitatory synaptic transmission. Moreover, the search for genetic variants impacting functional expression of the *CDH13* gene identified SNP (single nucleotide polymorphism) rs2199430 in intron 1 to be associated with differential mRNA concentrations in human post-mortem brain across the three genotypes *CDH13*^{G/G}, *CDH13*^{A/G} and *CDH13*^{A/A}. This work therefore aimed to further validate these findings in a complementary human model by using induced pluripotent stem cells (iPSCs). The application of human iPSCs in research has replaced the use of embryonic cells, resolving the ethical conflict of destructive usage of human embryos. Investigating *CDH13*'s mode of action in inhibitory synapses was predicted to facilitate mechanistic insight into the effects of *CDH13* gene variants on E/I network activity, which can then be targeted to reinstate balance.

Genome-wide association studies have identified rare copy number variants (CNVs) resulting in a deletion (or duplication) of *CDH13*. To reduce genetic background variance, a set of isogenic iPSC lines with a gene dose-dependent deficiency of *CDH13* (*CDH13*^{-/-} and *CDH13*^{+/-}) was generated by using the Clustered Regulatory Interspaced Short Palindromic Repeats/CRISPR-associated protein 9 (CRISPR/Cas9) system. These CRISPRed iPSCs carrying a single or two allele(s) with *CDH13* inactivation facilitate investigation of *CDH13* function in cellular processes, at inhibitory synapses and in neuronal network activity. In addition, iPSCs carrying allelic SNP rs2199430 variants were used to study the effects of common genetic variation of *CDH13*. These cell lines were differentiated into pure glutamatergic and GABAergic neurons and co-cultured to generate neuronal networks allowing its activity to be measured and correlated with electrophysiological signatures of differential *CDH13* genotypes. The work towards assessment of neuronal network activity of the iPSC lines was subdivided into three major steps: first, generating rtTA/Ngn2 and rtTA/Ascl1-positive iPSCs via a lentivirus-mediated approach; second, differentiating pure glutamatergic and GABAergic neurons from the genetically transduced iPSCs and co-culturing of pure glutamatergic and GABAergic neurons in a pre-established ratio (65:35) by direct differentiation upon supplementation with doxycycline and forskolin on a microelectrode array (MEA) chip; and, finally, recording of neuronal network activity of iPSC lines after 49 days *in vitro*, followed by extraction and analyses of multiple MEA parameters.

Based on the MEA parameters, it was confirmed that complete *CDH13* knockout as well as heterozygous deficiency influence E/I balance by increasing inhibition. It was further revealed that common SNP variation alters the signature of neuronal network activity. Specifically, *CDH13* deficiency resulted in a significant reduction in network burst duration (NBD), reduced number of detected spikes within a network burst and reduction in network burst rate (NBR) compared to the control (*CDH13^{G/G}*). *CDH13^{A/G}* and *CDH13^{A/A}* showed similarities with the CRISPRed *CDH13*-deficient networks by showing a significant reduction in the NBD and a reduced number of detected spikes within a network compared to *CDH13^{G/G}*. Strikingly, there was a significant increase in the NBR of the *CDH13^{A/G}* and *CDH13^{A/A}* compared to *CDH13^{G/G}* networks. *CDH13^{A/G}* networks exhibited significant differences in both parameters. At the cellular level, this indicates that signalling pathways which determine the length and frequency of network bursts differ among allelic variants of SNP rs2199430, thus confirming functional relevance of this intronic SNP.

In summary, *CDH13*-deficient isogenic iPSC lines were generated using CRISPR/Cas9, iPSCs were genetically transduced via a lentivirus approach, direct differentiation of glutamatergic/GABAergic neurons derived from transduced iPSCs were used to establish a scalable co-culture system, and network activity was recorded by MEA using pre-established parameters to extract and analyze activity information. The results indicate that iPSC-derived neuronal networks following CRISPR/Cas9-facilitated *CDH13* inactivation, as well as networks with allelic SNP variants of *CDH13*, moderate E/I balance, thus advancing understanding of *CDH13* function at inhibitory synapses and elucidating the effects of rare and common *CDH13* gene variation.

Zusammenfassung

Während das gesunde Gehirn auf der Basis einer ausgewogenen synaptischen Kommunikation zwischen glutamatergen und GABAergen Neuronen arbeitet, um Exzitation (E) und Inhibition (I) zu koordinieren, beeinträchtigt eine Störung des E/I-Gleichgewichts die synaptische Kommunikation, die Informationsverarbeitung und letztlich die Kognition. Zahlreiche Hinweise deuten darauf, dass ein eingeschränktes E/I-Gleichgewicht die pathophysiologische Grundlage eines breiten Spektrums psychischer Erkrankungen darstellt. Genetische Screening-Ansätze haben Cadherin-13 (*CDH13*) als Risikogen für neuropsychiatrische Erkrankungen identifiziert. *CDH13* reguliert mehrere zelluläre und synaptische Prozesse bei der Gehirnentwicklung und der neuronalen Plastizität im Erwachsenenalter. Neben anderen Funktionen ist es spezifisch an hemmenden Synapsen von Parvalbumin- und Somatostatin-exprimierenden GABAergen Neuronen lokalisiert. Als Hinweis für die Funktion von *CDH13* bei der Regulierung des E/I-Gleichgewichts ergaben elektrophysiologische Ableitungen von Hippocampusschnitten in einem *CDH13*-defizienten Mausmodell einen Anstieg der basalen inhibitorischen, nicht aber der exzitatorischen synaptischen Übertragung. Darüber hinaus wurde bei der Suche nach genetischen Varianten die sich auf die funktionelle Expression des *CDH13*-Gens auswirken, der SNP (*single nucleotide polymorphism*, Einzelbasenpolymorphismus) rs2199430 im Intron 1 identifiziert, der mit den mRNA-Konzentrationen im menschlichen post-mortem Gehirn in einer vom Genotyp *CDH13*^{G/G}- *CDH13*^{A/G}- und *CDH13*^{A/A}-abhängigen Weise assoziiert ist. Ziel dieser Arbeit war es daher, diese Ergebnisse in einem komplementären menschlichen Modell unter Verwendung induzierter pluripotenter Stammzellen (*induced pluripotent stem cells*, iPSCs) zu bestätigen, und damit zu validieren. Die Anwendung menschlicher iPSCs in der Forschung hat embryonale Zellen ersetzt und den ethischen Konflikt aufgelöst, der im Zusammenhang mit der verbrauchenden Verwendung menschlicher Embryonen besteht. Die Untersuchung der Wirkungsweise von *CDH13* in inhibitorischen Synapsen sollte einen mechanistischen Einblick in die Auswirkungen von *CDH13*-Genvarianten auf die Aktivität des E/I-Netzwerks ermöglichen, die dann gezielt zur Wiederherstellung des Gleichgewichts eingesetzt werden können.

Genomweite Assoziationsstudien identifizierten seltene Kopienzahlvarianten (*copy number variants*, CNVs), die zu einer Deletion (oder Duplikation) des *CDH13*-Gens führen. Um die genetische Hintergrundvarianz zu verringern, wurde mit Hilfe des CRISPR/Cas9-Systems (Clustered Regulatory Interspaced Short Palindromic Repeats/CRISPR-associated protein 9) eine Reihe isogener iPSC-Linien mit einem dosisabhängigen Mangel an *CDH13*-Gen (*CDH13*^{-/-} und *CDH13*^{+/-}) erzeugt. Die CRISPR-modifizierten iPSCs, bei denen *CDH13* auf einem einzelnen oder zwei Allel(en) inaktiviert wurde, ermöglichen die Untersuchung der *CDH13*-Funktion in zellulären Prozessen, an hemmenden Synapsen und in der Aktivität neuronaler Netzwerke. Darüber hinaus wurden iPSCs, die die allelischen Varianten des SNP rs2199430 tragen, verwendet, um die Auswirkungen der häufigen genetischen Variation des *CDH13*-Gens zu untersuchen. Diese Zelllinien wurden zu reinen glutamatergen und GABAergen Neuronen differenziert und ko-kultiviert, um neuronale Netzwerke zu erzeugen, deren Aktivität gemessen und mit elektrophysiologischen Signaturen unterschiedlicher *CDH13*-Genotypen korreliert wurde. Die Arbeiten zur Bestimmung der neuronalen Netzwerkaktivität der iPSC-Linien wurden in drei Hauptschritte unterteilt: erstens die Erzeugung von rtTA/Ngn2- und

rtTA/Ascl1-positiven iPSCs über einen Lentivirus-vermittelten Ansatz; zweitens die Differenzierung reiner glutamaterger und GABAerger Neuronen aus den genetisch transduzierten iPSCs und die Ko-Kultur reiner glutamaterger und GABAerger Neuronen in einem vorher festgelegtem Verhältnis (65: 35) durch direkte Differenzierung unter Zugabe von Doxycyclin und Forskolin auf einem Mikroelektroden-Array (MEA)-Chip; und schließlich die Aufzeichnung der neuronalen Netzwerkaktivität der iPSC-Linien nach 49 Tagen *in vitro*, gefolgt von der Extraktion und Analyse verschiedener MEA-Parameter.

Anhand der MEA-Parameter wurde bestätigt, dass sowohl kompletter *CDH13*-Knockout als auch heterozygote Defizienz das E/I-Gleichgewicht durch verstärkte Inhibition beeinflussen. Darüber hinaus zeigte sich, dass häufige SNP-Variation die Signatur der neuronalen Netzwerkaktivität verändert. Insbesondere führte *CDH13*-Defizienz zu einer signifikanten Verringerung der Dauer der Netzwerk-Bursts (NBD), einer geringeren Anzahl von erkannten Spikes innerhalb eines Netzwerk-Bursts und einer signifikanten Verringerung der Netzwerk-Burst-Rate (NBR) im Vergleich zur Kontrolle (*CDH13*^{G/G}). *CDH13*^{A/G} und *CDH13*^{A/A} wiesen Ähnlichkeiten mit den CRISPR-modifizierten *CDH13*-defizienten Netzwerken auf, indem sie im Vergleich zu *CDH13*^{G/G} eine signifikante Verringerung der NBD und eine geringere Anzahl von erkannten Spikes innerhalb eines Netzwerks aufwiesen. Auffallend war eine signifikante Zunahme der NBR in den *CDH13*^{A/G}- und *CDH13*^{A/A}-Netzwerken im Vergleich zu den *CDH13*^{G/G}-Netzwerken. *CDH13*^{A/G}-Netzwerke wiesen bei beiden Parametern signifikante Unterschiede auf. Auf zellulärer Ebene deutet dies darauf hin, dass sich die Signalwege, die die Länge und Häufigkeit von Netzwerk-Bursts bestimmen, zwischen den allelischen Varianten des SNP rs2199430 unterscheiden, was die funktionelle Bedeutung dieses intronischen SNP bestätigt.

Zusammenfassend wurden *CDH13*-defiziente isogene iPSC-Linien mit CRISPR/Cas9 erzeugt, iPSCs wurden mit Hilfe eines Lentivirus-Ansatzes genetisch transduziert, direkte Differenzierung von glutamatergen/ GABAergen Neuronen, die von transduzierten iPSCs abgeleitet wurden, wurden verwendet, um ein skalierbares Ko-Kultursystem zu etablieren. Die Netzwerkaktivität wurde mit MEA aufgezeichnet, wobei zuvor festgelegte Parameter verwendet wurden, um Aktivitätsinformationen zu extrahieren. Die Ergebnisse zeigen, dass iPSC-abgeleitete neuronale Netzwerke nach CRISPR/Cas9-vermittelten *CDH13*-Inaktivierung sowie Netzwerke mit allelischen SNP-Varianten von *CDH13* das E/I-Gleichgewicht beeinflussen, was das Verständnis der *CDH13*-Funktion an hemmenden Synapsen fördert und die Auswirkungen seltener und häufiger *CDH13*-Genvariationen aufklärt.

1. Introduction

1.1. Cadherins

Cadherins belong to an extended family of calcium-dependent transmembrane cell adhesion molecules. The functions of cadherins are organ, tissue, and cadherin dependent. The cadherin superfamily is divided into three different categories: type 1 (classical cadherins), type 2 (non-classical cadherins) and atypical cadherins. What all these categories have in common are the cadherin extracellular domains (EC). Cadherins, which contain five ECs are classified as classical cadherins. Non-classical cadherins can be made up of more than five ECs (Hirano & Takeichi, 2012). These are the domains, which are involved in calcium binding (Ciatto et al., 2010). Type 1 and type 2 cadherins differ in their amino acid sequence of their C-terminus resulting in different functions and different involvement in signalling pathways, as well as the presence of the transmembrane domain (Hirano & Takeichi, 2012). Type 1 cadherins are mostly expressed in epithelia, while type 2 cadherins in the nervous system and vasculature (Ciatto et al., 2010).

1.2. Classical Cadherins

Classical cadherins possess both a highly conserved C-terminal cytoplasmic domain and an N-terminal ectodomain, as well as a transmembrane region that spans the membrane once. The C-terminus is located intracellularly, and the N-terminus is located extracellularly. The N-terminus consists of five tandem repeats of about ~110 amino acid motifs (EC1-EC5), where the EC1 is located distalmost from the plasma membrane. These proteins mediate homophilic calcium-dependent adhesion between cells, where calcium ions are bound between the domains and play a role in the adhesive function (Huntley et al., 2002). Crystal structure studies have shown that classical cadherins are dimeric. The adhesion between two classical cadherins from different cells occurs through a formation of an interface based on strand swapping. This occurs when the tryptophan 2 from the EC1 domain from one cadherin protein is inserted into the EC1 hydrophobic core of a neighbouring cadherin protein (Chen et al., 2005; Ciatto et al., 2010).

Classical cadherins are intracellularly linked to members of the catenin family via their highly conserved cytoplasmic domain. This domain interacts with the catenin complex, which includes β -catenin, p120-catenin and α -catenin. The cadherin molecule binds at the juxtamembrane region with P120-catenin and at its distal region with β -catenin. β -catenin and α -catenin interact with each other and α -catenin binds to the actin cytoskeleton of the cell (Gumbiner, 2005). In classical cadherins, the highly conserved C-terminal cytosolic domain represents the binding point for α -, β - and γ -catenins, which bind and interact with actin filaments. This binding to the actin cytoskeleton is crucial for adhesive function (Huntley et al., 2002; Ranscht, 1994).

1.3. Cadherin-13

Cadherin 13 is also known as Heart (H)- or Truncated (T)-cadherin. *CDH13* was termed T-cadherin when it was first discovered in 1991 by Ranscht and Dours-Zimmermann, when they isolated an unknown 95 kDa glycoprotein out of the brain of a chicken embryo. It was classified as T-cadherin due to the lack of the transmembrane region and the cytoplasmic domain. In the human genome, the gene *CDH13* is localized on chromosome 16q24 and shows 80% amino acid sequence homology to the chicken *CDH13* (Takeuchi et al., 2000). *CDH13* was also named H-cadherin (heart cadherin) after the organ in which the expression level was found to be the highest in 1996 (Lee, 1996). *CDH13* encodes a calcium-dependent glycosylphosphatidyl inositol-anchored (GPI) cell adhesion molecule and therefore belongs to the atypical members of the cadherin super family. *CDH13* is expressed in the developing and adult brain as well as the cardiovascular system (Verweij et al., 2017).

Classical cadherins and *CDH13* revealed only a 30% sequence identity resulting in structural and functional differences (Dames et al., 2008). Firstly, these proteins differ in their linkage to the plasma membrane of a cell. When comparing with classical cadherins, *CDH13* shows a similar extracellular domain as the classical cadherins but lacks the transmembrane spanning region and the cytoplasmic domain. Instead, *CDH13* is anchored to the plasma membrane through phosphatidylinositol glycan (Philippova et al., 2008). Another difference between *CDH13* to other cadherins can be found in the ectodomain. The EC1 subunit in classical cadherins have a unique amino acid sequence, the so-called HAV (histidine-alanine-valine) motif (Dames et al., 2008; Yap et al., 1997). The HAV motif is involved in the function of cell binding and homophilic interactions. This HAV motif is missing in *CDH13* (Ranscht & Dours-Zimmermann, 1991; Rivero et al., 2013). Furthermore, Tryptophan at position 2, which is involved in forming the canonical strand exchange dimer in EC1 of classical cadherins, is replaced with isoleucine in *CDH13* (Dames et al., 2008). Through this finding, and by doing additional crystallographic research, it has been shown that the EC1 domain of *CDH13* is monomeric and that an X interface is formed by hydrophilic surface interactions, which replaces the strand-swapping mechanism, which occurs in classical cadherins (Ciatto et al., 2010).

1.3.1. Domains, processing, and activation of *CDH13*

As mentioned before, *CDH13* is made up of five ectodomains depicted in different colours (Fig. 1). Additionally, there are three domains, which are crucial for processing, translocation, and post-translational modifications of the protein: Signalling Peptide (S.P) at the N-Terminal and the Propeptide located at the N- and C-terminal (Mavroconstanti et al., 2013). Within the EC5 domain and the Propeptide at the C-Terminal, a “GPI addition signal” is present (Mavroconstanti et al., 2013). This GPI addition signal is made up of approximately 20-30 amino acids. This signal originates at the ω site, which is the amino acid at which the GPI is attached (Gerber et al., 1992). Around 10 polar amino acids succeed the ω site which are followed by 15-20 hydrophobic residues (Kinoshita, 2020) (Fig. 1)

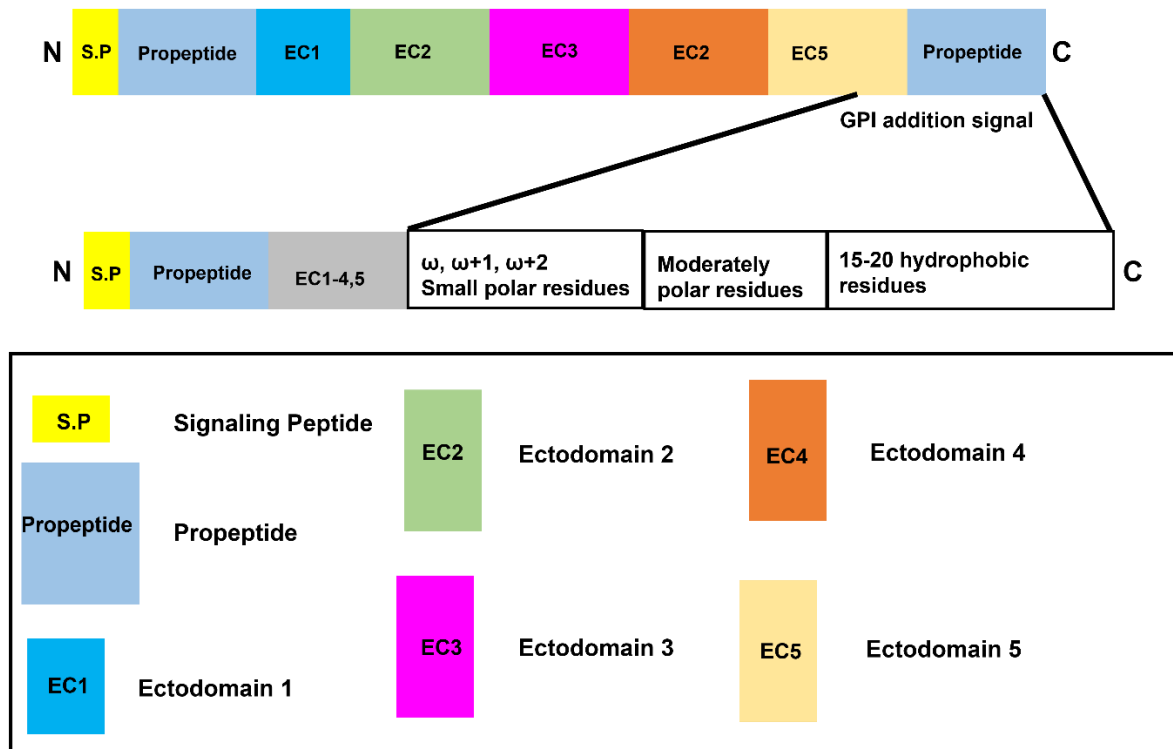


Figure 1. Structural domains of *CDH13*

Structural domains of *CDH13*. *CDH13* is made up of five ectodomains (EC1-5), a signalling peptide at the N-terminal and a propeptide located at the N- and C-terminal. Within the EC5 and the propeptide at the C-terminal, a GPI addition signal is present responsible for the GPI attachment.

CDH13 is translocated into the endoplasmic reticulum (ER) lumen with the aid of the signalling peptide and the propeptide at the N-terminal. These aiding cassettes are then removed to generate a proprotein. The propeptide at the C-terminal functions as a signalling peptide, which is recognized by the GPI transamidase. The GPI transamidase cleaves at the ω site and adds a preassembled GPI by transamidation forming a precursor GPI-anchored protein (GPI-AP)(Mavroconstanti et al., 2013) . Maturation of the GPI-AP enables the protein to be active and carry out its cell-type specific function (Figure 2).

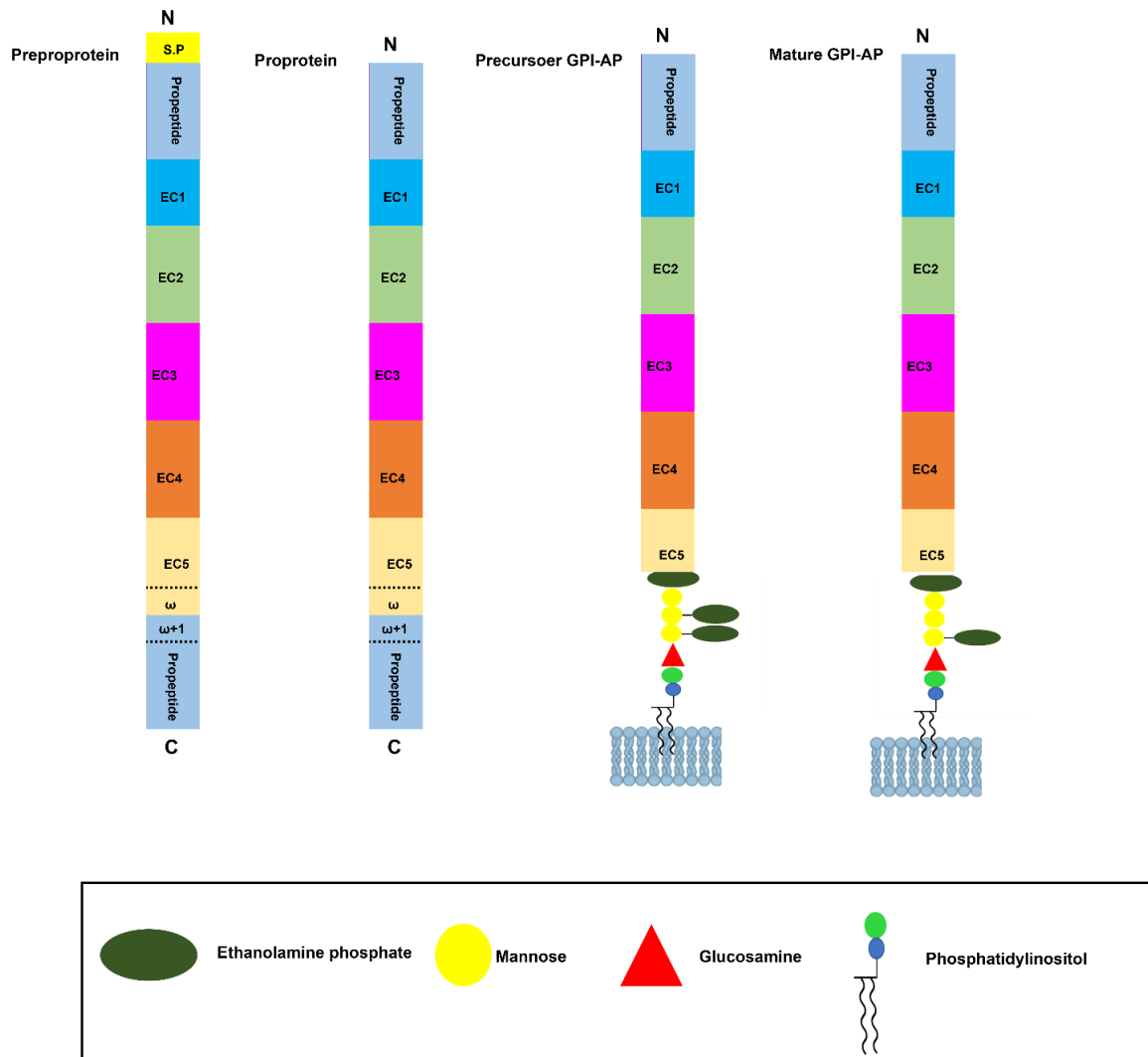


Figure 2. Translocation and processing of *CDH13*

Translocation and processing of *CDH13* The signalling peptide and the propeptide at the N-Terminal aid in the translocation of *CDH13* to the ER. These cassettes are removed and cleavage of the ω site occurs allowing a preassembled GPI to be added at the C-terminal forming a GPI-AP. The GPI-AP undergoes maturation steps to enable activation of the *CDH13*.

CDH13 is only functional if the X-dimer interface formation occurs (Ciatto et al., 2010). The X-dimer interface is composed of conserved amino acids found in the interdomain linker region (in red print), the N-terminal of EC1 (blueprint and red highlight), EC1-EC1 interaction contact point (blueprint and green highlight) and the EC2 domain (green print and blue highlight) (Ciatto et al., 2010) (Fig. 3). The latter forms the core of the X-dimer. The X-dimer interface formation is calcium dependent. Comparing Ca^{2+} -bound vs. Ca^{2+} -free *CDH13* crystal structures, demonstrated the calcium dependency. The absence of Ca^{2+} prevented the formation of the X-dimer because of a non-rigid interdomain linker and inappropriate orientation of the EC1-EC2 domains (Ciatto et al., 2010; Pokutta et al., 1994). The X-dimer interface is considered the functional region of *CDH13* as its disruption led to the abolishment of some fundamental *CDH13* functions, which are known so far. Mutations at the interface disrupted Ca^{2+} -dependent cellular adhesion and eliminated the inhibitory effect on neurite length (Ciatto et al., 2010; Harrison et al., 2010).

MQPRTPLVLCVLLSQVLLLSAEDLDCTPGFQQKVFHINQPAEFIEDQSILNLTFS DCKG	60
NDKLRYEVSSPYFKVNSDGGGLVALRNITAVGKTLFVHARTPHAEDMAELVIVGGKDIQGS	120
LQDIFKFARTSPVPRQKRSVVSPIIPENQRQPFPRDVGKVDSDRPERSKFRLTGKGV	180
DQEPKGIFRINENTGSVSVTRTLTDREVIAYVQLFVETTDVNGKTEGVPVLEVIVDQND	240
NRPIFREGPYIGHVMEGSPTGTTVMRMTAFDADDPATDNALLRYNIRQQTPDKPSPNMFY	300
IDPEKGDIVTVVSPALLDRETLENPKYELIEAQDMAGLDVGLTGTATATIMIDDKNDHS	360
PKFTKKEFQATVEEGAVGVIVNLTVEDKDDPTTGAWRAAYTIINGNPGQSFEIHTNPQTN	420
EGMLS VVKPLDYEISAFHTLLIKVENEDPLVPDVS YGSPSTATVHITVLDVNEGPFVFPD	480
PMMVTRQEDLSVGSVLLTVNATDPDSLQHQ TIRYSVYKDPAGWLNINPINGTVDTTAVLD	540
RESPFVDNSVYTALFLAIDSGNPPATGTG TLLITLEDVNDNAPFIYPTVAEVCDDAKNLS	600
VVILGASDKDLHPNTDPFKFEIHKQAVPD KVVWKISKINNTHALVSLQNLNKANYNLPIM	660
VTDSGKPPMTNITDLRVQVCS CRNSKVCNAAGALRFSLPSVLLLSLFLACL	710

RTPHAE: Interdomain linker region in the propetide domain

V,S,V: N-terminal of EC1

L,E,I: EC1-EC1 interaction contact points

M,V,L: EC2 domain

Figure 3. Amino acid sequence of *CDH13*

Amino acid sequence of *CDH13* in the colours representing the domains of *CDH13* including highlighted essential functional amino acids (Figure generated using UniProtKB - P33150 and (Ciatto et al., 2010) information).

1.4. *CDH13* in neurodevelopmental and psychiatric disorders

Genome-wide association (GWA), copy number variant (CNV), mouse model and cell culture studies have associated *CDH13* to neurodevelopmental and psychiatric disorders which will be discussed in the following section.

GWAS suggested an association of *CDH13* with attention-deficit/hyperactivity disorder (ADHD). *CDH13* variants were found to be among top candidates for ADHD in various GWAS studies (Franke et al., 2009; Lasky-Su et al., 2008; Lesch et al., 2008; Neale et al., 2010; Zhou et al., 2008) even though no genome wide statistical significance was ever observed due to

limited sample size. Despite this, *CDH13* remains one of the most relevant and studied genes associated with ADHD. *CDH13* has been associated to working memory performance in children with ADHD (Arias-Vásquez et al., 2011), hyperactive/impulsive symptoms in youths with ADHD (Salatino-Oliveira et al., 2015). Recently, a common *CDH13* variant has been associated with low agreeableness and neural responses to working memory tasks in adults with ADHD (Ziegler et al., 2021).

In psychiatric disorders, it is very common that the patients develop comorbidities. ADHD comorbidities disorders, such as violent behaviour (Tiihonen et al., 2015), substance abuse including cigarette smoking (Drgon et al., 2009), methamphetamine intake (Uhl et al., 2008), and alcohol dependence (Johnson et al., 2011) have been associated with *CDH13*. Additionally, *CDH13* has been identified as a potential risk gene in major depression (Howard et al., 2019), bipolar disorder (Prata et al., 2019), and schizophrenia (Otsuka et al., 2015). *CDH13*'s role in neurodevelopmental processes has been studied using genetically modified mouse models as well as iPSCs, which provided a greater insight into its underlying mechanisms involved in neurobiology. Based on research over the past years, different cell types have been found to express *CDH13* suggesting a cell-type specific mode of action. The expression has been found in motor neurons (Ciatto et al., 2010; Fredette et al., 1996; Fredette & Ranscht, 1994) cortical neurons, GABAergic interneurons, dopamine-specific neurons (Drgonova et al., 2016; Paradis et al., 2007; Rivero et al., 2015) and serotonin-specific neurons (Forero et al., 2020; Forero et al., 2017).

1.5. *CDH13* signalling pathways

CDH13 acts on a variety of signalling molecules, thereby affecting their respective signalling pathways (Rivero et al., 2013). The GPI-anchored nature of *CDH13* implies that it is required to bind to other membrane-bound proteins to exert its functions. So far, the following membrane bound proteins have been identified to interact with *CDH13*: GABA_A receptor $\alpha 1$ subunit (GABA_A $\alpha 1$), Integrin $\beta 3$ (ITG $\beta 3$), Integrin $\beta 1$ (ITG $\beta 1$), Insulin-like growth factor 1 (IGF-1), Brain derived neurotrophic factor (BDNF), and Tropomyosin-related kinase B (TrkB) (Joshi et al., 2007; Mossink et al., 2022; Philippova et al., 2008; Rivero et al., 2013). The latter five proteins activate intracellular downstream signaling pathways such as the protein kinase B (AKT) and mammalian target of rapamycin (mTOR) pathways, which are essential in neurite outgrowth, synapse formation and transmission, neuron survival and dendrite formations (Ahn, 2014; Joshi et al., 2005; LiCausi & Hartman, 2018; Read & Gorman, 2009). *CDH13* can also engage in homophilic interactions, which triggers the activation of the Ras homolog family member A (RhoA) / Rho-associated protein kinase (ROCK) and Ras GTPase pathways. The Rho/ROCK pathway has been shown to be involved in axon pathfinding, neurite outgrowth and differentiation, axon pathfinding and dendritic spine formation and maintenance (Govek et al., 2005). Activating Rac GTPase regulates the actin cytoskeleton, in turn, affecting axon outgrowth and guidance (Norgaard & Pocock, 2019). Furthermore, Rac GTPases are required for the establishment of neural polarity and neurite branching (de Curtis, 2008, 2019).

1.6. Effects of *CDH13* axonal migration and outgrowth

The established main function of *CDH13* is that it acts as a negative regulator in axonal migration and outgrowth. It was hypothesized as early as 1994 that *CDH13* acts as an avoidance cue to restrict the pathway of motor axons and thus involved in motor axon organization (Fredette & Ranscht, 1994). Following this, research identified *CDH13* as the first cadherin to act as a neurite growth inhibitor by comprising the extracellular domains and observing its effects (Fredette et al., 1996). This was later confirmed in a crystallography study to identify the sequence sites responsible for the adhesive property of *CDH13*. Neurite outgrowth regulation was prevented when the regulatory region responsible for adhesion was disrupted (Ciatto et al., 2010).

1.7. Induced pluripotent stem cells

The reprogramming technique was developed in 2006 with the aim to eliminate research being conducted using embryonic stem cells (ESCs) and replace them with iPSCs. Reprogramming consists of the molecular manipulation of somatic cells by introducing four transcription factors: octamer-binding transcription factor 3/4 (*Oct3/4*), *SRY-box 2* (*Sox2*), avian myelocytomatosis viral oncogene homolog (*c-Myc*) and Kruppel-like factor 4 (*Klf4*) called the Yamanaka factors (Takahashi & Yamanaka, 2006). The Yamanaka factors can be introduced into the cells by either an integrative method (e.g. lentivirus) or a non-integrative method (e.g. Sendai virus) (Fusaki et al., 2009; Romli et al., 2013). The reprogrammed cells are referred to as “iPSCs” (Takahashi et al., 2007). iPSCs have many of the regenerative properties as ESCs such as morphology, growth behaviour, pluripotency capacity and differentiation into all human cell types as they can differentiate in all three germ layers (mesoderm, ectoderm, endoderm). iPSCs have widely been acknowledged as a breakthrough in personalized medicine covering many diverse research areas such as regenerative medicine (Walmsley et al., 2014), drug screening (Elitt et al., 2018), disease modelling (Kim, 2015) and cell therapy (Flahou et al., 2021). iPSCs are an invaluable tool in basic research since they can be used to examine and understand molecular mechanisms underlying diseases in a patient-specific manner. The application of iPSCs is expanding across the world’s research labs, but there are still no uniform and standardized guidelines to reduce iPSC model variation (Volpato & Webber, 2020). Variation arises primarily from differences in donors, which affect critical iPSC characteristics such as morphology, DNA methylation, transcriptomic and proteomic signatures as well as pluripotency and differentiation capacity (Guhr et al., 2018; Kilpinen et al., 2017). Naturally, all this variability affects iPSCs differentiation and since iPSC differentiation and culture involve several steps, small variations at each step can inevitably lead to substantial differences in results (Ghaffari et al., 2018; Popp et al., 2018; Volpato et al., 2018). To minimize variability in our experiments, we chose to generate a set of isogenic cell lines with a gene dose-dependent deficiency of *CDH13* using the CRISPR/Cas9 system (Vitale et al., 2021). Using isogenic cell lines can reduce genetic variance between control and disease-state iPSCs since they differ only by one gene of interest (Bassett, 2017; Kim et al., 2014).

1.8. Genetic engineering

Commencement of genetic engineering approaches dates to the late 1990s and involves the targeted modification of the genome (Woolf, 1998). These modifications include insertion, deletion, or replacement of specific gene sequences of interest. Since its conception, this technology has advanced in specificity and has gained enormous impact in various scientific fields: animal research (Sakurai et al., 2020), aquaculture (Wargelius, 2019), plants (Townsend et al., 2009), and gene therapy (Barrangou & Doudna, 2016; Carroll, 2008). The best-known genomic engineering technologies are the CRISPR, TALEN, and Zinc-finger technologies (Becker & Boch, 2021; Ran et al., 2013; Urnov et al., 2010). Since the CRISPR/Cas9 system is the approach used in the present work to knockout *CDH13*, it will be described in more detail.

1.8.1. CRISPR/Cas9

Adaptive immune systems based on CRISPR in bacteria have been modified for genetic engineering (Bhaya et al., 2011). CRISPR systems include a single-guide RNA (sgRNA) and Cas proteins which need to be co-expressed when generating a knockout cell line (Fig.4A). The sgRNA consists of a scaffold sequence required for Cas-binding and a spacer which is a user-defined 20-nucleotide sequence defining the genomic target to be modified (Sternberg et al., 2014). The spacer must be a unique sequence within the genome, and it must be preceded by a Protospacer Adjacent Motif (PAM) (Anders et al., 2014). The exact PAM sequence is dependent on which Cas protein is used: for the *S. pyogenes* Cas9 (SpCas9), a 5' NGG PAM sequence is required. The Cas9 protein undergoes a conformational change when it forms a complex with the scaffold sequence of the sgRNA (Fig.4B). This active DNA-binding complex binds to the target sequence with the aid of the sgRNA spacer sequence (Fig. 4C). During the second conformational change, the Cas9 induces a double-strand break (DSB) within the target DNA that occurs 3-4 nucleotides upstream of the PAM sequence (Fig.4D) Either the DSB can be repaired by non-homologous end joining (NHEJ) pathways or the homology directed repair (HDR) pathway, both causing small insertions and deletions (INDELs) (Bennett et al., 2020) at the DSB site (Deltcheva et al., 2011; Ma et al., 2014; Ran et al., 2013; Thurtle-Schmidt & Lo, 2018). When INDELs are introduced in the protein coding sequence, the reading frame is shifted causing an alteration in protein translation which often leads to a gene deletion.

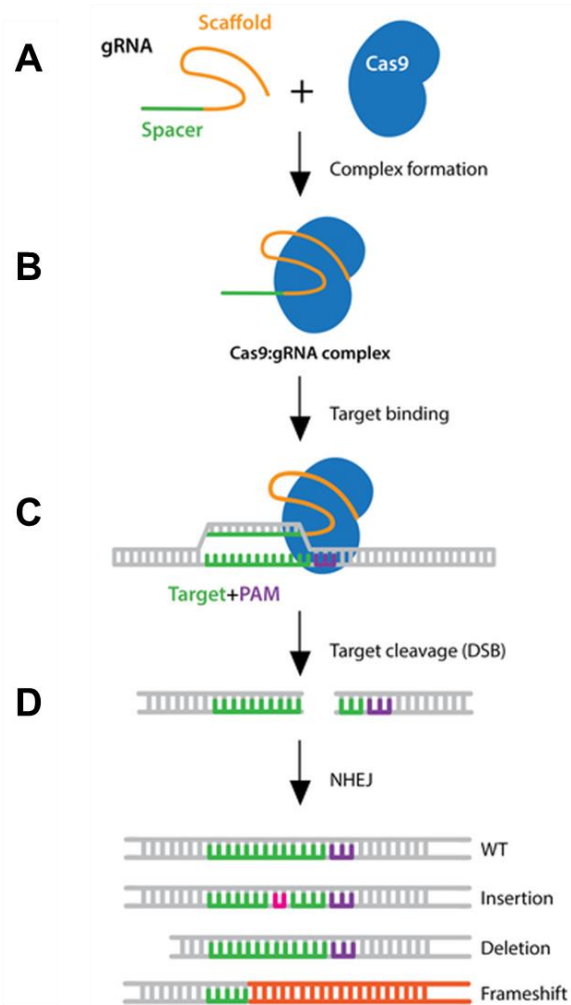


Figure 4. CRISPR/Cas9 mode of action

A. The sgRNA and Cas9 protein must be co-expressed. **B.** Conformational change occurs when the sgRNA and the Cas9 protein form a complex. **C.** This active DNA-binding complex binds to the target sequence. **D.** After a second conformational change, the Cas9 induces a DSB which is repaired by NHEJ resulting in nucleotide insertions/deletions causing frameshifts in the genetic sequence. Figure taken from Addgene (Source: www.addgene.org, accessed 10.06.2022)

In spite of the fact that Cas9 targeting specificity is thought to be strictly controlled by the sgRNA and the PAM sequence, potential unintended mutations may still occur: these are called off-target effects (Cong et al., 2013; Fu et al., 2013; Hsu et al., 2013; Mali et al., 2013; Zhang et al., 2015). Off-target effects can be reduced by increasing sgRNA specificity in the seed sequence, which is 10-12 bp adjacent to the PAM sequence (at the 3' end of sgRNA) influencing Cas9 specificity (Cong et al., 2013; Jinek et al., 2012). Cas9 specificity is dependent on the GC content of the seed sequence (Ren et al., 2014): the right balance of the GC content is critical, since extreme levels of GC content can reduce sgRNA activity (Cencic et al., 2014), whereas a guanine-rich seed sequence within the extreme levels can fold into stable G-quadruplexes *in vivo* which contribute to sgRNA stability (Moreno-Mateos et al., 2015). Uridine-rich seed sequences decrease the sgRNA abundance as uridine induces termination of sgRNA transcription (T. Wang et al., 2014; Wu et al., 2014). All these parameters are considered when

designing the sgRNAs on online platforms, but nonetheless, off-target effects must be checked after genetically engineering cell lines.

1.9. Excitatory/inhibitory balance

There are different types of neurons within neural networks, and they all perform different functions to maintain network integrity. Neuronal networks and information processing depend on the balance between excitatory (glutamatergic) and inhibitory (GABAergic) γ -aminobutyric acid (GABA) neurons. In line with this hypothesis, excitation-inhibition (E/I) imbalances are believed to be a pathophysiological cause of many mental disorders (Selten et al., 2018) such as autism spectrum disorder (ASD) (Culotta & Penzes, 2020) and schizophrenia (Gao & Penzes, 2015)

1.9.1. E/I balance: physiology

On dendritic spines are glutamatergic synapses (Penzes et al., 2011), while GABAergic synapses are found along the shaft of the dendritic nerve fiber, along the somata, and along the initial segments of axons (Fritschy & Brünig, 2003). The electron-dense postsynaptic density (PSD) is a major characteristic of excitatory synapses which extends directly opposite the presynaptic active zone, while inhibitory synapses lack this feature and are found to be more symmetrical in structure. Pre-synaptically, excitatory and inhibitory neurons are distinguished by the presence of vesicular glutamate transporters (VGLUTs) and vesicular GABA transporters (VGATs), respectively. These transporters are responsible for trafficking of the respective neurotransmitters: glutamate and γ -aminobutyric acid (GABA) from the pre-synapse to the post-synapse. Post-synaptically, different adaptor proteins facilitate the assembly of receptors at the surface enabling neurotransmitters to bind and initiate a receptor-dependent ion influx which induces polarization dependent on the type of receptor which is activated. The pre- and post-synapse are held together in close proximity by trans-synaptic adhesion with the aid of adhesion molecules such as neuroligin, neurexin, cadherins, Slitrk, Leucine-rich-repeat transmembrane neuronal proteins (LRRTMs), integrins, MAM Domain Containing Glycosylphosphatidylinositol Anchor 2 (MDGA2), Fibronectin leucine-rich transmembrane protein 3 (FLRT3), Immunoglobulin superfamily member 11 (IgSF11), Netrin-G ligand-2 (NGL-2), Extracellular leucine-rich repeat and fibronectin type III domain containing 1 (Elfn1) (Gatto & Brodie, 2010; Jang et al., 2017; Mossink et al., 2022) (Fig. 5).

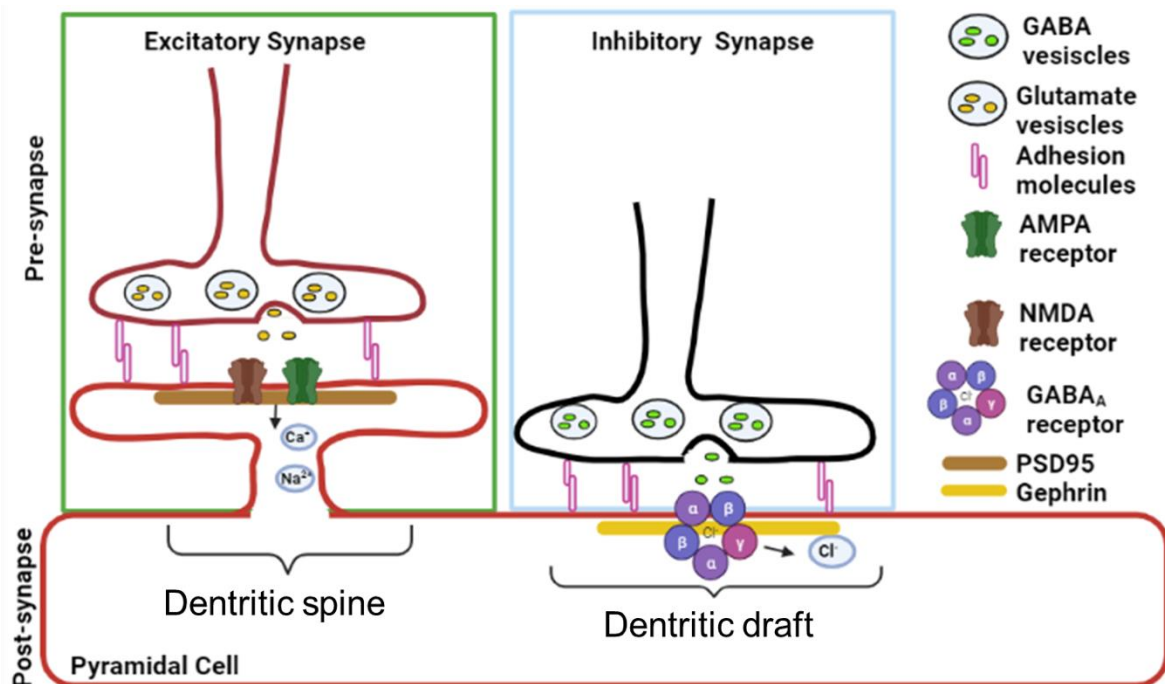


Figure 5. The physiology of a balanced E/I synapse

Glutamatergic synapses (excitatory) are located on dendritic spines while GABAergic synapses (inhibitory) are located along the shafts of dendritic nerve fibres. Excitatory synapses are characterized by the PSD zone, VGLUTs and the neurotransmitter glutamate. Inhibitory synapses are characterized by VGATs and the neurotransmitter GABA. The pre- and post-synapse and held together in proximity by trans-synaptic adhesion with the aid of adhesion molecules. Figure created with Biorender.

The interplay between excitatory and inhibitory neurons results in the correct E/I ratio, thus allowing correct information flow throughout the network. Pyramidal cells are considered as the largest neuronal population responsible for glutamatergic transmission. These neurons have long-projecting axons with many spine-studded pyramidal-shaped arbors, increasing the neuron's ability to receive both excitatory as well as inhibitory input (Spruston, 2008). Pyramidal cells occur mostly in the cortex (Elston, 2003; Spruston, 2008) and amygdala (McDonald, 1992; Muller et al., 2006) which are also the brain regions of major interest in mental disorders as the cortex is responsible for cognition (Parenti et al., 2020; Schubert et al., 2015) and the amygdala was shown to be involved in depression (Satterthwaite et al., 2016), anxiety (He et al., 2016) and schizophrenia (Kim et al., 2020). The GABAergic neurons provide inhibitory input: GABAergic neurons account for only 10-15% of the total number of neurons in the brain, but their ability to synthesize the inhibitory neurotransmitter GABA as well as their synaptic strength, and high-activity rate makes them crucial in regulating neuronal excitability (Markram et al., 2004). A significant influence of E/I modulation is exerted by GABAergic interneurons that contain the calcium-binding protein parvalbumin. Parvalbumin-positive (PV+) neurons are crucial in the generation and timing of action potentials of excitatory neurons due to the inhibitory synapse location as well as their electrophysiological properties which enable fast spiking activity (González-Burgos et al., 2005; Kawaguchi, 1995). Two majorly investigated PV+ neurons subtypes are basket cells (Kawaguchi, 1995; Lewis & Lund, 1990) and chandelier cells (Freund & Katona, 2007). Chandelier neurons show fast-spiking

firing patterns and have cartridges, long linear axon terminals that form synapses on pyramidal neurons' initial axon segments. Basket neurons exhibit similarly fast-spiking electrophysiological characteristics. Its axons, however, target pyramidal neurons' cell bodies and proximal dendrites. Both PV+ neurons are strategically placed, so they can both control the excitatory cell's firing rhythm but also generate fast, synchronized inhibition patterns at the same time as receiving rhythmic feedback inhibition from the pyramidal cells. This synchrony is crucial to the generation of dynamic network oscillations i.e., network activity (Williams & Boksa, 2010) (Figure 6).

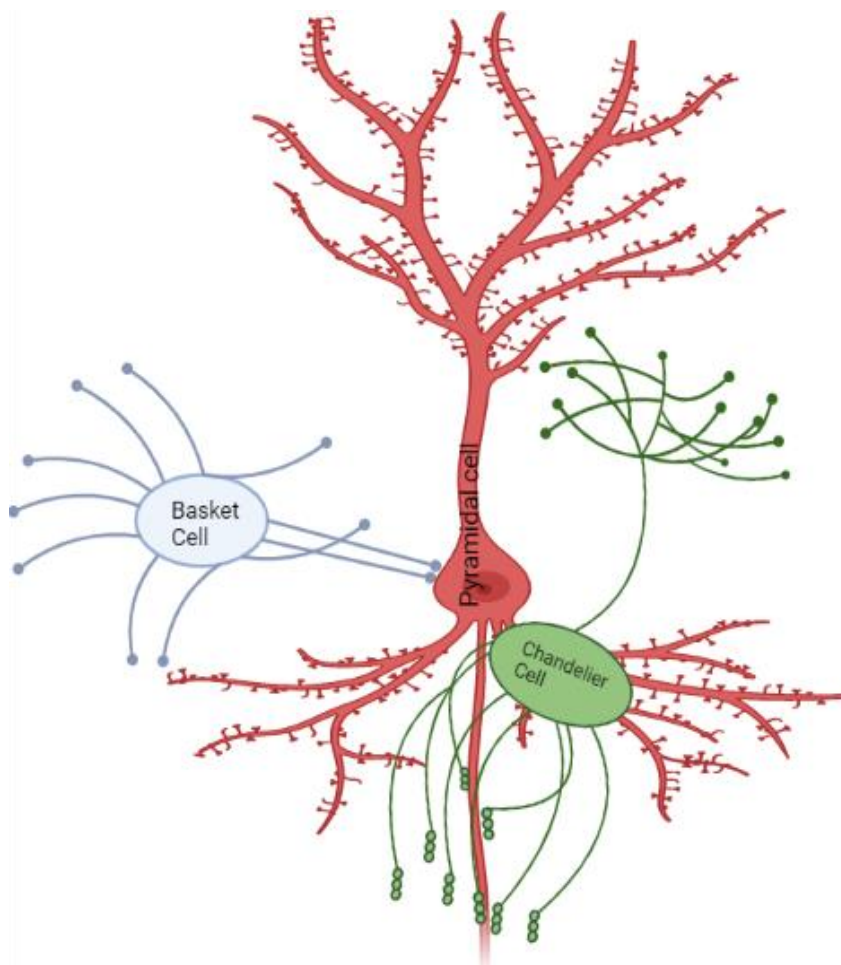


Figure 6. Chandelier and Basket neurons acting on Pyramidal cell

Chandelier neurons have cartridges, long linear axon terminals that synapse onto pyramidal neurons' initial axon segments. Basket neurons, target pyramidal neurons' cell bodies and proximal dendrites. Created with Biorender.

1.9.2. E/I balance: mode of action

An effective functional neuronal network depends on precise output signals derived from single excitatory and inhibitory neurons (Beierlein et al., 2000; Megías et al., 2001; Szabadics et al., 2001). Action potentials are fired via excitatory synapses stimulated by glutamate as opposed

to inhibitory synapses, which are activated by GABA. Both forms of neuronal activation occur when the cells are depolarized. Cortical interneurons control pyramidal cells to fire specific oscillatory patterns by rhythmic inhibition (Tamás et al., 2000). These specific oscillatory patterns occur at 30-80 Hz, also known as gamma frequencies/gamma oscillations. Gamma oscillations derive from the synchronized interplay firing between glutamatergic and PV+ neurons with the E/I balance regulating its frequency (i.e., power). Gamma frequency synchronization of neuronal networks in the cortex and hippocampus is crucial for successful information transfer between cerebral regions affecting cognition, including learning and memory (Bartos et al., 2007; Gatto & Broadie, 2010; Li et al., 2021).

It is noteworthy that, in addition to the crucial role the E/I synaptic ratio plays in generating the correct overall firing patterns of cells (Eichler & Meier, 2008), this ratio varies greatly across developmental stages and even between neuron subtypes. Researchers have observed that glutamatergic neuron E/I ratios in hippocampal neuron cultures vary between 14 and 19 days (2:1 and 4:1, respectively) (Liu, 2004). From day 14 to day 19, these ratio changes were also observed among inhibitory neurons in specific PV+ and calretinin+ interneurons in the culture, as the ratios varied from 14:1 to 3:1, respectively (Gulyás et al., 1999). “Synaptic scaling” activates compensatory mechanisms responsible for neuronal homeostatic control which enable the regeneration of network circuits, for example, during development, when the external conditions of the cells inevitably change (Turrigiano, 2011; Turrigiano et al., 1998). Genetic mutations in the neuronal homeostatic mechanisms are the pathophysiological origin of neurodevelopmental and psychiatric disorders as they cause destabilization of the E/I balance and thus of the neuronal network circuitry. Especially mutations in specific transcriptional regulators, translational regulators, scaffolding proteins, cell adhesion molecules, and channels/receptors impact the E/I balance (Gatto & Broadie, 2010).

1.9.3. *CDH13* involved in the E/I balance

CDH13 is expressed in presynaptically in PV+ and SOM inhibitory neurons (Mossink et al., 2022; Rivero et al., 2015). A previous investigation showed that hippocampal neurons from *CDH13*^{-/-} mice received an increased inhibitory input, while excitatory input is not altered, implying an imbalance in the E/I (Rivero et al., 2015). Considering the location and effect of *CDH13* removal, it is clear that *CDH13* has a critical regulatory role in inhibitory functions in which it modulates synaptic activity and turnover (Rivero et al., 2015) The inhibitory system controls hyperexcitability in a given neuron circuitry (Shepherd, 2004), so if this system malfunctions, the E/I balance is disrupted causing altered information and signalling processing initiating instability in neuron networks. With regards to the absence of *CDH13*, E/I imbalance is most likely due to increased stability of GABAergic synapses (Rivero et al., 2015). Synaptic (de)stabilization from cadherins has been reported before (Aloy et al., 2006; Andreyeva et al., 2012), where they may interact heterophilically with either postsynaptic or presynaptic molecules such as GABA-A α 1 (Philippova et al., 2008), integrin- β 1 and integrin- β 3 (Mossink et al., 2022). Through such interactions, changes in actin cytoskeleton dynamics can be induced, which destabilize GABAergic synapses (Rivero et al., 2015) which in turn disrupts the E/I balance.

2. Aims of the thesis

The first aim of this thesis was to generate and characterize a set of isogenic iPSC cell lines using the CRISPR/Cas9 system to investigate the effects of *CDH13* deficiency in GABAergic neurons in neuronal network activity. After that, two further iPSC cell lines were characterized to study the differential effects of *CDH13* SNP variants in GABAergic neurons in neuronal activity. Once all cell lines were established, the next aim was to transduce these cell lines with two specific vectors (rtTA/Ngn2 and rtTA/Ascl1) which when activated with supplements, induce differentiation of glutamatergic- (excitatory-E) and GABAergic- (inhibitory-I) neurons respectively. These two individual cultures were qualitatively verified for each cell line, before establishing a scalable co-culture system, to investigate how differential *CDH13* genotype affects the E/I balance by using the MEA system to extract network activity data. This work was done to confirm a previous mouse study which shows an increase in inhibition in *cdh13* deficient neurons indicating the potential influence CDH13 has in synaptic (de)stabilization which in turn affects neuronal circuits.

3. Methods

3.1. Cell culture methods

3.1.1. Cells

A written informed consent was signed by all study participants and the study was approved by the Ethics Committee of the Medical Faculty, University Hospital Würzburg (approval number 96/11). Primary human fibroblasts and human iPSCs were used as cell culture models. For this purpose, dermal fibroblasts isolated from healthy volunteers were reprogrammed into induced stem cells and quality control checks were carried out. The healthy probands were screened with the Structured Clinical Interview for DSM-IV (SCID-I) to exclude axis 1 mental disorders. Stocks of the original virus-induced stem cells ("mother plates") and of mother-plate-derived and established iPSC lines are stored in the liquid nitrogen storage tanks of the Division of Molecular Psychiatry, Laboratory of Translational Neuroscience, Center of Mental Health, University Hospital Würzburg for future studies. This was carried out by Dr. Jansch and Dr. Ziegler.

3.1.2. Culturing and passaging human induced pluripotent stem cells

Frozen iPSCs were thawed at 37°C. Still containing small pieces of ice, the sample was transferred into a falcon tube with fresh DMEM/F12. After centrifugation at 1200 rpm for 5 min, the supernatant was discarded, and 1.5 ml of fresh StemMACS™ iPS-Brew XF was carefully pipetted to the cell pellet avoiding the separation into single cells. The cell suspension was then transferred into a matrigel-coated well plate in StemMACS™ iPS-Brew XF supplemented with 10 µM Rock inhibitor (RI) and the cells were kept at 37°C, 5% CO₂ in an incubator. The stem cell culture medium was changed every day and cell densities checked under an inverted

light microscope. Once iPSC colonies reached 70-80% confluency, they were split in a specific ratio dependent on planned experiment as follows: after washing the human iPSCs with 1 mL 1x PBS, 500 μ l accutase were added to the cells and incubated for 3-5 min at 37°C. After that, 2 mL of DMEM/F12 were added to the well to stop the activity of the accutase (cell detachment reagent). Cells were transferred to a falcon tube with 2 mL DMEM/F12 and centrifuged at 1200 rpm for 5 min, the supernatant was discarded, and 1 mL of fresh StemMACS™ iPS-Brew XF was added to the cells. A precise ration of the cell suspension was transferred into a matrigel-coated 6-well plate that had been washed once with 1x PBS (1 mL) and contained 1.5 mL of fresh StemMACS™ iPS-Brew XF supplemented with 1 μ l/mL RI. From this time point, cells needed approximately 3-4 days to reach confluency again.

3.1.3. Coating for human iPSC cultures

Matrigel is a widely used coating strategy for human iPSC cultures. It is extracted from the Engelbreth-Holm-Swarm (EHS) mouse sarcoma, a tumor rich in extracellular matrix proteins. Matrigel is a reconstituted basement membrane preparation which is composed of approximately 60% laminin, 30% collagen IV and 8% entactin. Growth factors which naturally occur in the EHS tumor such as Heparan sulfate proteoglycan (perlecan), TGF- β , epidermal growth factor, insulin-like growth factor, FGF, tissue plasminogen activator, metalloproteinases and other are also an essential component of the Matrigel matrix. Each Matrigel vial is delivered with a specific dilution factor which indicates the amount of Matrigel that should be diluted in 25 mL of DMEM/F12 to coat plates. The Matrigel solution was then pipetted to the respective well and incubated for 1 h at room temperature (RT). After the incubation period, the plates were sealed using Parafilm and stored at 4°C for up to 4 weeks. Before use, the Matrigel solution was removed, and the culture plate was washed once with DPBS.

Due to the Corona virus pandemic, Matrigel availability became scarce. Therefore, the coating strategy was switched to Geltrex LDEV-Free Reduced Growth Factor Basement Membrane Matrix. Here again, a specific dilution factor indicating the amount of Geltrex that should be diluted in 25 mL of DMEM/F12 was provided by the company. After pipetting the Geltrex in the plates, the plates were placed for 60 min at 37°C. After that, they were placed for 15 min at RT before storing them at 4°C or using them to seed iPSCs.

3.2. Genetic editing

3.2.1. Sequencing region of interest

Section 3.2.1-3.4.6 were performed together with Johanna Zöller.

The region of interest to be modified was sequenced before designing the guideRNAs. The following primers were used for sequencing of *CDH13* exon 1:

Table 1. Primers used to sequence exon 1 of *CDH13*.

Target	Forward/Reverse primer (5'–3')
<i>CDH13</i> exon 1	CATTGCCAGCGTGATTTGTGAG TCCCTACCGAGCCCCGATCTG

3.2.2. Designing sgRNAs

The sgRNAs were designed with the software tool 'Design CRISPR Guides' from Benchling (<https://www.benchling.com/>): sgRNAs are selected based on the predicted on-target and off-target activity. Two sets of sgRNAs were chosen for generating the *CDH13* knockout (sgRNA #2) and heterozygotic (sgRNA #1) iPSC cell line:

Table 2. sgRNAs used to generate the *CDH13* knockout (sgRNA #2) and heterozygous (sgRNA #1) iPSC lines.

sgRNAs for <i>CDH13</i> ^{+/-} and <i>CDH13</i> ^{-/-} iPSC lines	Sequence
sgRNA #1 (<i>CDH13</i> ^{+/-})	CACAGAACGAGCGGAGTTCT
sgRNA #2 (<i>CDH13</i> ^{-/-})	AGGAGAACGCACAGAACGAG

The benchling program automatically designs two oligos (sgRNA-top and sgRNA-bottom) to synthesize each sgRNA. These oligos were ordered and each pair were phosphorylated and annealed before ligating the sgRNAs into the pSpCas9(BB)-2A-Puro (PX459) V2.0 plasmid (Addgene: #62988). After that, the newly ligated plasmid was cloned into DH5 α -*E. coli* cells.

3.2.3. pSpCas9(BB)-2A-Puro (PX459) V2.0 plasmid5 digestion and phosphorylation and annealing of sgRNA

The pSpCas9(BB)-2A-Puro (PX459) V2.0 plasmid digestion was carried out by setting up the digestion. The digestion reaction was incubated for 30 min at 37°C. The DNA was then purified using the NucleoSpin Gel and PCR Clean-up Kit. In parallel, the phosphorylation-annealing reaction was set up for the ordered oligos pair. When the reaction was over, the guide mixture was diluted 1:100 in H₂O (1 µl guide mix in 99 µl H₂O). The guide mixture was then ligated into the digested plasmid. Once the reaction was finished, the newly ligated plasmid was confirmed on an agarose gel and then cloned into DH5α-*E. coli* cells.

3.2.4. Cloning of sgRNAs

The cloning procedure was carried out as follows: a 50 µl tube of DH5α-*E. coli* cells was thawed on ice for 10 min for each sgRNA. 2 µl of each sgRNA guide was added to the DH5α-*E. coli* cells and gently mixed by inverting the tube 4-5 times. This reaction mix was incubated on ice for 20 min and then heat-shocked at 42°C for 30 s. After that, the cells were immediately placed on ice for 5 min 1 ml of pre-warmed Outgrowth medium was added to each reaction. The reaction was placed at 37°C for 60 min on a shaker at 250 rpm. After that, the whole tube is plated onto LB plates with 1000 µg/mL ampicillin. The plates were then incubated overnight at 37°C. The following day, single colonies which grew on the LB plates were picked to check for the correct insertion of the sgRNA. For this, every colony was inoculated into a 5 ml culture of LB medium with 1000 µg/mL ampicillin. The cultures are placed on a shaker at 37°C overnight. The following day, the plasmid was isolated from the culture using the Wizard®*Plus* SV Minipreps DNA purification system. The DNA concentration was measured and sent to sequence (100 ng/µl DNA in 30 µl total volume) using the following primers:

Table 3. Primers used to confirm insertion of sgRNA.

Target	Forward/reverse primer (5'–3')
sgRNA #1 (<i>CDH13</i> ^{-/-})	GCACAGAACGAGCGGAGTTCT AGAACTCCGCTCGTTCTGTGC
sgRNA #2 (<i>CDH13</i> ^{-/-})	GAGGAGAACGCACAGAACGAG CTCGTTCTGTGCGTTCTCCTC

3.2.5. Nucleofection of the plasmids

Nucleofection of 800,000 healthy iPSCs with 5 µg plasmid was performed by using the Amaxa™ P3 primary Cell 4D-Nucleofector™ X Kit L and the Nucleofector™ X-Unit program 'CA137'. For this purpose, iPSCs are collected and centrifuged to obtain a pellet. The supernatant is removed, and the pellet is resuspended in 1 ml StemMACS™iPS-BrewXF

supplemented with 10 μ M Y27632. The resuspension should be done carefully but thoroughly to ensure a single cell suspension crucial for nucleofection efficiency. 800,000 cells were then counted, placed in a separate Eppendorf tube, centrifuged and the supernatant removed. The pellet was resuspended in 100 μ l P4 Primary Cell Nucleofector[®] Solution + supplement 1 (provided in Amaxa[™] P4 primary Cell 4D-Nucleofector[™] X Kit L. 5 μ g of either the sgRNA - pSpCas9(BB)-2A-Puro (PX459) V2.0 plasmid, or the sgRNA - pCas9(BB)-2A-GFP; (Addgene: #48138) were added to the resuspended pellet and gently pipetted two times up and down. This mix was then carefully added to the lonza cuvette and introduced into the machine. After nucleofection, StemMACS[™]iPS-BrewXF supplemented with 10 μ M Y27632 media was taken up with a small plastic pipette dropper provided from the kit and carefully added to the cuvette containing now the nucleofected iPSCs. This suspension was mixed thoroughly and then transferred to the culturing plate. This transfer step was repeated several times to ensure entire collection of nucleofected iPSCs into the culturing plate.

3.2.6. Colony selection

Selection of the colonies was carried out using puromycin as follows: Once the control plasmid expressed GFP, 700 ng/ml of puromycin was added to the iPSCs, carrying the pSpCas9(BB)-2A-Puro. As soon as the GFP expression in the parallel control experiment was over, puromycin was removed from CRISPR/Cas9 experiment. After three weeks, surviving colonies were manually picked and individually transferred into Matrigel[™] pre-coated wells.

After clonal expansion and single cell expansion of the selected colonies (4-5 months), different procedures were carried out to validate the genetic modification in the obtained colonies and the chosen colonies were further characterized.

3.3. Validation of genetic modifications

3.3.1. Trilineage differentiation

Since *CDH13* is not expressed in iPSCs, the StemMACS[™] Trilineage Differentiation Kit was used to direct differentiate the iPSCs into ecto-, meso- and endoderm and determine in which lineage *CDH13* could be detected. The mesodermal lineage exhibited expression of *CDH13*. For this reason, the picked colonies were differentiated into the mesodermal lineage and the cells collected for protein analysis via Western blotting. The iPSC clones which expressed *CDH13* at the protein level were immediately taken out for further validation.

3.3.2. PCR cloning for verification of biallelic modifications

Transformation was carried out in the same way as Section 3.2.4 with the differences being the type of cells used for transformation and the primers used for sequencing. The primers used for sequencing can be found in Section 3.2.1. For each investigated iPSC line, 30 colonies were picked to isolate the plasmid and sequence to identify alterations on the alleles. SnapGeneViewer (version: 4.2.6) was used to detect genomic alterations. Using the PCR

cloning kit selected clones were investigated for allelic modifications. First the gDNA for every clone was isolated using the PureLink™ Genomic DNA kit. Then the insert-DNA (i.e., *CDH13*) was amplified. 3µl of the PCR product were taken to be analysed on a 2% agarose by gel electrophoresis. Once the expected band size was observed, the remaining PCR product was ligated with the vector provided by the kit. The ligation reaction was incubated at RT for 15 min. After that it was immediately placed on ice for 2 min. The ligation reaction was then immediately transformed into the NEB 10-beta Competent *E. coli* cells.

3.3.3. Identification of potential CRISPR/Cas9 off target effects

Off-target effects were checked for the *CDH13* knockout and heterozygotic iPSC line. For each sgRNA, the benchling program automatically calculates the sequence where an off-target binding may occur. The top three off-target sequence hits for every sgRNA were chose to be analyzed and shown below:

Table 4. Accession number and off-target sequences.

Accession number for sgRNA #1 (<i>CDH13</i> ^{+/-})	Off-target sequences for sgRNA #1 (<i>CDH13</i> ^{+/-})	Accession number for sgRNA #2 (<i>CDH13</i> ^{-/-})	Off-target sequences for sgRNA #2 (<i>CDH13</i> ^{-/-})
NM_001146274	AGAAACTCCGGTCCTTCTGGA	NM_207116	AGCAGAAGACACAGA ACGAG
NM_004853.3	AGAACTCCACTCTGTCTGTG	NM_001369490	AGGTCAACACACAGA ACGAG
NM_001040000.3	AGAGCTCCGCTCCTTCTGCC	NM_003800.5	CTCGTTCTGTTTCATTC TTTT

The DNA of the iPSC lines was isolated and amplified by PCR. PCR products were purified with the NucleoSpin Gel and PCR Clean-up Kit and sequenced with the following primers:

Table 5. Primers used to check the off-target sequences.

Target	Accession number	Forward/reverse primer (5'-3')
sgRNA#1 <i>CDH13</i> ^{+/-}	NM_001146274	TTCTGCTGTGAGTGGTTTTGA ACTTCCAACCCAAACTGACCC
	NM_004853.3	GCCGGAGTAGAGTTACAGCC CCTGGGCATCCTGAGACTTG
	NM_001040000.3	GGGGAAGTGTGAGCCATAGA

		CTAATTGCCCCCTGTCACCC
sgRNA#2 <i>CDH13</i> ^{-/-}	NM_207116	TCTGCTGACTCACCTCCTCA GCTGTTTTGATGGGAACGGG
	NM_001369490	GAGGTCAGAGAATGTGCACCA GTCAGGATTCAGGGCCAGTG
	NM_003800.5	GGTGGTGTATTGGTTTAAG CTTATAGTCCCTAGGCTAAG

3.4. iPSCs characterization

3.4.1. Germ layer differentiation

IPSCs were seeded on ultra-low attachment plates in differentiation medium (DMEM, 10% FBS, 1% NEA, 100 μ M β -mercaptoethanol) with 10 μ M Y27632. After seven days in suspension, embryonic bodies (EBs) were plated on 0.1% gelatine-coated plates for undirected differentiation and specific germ layer markers were tested by immunofluorescence three weeks later for the following markers: α -SMA (alpha-smooth muscle actin) (mesoderm), AFP (alpha-1- fetoprotein) (endoderm) and β -Tubulin (ectoderm).

3.4.2. Pluripotency expression markers

All iPSC lines were investigated for the expression of pluripotency markers via immunofluorescence (OCT 3/4, SSEA-4, TRA-1–60) and quantitatively determined by quantitative reverse transcription polymerase chain reaction (qRT-PCR) with the following primers:

Table 6. Primers used to quantitatively determine pluripotency markers.

Target	Forward/reverse primer (5'–3')
<i>REX1</i>	AGGTGGCATTGGAAATAGCAGA AGTGGGGTGGGTTTGCCTA
<i>OCT3/4</i>	CCCACACTGCAGCAGATCA TGTGCATAGTCGCTGCTTGA
<i>NanoG</i>	CTGAGATGCCTCACACGGAG TGTTTGCCTTTGGGACTGGT

3.4.3. Sendai transgene analysis

To prove the absence of the that the CytoTune™ 2.0 reprogramming vectors and transgenes in the reprogrammed cells, RT-PCR was performed. For this purpose, RNA was isolated, and reverse transcribed. The following primers were used for each investigated transgene:

Table 7. Primers used to confirm absence of CytoTune™ 2.0 reprogramming transgenes.

Target	Forward/reverse primer (5'–3')
SeV (Sendai Virus)	GGATCACTAGGTGATATCGAGC ACCAGACAAGAGTTTAAGAGATATGTATC
KOS (hKlf4, hOct3/4, hSox2)	ATGCACCGCTACGACGTGAGCGC ACCTTGACAATCCTGATGTGG
Klf4 (Kruppel-like factor 4)	TTCCTGCATGCCAGAGGAGCCC AATGTATCGAAGGTGCTCAA
c-Myc (Myc gene)	TAACTGACTAGCAGGCTTGTCTG TCCACATACAGTCCTGGATGATGAT

3.4.4. Karyotype analysis

Karyotypes were verified by G-bands by trypsin using Giemsa (GTG)-banding analysis and carried out by Creative Biarray using 20 metaphases for *CDH13*^{+/+}. For *CDH13*^{+/-} and *CDH13*^{-/-}, the analysis was carried out by the Institute of Human Genetics, University of Würzburg, using 10 metaphases. Samples were examined with a resolution of 450–500 bands using an Axioskop microscope.

3.4.5. Mycoplasma contamination detection

The absence of mycoplasma contamination was confirmed using LookOut® Mycoplasma PCR Detection Kit.

3.4.6. Short Tandem Repeat analysis

Short Tandem Repeat (STR) analysis was conducted by Eurofins genomics. DNA was isolated from cell pellet. Genetic characteristics were determined by PCR single-locus technology. Sixteen independent PCR-systems D8S1179, D21S11, D7S820, CSF1PO, D3S1358, TH01, D13S317, D16S539, D2S1338, AMEL, D5S818, FGA, D19S433, vWA, TPOX and D18S51 were investigated. ASN-0002 core markers are colored grey, Thermo Fisher, AmpFISTR® Identifiler® Plus PCR Amplification Kit. In parallel, positive, and negative controls were carried

out yielding correct results. The analysis showed that parental fibroblasts and newly created iPSCs shared alleles with a 100% match.

3.4.7. *CDH13* SNP rs2199430 genotype sequencing

Identifying the *CDH13* SNP variants for rs2199430 in the iPSC lines used in this study was carried out as follows: First, the gDNA for every iPSC line was isolated using the PureLink™ Genomic DNA kit. Then our insert-DNA (in our case *CDH13*) was amplified and then sent to sequence. The reverse primer was used to detect the SNP variant of the iPSC lines. The following primers were used for *CDH13*-SNP rs2199430 verification:

Table 8. Primers for SNP rs2199430 verification.

Target	Forward/Reverse primer (5'–3')
<i>CDH13</i>	AGACATCAGAGGCATTTCCAGG TCTCCACGTCTTTGTGGTGC

3.5. Direct neuronal differentiation

3.5.1. Lentivirus generation and harvesting

A lentivirus was produced by transfecting HEK 293 cells with the plasmids expressing the desired gene, vesicular stomatitis G protein (VSV-G) envelope expressing plasmid and a packaging plasmid. For this purpose, the HEK 293 cells should be not more than 50% confluent, as they need space to grow for the virus production. The Jetprime transfection Kit was used which included all the necessary materials. First, three 2 ml Eppendorf tubes (Eppi) were filled with 1 ml Jetprime buffer, 7.5 µg pPax plasmid (addgene #12260) and 2.5 µg pMD2.G plasmid (addgene #12259). After that, the tubes were shortly shaken and 10 µg of the required plasmid (reverse tetracycline-controlled transactivator (rtTA) or Neurogenin 2 (Ngn2) or Achaete-scute homolog 1 (Ascl1)) (and 40 µl Polyplus reagent were added (one plasmid per Eppi) and the Eppis were shaken. After 3 min of centrifugation, the Eppi was incubated at RT for 10 min. During the incubation time, the media of the HEK-293 cells was removed and exactly 10 ml were added to the cells, as the concentrations of the plasmids are dependent on the amount of media affecting the dilutions. After 10 min, the whole solution of the buffer with the plasmid was added dropwise to the cells in the plate. The solution was mixed in a cross way and placed in the incubator (37°C, 5% CO₂) for 6 h. From here on, these cells were virus-producing cells. After the incubation time, the cells were washed with PBS and new media was added. Virus particles were harvested two days after the HEK 293 cells had been transfected. The supernatant from each plate was collected separately and centrifuged for 2 min at 40 rpm. The supernatant of each plasmid was filtered through a syringe with a 0.45 µm filter. This resulted in solutions that contained virus particles. The virus particles were either stored at -80°C or used directly for transduction of the iPSCs.

The work with lentivirus vectors was approved by the Government of Lower Franconia (approval number: 8791.25-41-4).

3.5.2. Generation of rtTA/Ngn2- and rtTA/Ascl1-positive iPSCs

The transduction of iPSCs (Frega et al., 2017; Mossink et al., 2022) was carried out as follows: the supernatant of the HEK-293 cells, which contains one of the lentivirus particles rTA, Ngn2, or Ascl1, was used for the transduction of the hiPSCs. iPSCs were then transduced with either the virus particle combination rtTA/Ngn2 or rtTA/Ascl1. The lentivirus integrates into the genome, but no self-replication is possible because the 5' and 3' long terminal repeats (LTRs) are cut off. After 6 h, the media (StemMAC + 10 µM rock inhibitor) was changed. On the third day, the iPSCs were selected with puromycin (7 µg/ml) and G418 (35 µg/ml). The selection lasted for 5 days. After that, a quantitative lentiviral titer test was performed with the Lenti-X GoStix Plus kit to check for the absence of the lentivirus particles in the cultures.

The Ngn2- and Ascl1-lentivirus vectors were transduced into iPSCs in combination of rtTa as they are both under a Tet-controlled promoter. Mechanistically, the rtTA vectors' transcription is turned on by doxycycline, a derivative of tetracycline. The resulting rtTA protein binds to the Tet-promoter on the Ngn2 and Ascl1 vector initiating glutamatergic or GABAergic neuron differentiation, respectively. In addition to doxycycline, forskolin is required for successful GABAergic differentiation (Shi et al., 2016).

3.5.3. Confirmation of rtTA, Ngn2 and Ascl1 vector integration in iPSCs

The cells of each transduced clone were first activated and then collected and centrifuged to obtain a pellet. This pellet was washed with PBS and transferred to an Eppi. The gDNA was isolated from the pellet using the PureLink Genomic DNA kit using the following primers:

Table 9. Primers used to confirm the presence of rtTA, Ngn2 and ASCL1.

Target	Forward/reverse primer (5'–3')
rtTA	CTGGGAGTTGAGCAGCCTAC AGAGCACAGCGGAATGACTT
Ascl1	GTCCTGTGCCCCACCATCTC CAGCAGCTCTTGTTCCCTCTG
Ngn2	AGACGGTGCAGCGCATCAAGAA AGCGTCTCGATCTTCGTGAGCT

The 3 µl of the PCR product was analyzed using a 2% agarose gel. If the sample showed a positive band (~200 bp) for its respective integrated vector, the rest of the PCR product was cleaned up using the PCR clean-up kit. Once the PCR product was cleaned up, the samples were sent to sequence to LGC Genomics.

3.5.4. Glutamatergic neuron differentiation

rtTA/Ngn2-positive iPSCs were induced by adding 4 µg/ml doxycycline. For a 24-well-format, 40,000 cells were seeded on polyornithine/laminin coated plates in StemMACS medium + Rock Inhibitor + 4 µg/ml doxycycline on day 1. On day 2, the media was changed to DMEM/F12 with 1:100 N2, 1:100 MEM non-essential amino acid solution (100x) (NEAA; 0.1µg/ml primocin, 10 ng/ml Neurotrophin type 3 (NT3), 10 ng/ml BDNF; 4 µg/ml doxycycline. This was warmed in a water bath and then 0.2 µg/ml of laminin was added. On day 3, astrocytes must be added to the culture in a 1:1 ration as the number of seeded cells. Astrocyte isolation was done following (Frega et al., 2017). On day 4, the media was changed to neurobasal medium with 1% B27, 1% Glutamax, 0.1 µg primocin, 10 ng/ml NT3, 10 ng/ml BDNF and 4 µg/ml doxycycline and 1:1000 1x gentamycin. This medium was changed every second day. From day 10 onwards, doxycycline was removed from the media.

3.5.5. GABAergic neuron differentiation

rtTA/Ascl1-positive iPSCs were induced by adding 4 µg/ml doxycycline and 10 µM forskolin. On day 1, iPSCs were seeded on polyornithin/laminin coated plates in StemMACS medium, 10 µM RI, 4 µg/ml doxycycline and 10 µM forskolin. On day 2, the media was changed to DMEM/F12 with 1:100 N2, 1:100 NEAA, 0.1 µg/ml primocin, 10 ng/ml NT3, 10 ng/ml BDNF; 4 µg/ml doxycycline, 10 µM forskolin. This was warmed in a water bath and then 0.2 µg/ml of laminin was added. On day 3, astrocytes were added to the culture in a 1:1 ration as the number of seeded cells. On day 4, the media was changed to Neurobasal medium with 1% B27, 1% Glutamax, 0.1 µg primocin, 10 ng/ml NT3, 10 ng/ml BDNF and 4 µg/ml Doxycycline, 10µM Forskolin and 1:1000 1x gentamycin. This medium was changed every second day. From day 10 onwards, doxycycline and forskolin were removed from the media.

3.5.6. Glutamatergic/GABAergic co-culturing differentiation

The co-culturing experiments were done in a 65:35 ratio, with glutamatergic and GABAergic neurons respectively. For a 24-well plate format, 114,000 cells per well were seeded. For a well on the MEA chip, 750,000 cells were seeded in each well. For both experiment set-ups, the following protocol was used: On day 1, the rtTA/Ascl1 cells were seeded in the wells using the medium used for the GABAergic differentiation (Section 3.5.5). After 5 h, the rtTA/Ngn2 cells were seeded on top of the rtTA/Ascl1 cells using the same media. From here on the procedure was the same as for the differentiation of GABAergic neurons. The differentiation was kept for 49 DIV, since this was the time point at which the inhibitory system was found to be fully functional and mature (Mossink et al., 2022)

3.5.7. Astrocyte isolation for neuron differentiation support

Neurons require support from astrocytes to mature and develop functional synapses. It is known that astrocytes play a major role in neural circuit development by controlling synapse formation, maintenance, and elimination, all of which are enable neuronal functioning. When

co-culturing the glutamatergic and GABAergic neurons, freshly prepared mouse astrocytes were co-cultured in a 1:1 ratio, as it has been shown that they are involved in a variety of processes crucial to development of neural circuits, including synapse formation and maintenance (Farhy-Tselnicker & Allen, 2018)

3.5.7.1. Dissection of the brain from newborn mice

To prepare fresh astrocytes, mice pups (P0-P3) from a mouse line on a C57BL/6N background, were decapitated using micro-preparation scissors. The head was then held back with anatomical forceps at the nose and the skin of the head cut with Vannas cataract scissors starting from the neck in rostral direction to free the skull. The skin was lifted aside with Dumont forceps N°7. The skull was then opened from foramen magnum in rostral direction with the Vannas cataract scissors. The brain was removed from the skull by using a small spoon and placed immediately in a petri dish filled with cold DMEM (without serum) on ice. This was repeated for every pup (Beaudoin et al., 2012) (Supplementary figure 12).

3.5.7.2. Removing the meninges

The brain was then gently held with Dumont forceps N°5 at the level of the cerebellum. With the aid of a scalpel N°10, a gentle cut was performed from caudal to rostral along the interhemispheric fissure to open the meninges. Using the scalpel, the hemispheres were separated from the midbrain at the levels of the basal ganglia. The meninges were then carefully removed from each hemisphere with Dumont Forceps N° 5. The removal of the meninges prevents fibroblast contamination of the astrocyte culture (<https://www.youtube.com/watch?v=eHDapIC6QvY>). This video was made by the Fritschy Lab at the University of Zurich) (Supplementary figure 13).

3.5.7.3. Astrocytes isolation

2-3 brains from P0 to P3 mice were then homogenized with a 1 ml pipette until the solution was turbid. This solution was transferred through a 70 µm cell strainer placed on top of a 50 ml centrifuge tube, which was then centrifuged at 4600 rpm and 4°C for 15 minutes (Hettich Zentrifuge). The supernatant was discarded, the pellet resuspended in cold DMEM (without serum) and centrifuged like before. This washing step was repeated 2 times. The third washing step was carried out with DMEM/10% Fetal Calf Serum (FCS) media. After the final washing step, 10 ml of warm DMEM/10% FCS was added to the falcon tube, the pellet resuspended and plated in a T75 culturing flask. The flasks were placed in the incubator at 37°C, 5% CO₂. After two days, the media was changed with DMEM/10% FCS and then every 3 days for 10 days. After 10 days, the culture should reach 90% confluency. The astrocytes appear as a densely packed tessellated monolayer with microglia and oligodendrocytes lying on top and intermixed. To remove the contaminating glial cells, the flask is shaken on a shaker for 5 hours

at 350 rpm at RT. The media removed and replaced, and then shaken overnight in the incubator at 350 rpm. The following day a complete media change was done and from then on, every third day. Two criteria were used to check if the astrocytes were of good quality: first, the culture should be able to grow confluent within 10 days after isolation. Second, the culture should be able to form a confluent tessellated monolayer (Frega et al., 2017) (Supplementary figure 14).

3.6. Molecular biology methods: RNA analysis

RNA isolation was carried out using the RNeasy Plus mini kit was used (#74134). The spectrophotometer NanoDrop ND1000 was used to quantify and to control the quality of the isolated RNA. The isolated RNA concentration was estimated by measuring the optical density (OD) at 260 nm, considering a concentration of 40 ng/μl at an OD260 of 1. Furthermore, contamination with proteins and the presence of other impurities was detected by the OD260/OD280 and OD260/OD230 ratios. A ratio of approximately 2.0 was considered as highly pure for RNA.

3.6.1. Complementary desoxyribonucleic acid (cDNA) synthesis

The complementary DNA (cDNA) synthesis was conducted using the iScript™ cDNA synthesis kit. 1000 ng of isolated total RNA were used for the cDNA synthesis. Approximately after 45 min, the run was finished, and the obtained cDNA was diluted 1:5 in 1x Tris-EDTA (TE) buffer and aliquoted for storage at -20°C.

3.6.2. Quantitative real-time polymerase chain reaction

qRT-PCR was conducted to analyse and compare the expression level of different genes of interest. The iQ™ SYBR® Green Supermix (BioRad) was used that contains the fluorescence stain SYBR, iTaq™ DNA polymerase, reaction buffer with desoxyribonucleotide triphosphates (dNTPs), magnesium chloride and stabilizers. SYBR green, an asymmetrical cyanine dye used as a nucleic acid stain, bound to the new synthesized DNA strands and in every cycle, the fluorescence increased proportional to the amount of new synthesized DNA. The number of cycles needed to reach the fluorescence threshold was presented by the quantification cycle (Cq) value.

For all conducted qRT-PCRs, samples were tested in triplicates using 384-well plates. All PCRs were run in the thermocycler CFX384 controlled by the software CFX manager 3.0.

For each qRT-PCR experiment, Glyceraldehyde 3-phosphate dehydrogenase (GAPDH), Actin beta (ACTB), Ubiquitin C (UBC), 5'-Aminolevulinic Synthase 1 (ALAS), TATA-Box Binding Protein (TBP), Hypoxanthine Phosphoribosyltransferase 1 (HPRT1), Glucuronidase Beta (GUSB), Transferrin Receptor (TFRC) were used as reference genes for normalization of the data and qRT-PCR data analysis was done using the programs CFX- Manager 3.0, Microsoft Excel 2016, LinReg and qBase+. Cq values from CFX manager 3.0 imported into Microsoft Excel 2016 were formatted for further analyses via LinReg and QBase. The software LinReg

allows the calculation of the amplification efficiency per well from a slope of the amplification curve in the exponential phase. A PCR efficiency of 100% illustrates a duplication of the amount of amplicon in each cycle ($E=2$), whereas a value of 1 means no amplification. Finally, an average amplification efficiency for each amplicon was calculated. Subsequently, the software qBase+ was used to process the data output and to calculate normalized gene expression values, considering the efficiency values provided by LinReg software as well as using the most stably expressed reference genes to normalize the data.

3.7. Molecular biology methods: Protein analysis

Protein analysis was carried out by adding lysis buffer (RIPA-buffer 1x (Sigma), Complete Protease Inhibitor Cocktail 7x (Roche), PhosStop 10x (Roche) to the cell pellet and resuspended. The sample was then sonicated to disrupt cell membranes and to release cellular contents and centrifuged for 2 min at 10000 rpm and 4°C. The supernatant containing the protein was then transferred to a fresh tube and stored at -80°C for later protein quantification using the Precision Red reagent.

3.7.1. Western blot procedure

In this study, the knockout of *CDH13* in iPSCs was confirmed by Western blot (Liu et al., 2014). *CDH13* (1:200) was used as the target protein and β -tubulin (1:1000) as the reference protein. The dilution of the secondary antibodies for the target protein was 1:5000 (donkey anti-goat) and 1:10000 for the reference protein (donkey anti-mouse). Detection of fluorescence was recorded using Fusion FX imaging system at 680 nm and 800nm.

3.8. Immunocytochemistry

3.8.1. Immunocytochemistry procedure

Immunocytochemistry was carried out as follows: 4% of paraformaldehyde (PFA) was added to the cells which were still in their culturing media for a pre-fixation step for 10 min at RT. After that, the whole solution was removed, and 4% of PFA was added to the cells and incubated for 15 min (the amount of PFA used is dependent on the wells' size). Following this step, the cells werewashed two times for 5 min with DPBS 1x before adding the blocking solution for 45 min at RT. Depending on whether the proteins of interest were located intracellularly/extracellularly, the blocking solution contains/lacks the permeabilization reagent Triton X-100 respectively. Permeabilization and blocking were done using 0.1% Triton X-100, 10% FBS, and 1% BSA in DPBS. In case permeabilization was not required, Triton X-100 was simply not added. Primary antibodies were added to the samples diluted in the blocking solution and incubated over night at 4°C. The following day, the cells were washed three times with DPBS 1X each time for 5 min. After that the secondary antibodies were added to the samples diluted in the blocking solution for one hour in the dark at RT. To visualize the cell nuclei, a counterstaining with 4', 6-diamidino-2-phenylindole (DAPI) was also added to the secondary antibody solution.

3.8.2. Epifluorescence

Images were obtained using an Olympus inverted system microscope IX81. Pictures were taken at 10x, 20x, and/or 40x magnifications through the exposure channels for Alexa Fluor 488, Alexa Fluor 555, Alexa Fluor 647 and DAPI. Images were then processed using software CellSense (Olympus) and ImageJ.

3.9. Microelectrode array (MEA) recording and data analysis

For this study, glutamatergic and GABAergic neurons were co-cultured in a 65:35 ratio on MEA chips to measure their spontaneous activity as this ratio exhibited the strongest GABAergic modulation when compared to cultures with different E/I ratios. MEA chips were used to measure neuronal network activity in a non-invasive manner. MEA measurement reveals three neural activity patterns: random spiking, local bursting, and network-wide bursts (Mossink et al., 2022)

All recordings were performed using the MEA2100-System (Multichannel Systems) and the 60-6wellMEA200/30iR-Ti-rcr chip. Spontaneous electrophysiological activity of E/I networks was recorded for 10 min at 37°C and constant flow of humidified gas (5% CO₂ and 95% O₂) using the Multi Channel Experimenter software. The activity of neuronal networks growing on MEAs was recorded for 10 min (after a 10 min acclimatization period).

The raw signal was sampled at 10 kHz. Analysis was performed off-line by extracting the spike using the Multi Channel DataManager software and in-house algorithms in Python 3.9 written by Antonio Vitale (Appendix-CD) that allows the extraction of MEA parameters and parameters describing the burst shape. The parameter extracted in the thesis include network burst duration (NBD; ms) and network burst rate (NBR, bursts/min). We detected bursts per electrode based on the maximum interspike interval (ISI) of 30 ms to start or end a burst. If the ISI was shorter than 30 ms, spikes were included in the burst, if the ISI was larger than 30 ms the burst ends. All bursts that were <65 ms apart were merged. All bursts that had a duration of <50 ms or had <4 spikes were removed from the analysis. When a burst occurs simultaneously in more than 80% of the active channels, it was considered as a network burst. A schematic representation of how spontaneous electric activity patterns measured on MEAs look like can be seen in the Supplementary figure 15.

3.9.1 Statistical analysis

The statistical analysis for all experiments was performed using Python 3.9. The data were tested for normal distribution by using Kolmogorov Smirnov test and because the data were not normally distributed, non-parametric tests were carried out. Statistical analysis

was performed with Kruskal–Wallis ANOVA with post-hoc Dunn’s correction for multiple testing (Fig. 34D, Supplementary figure 11C). When comparing means of two variables at one individual time-point, we used Mann-Whitney U-test and corrected for multiple testing using Bonferroni correction (Figure 32C, Supplementary figure 11A, Figure 33C, Supplementary figure 11B). Statistics on histograms were performed using Multiple t-test on bins using the Holm–Sidak method (Figure 32D, Figure 33D, Fig. 34D). All data represent means \pm SEM, * $p > 0.01$; ** $p > 0.001$; *** $p < 0.001$ and reported in Supplementary table 1.

4. Results

4.1 Generation of a *CDH13* knockout and heterozygotic iPSC line

4.1.1. Sequencing *CDH13*’s open reading frame

The first step in generating a set of isogenic cell lines was to sequence the target region so that site-specific sgRNAs could be designed. In this case, the start of *CDH13*’s open reading frame (exon 1) was targeted to ensure a nucleotide frameshift affecting *CDH13*’s translation



Figure 7. Start of the open reading frame (NM_001257.5)

SgRNAs were then ligated into the pSpCas9(BB)-2A-Puro (PX459) V2.0 plasmid5 (Addgene: #62988). Following ampicillin selection, the colonies were picked, the plasmids isolated, and sequenced to determine whether sgRNAs had been incorporated into the plasmids.

4.1.2. Nucleofection of plasmids and colony selection

Once the integration was confirmed, the plasmids were nucleofected in the *CDH13*^{+/+} iPSCs. Nucleofection of 800,000 viable iPSCs with 5 μ g plasmid was performed by using the Amaxa™ P4 primary Cell 4D-Nucleofector™ X Kit L and the Nucleofector™ X-Unit program ‘CA137’. For colony selection, puromycin was applied one day after nucleofection with a

concentration of 0.7 $\mu\text{g/ml}$ for 48 h. After that, the medium was changed every three days. 5 days post-nucleofection the first colonies were observed and monitored up to 10 days (Fig. 8).

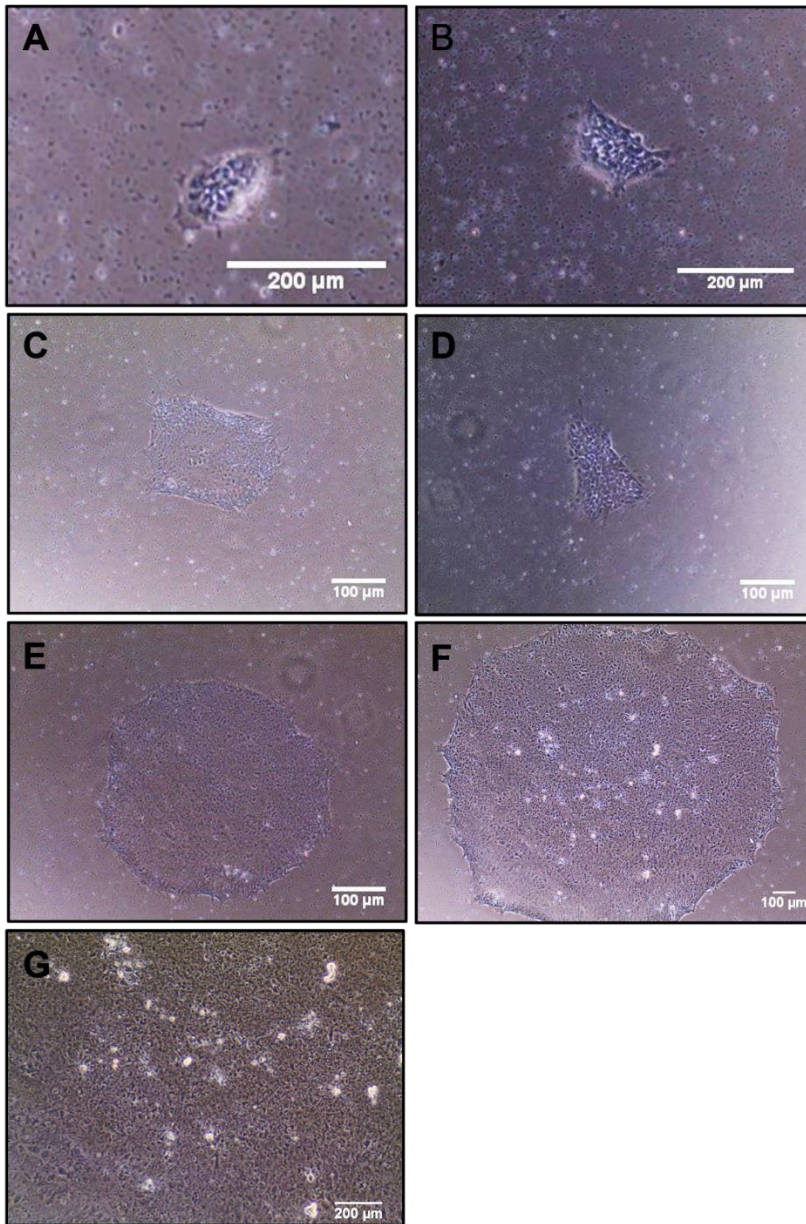


Figure 8. Colonies start to grow 5 days post nucleofection and monitored up to 10 days
A 5 days post nucleofection. B 6 days post nucleofection. C 7 days post nucleofection. D 8 days post nucleofection. E 9 days post nucleofection. F and G 10 days post nucleofection. C, D, E, F. Scale bar: 100 μm . A, B, G. Scale bar: 200 μm .

4.1.3. Sequencing of CRISPRed clones

After three weeks, 15 clones were manually picked and individually transferred into Matrigel™ pre-coated wells. These clones were upscaled from a petri dish to a 6-well plate format. Expansion of the individual clones was then done to guarantee backup samples. After clonal

expansion, the DNA was isolated for DNA sequencing to determine if a frameshift mutation was introduced in our CRISPRed clones. As indicated in Figure 9 the chromatograms representing the sequencing results were found to be noisy for every clone we had collected. Ideally, a chromatogram should have evenly spaced peaks, each with a single color not like in this case, where multiple peaks can be seen at a specific base pair position.

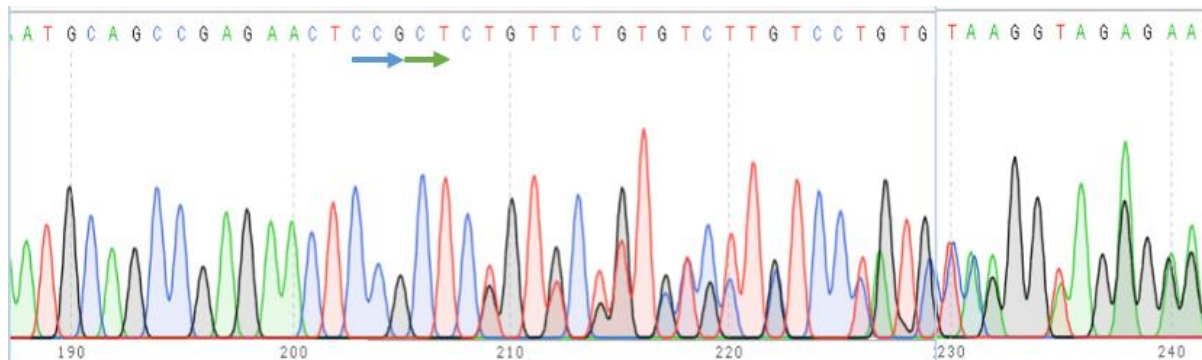


Figure 9. Exemplary noisy chromatogram of a CRISPRed colony
CCG (blue arrow) is our PAM sequence. 3-4 bp upstream, Cas9 introduced DSB.

4.1.4. Single cell expansion of CRISPRed clones

For this reason, it was assumed that our clones were not made up of a homogenous cell population. Therefore, we decided to single cell expand three of the 15 clones to obtain homogenous cell lines. This was done by seeding 4-5 cells per well in 96-well plates. Five days after seeding, colony growth had started, and the colonies were ready for upscaling after 14 days (Figure 10).

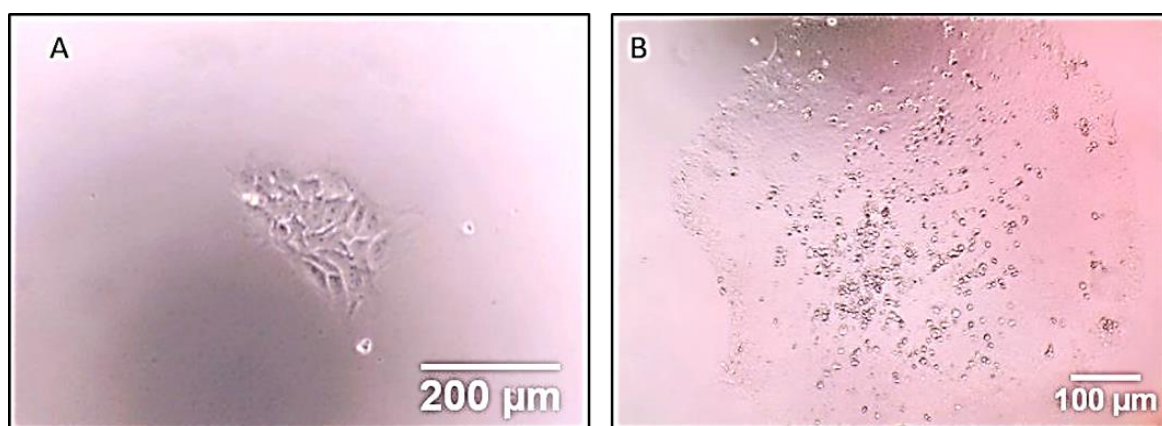


Figure 10. Growth of colonies in a 96-well format for 14 days
A. Growth of colony after 5 days of seeding. Close-up picture, scale bar: 200 µm. **B.** At day 14, colony ready to be picked and upscaled. Scale bar: 100 µm.

The DNA of the three single cell expanded colonies was isolated and sent to sequence. Similarly, the colonies presented noisy sequencing results. This indicated that a change had occurred on the genetic level, but that the specific frameshifts on the allelic level could not be determined. Which is why our next approach involved allelic separation in each of our clones.

4.1.5. Allelic separation using PCR cloning

A well-established method for allelic separation is PCR cloning performed together with Johanna Zöller and Franziska Benz using the NEB® PCR Cloning Kit. In brief, this technology consists in ligating an amplified DNA fragment into a vector, transforming the plasmid into NEB 10-beta Competent E. coli cells, selection of transformed colony by antibiotic resistance and then finally plasmid isolation and sequencing. This enables the detailed investigation of the region of interest on the separate alleles since only one allele is transformed into each bacterial cell. Therefore, to balance out the ratio between allele 1 to allele 2, 30 colonies were picked for each of the following clones: 1.1+1.3#3, 1.1+1.3#1, 1.1#4, 1.1#10, C115#3 and C123#7.

The first step of PCR cloning consisted of amplifying the sequence of interest (*CDH13*) resulting in a band size of 516 bp shown in Figure 11.

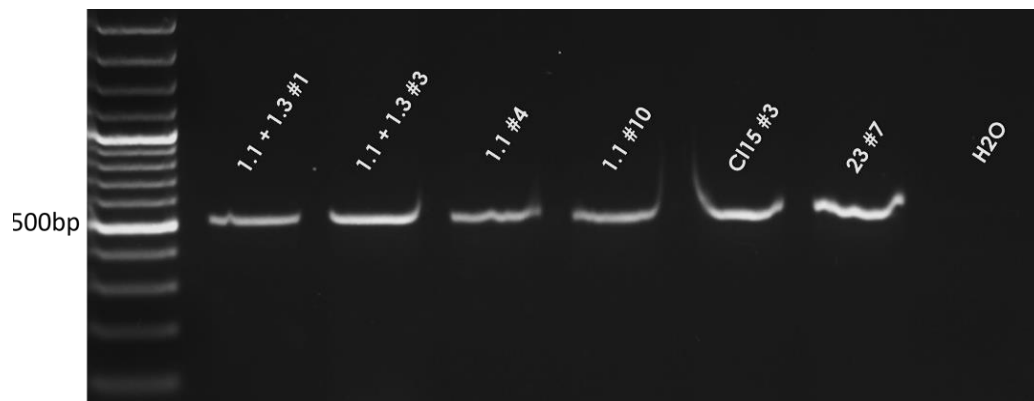


Figure 11. Amplification of CRISPRed clones
1.1+1.3#3, 1.1+1.3#1, 1.1#4, 1.1#10, C115#3 and C123#7.

The PCR products were ligated in the linearized pMiniT 2.0 Vector provided in the kit. The plasmids were then transformed into NEB 10-beta Competent E. coli cells. Selection of the colonies occurred using ampicillin selection. To validate the integration of our sequence of interest into the vector, colony PCR was performed. 5 random colonies were picked for each clone. The primers used from the kit anneal 155 bp upstream and 154 bp downstream from cloning insertion site, ensuring coverage of the insert. The success of the colony PCR was confirmed by the amplicon's correct band size (825 bp) on the agarose gel. The amplicon size is made up of the *CDH13* insert (516 bp) and the upstream/downstream base pairs (309 bp) (Figure 12).

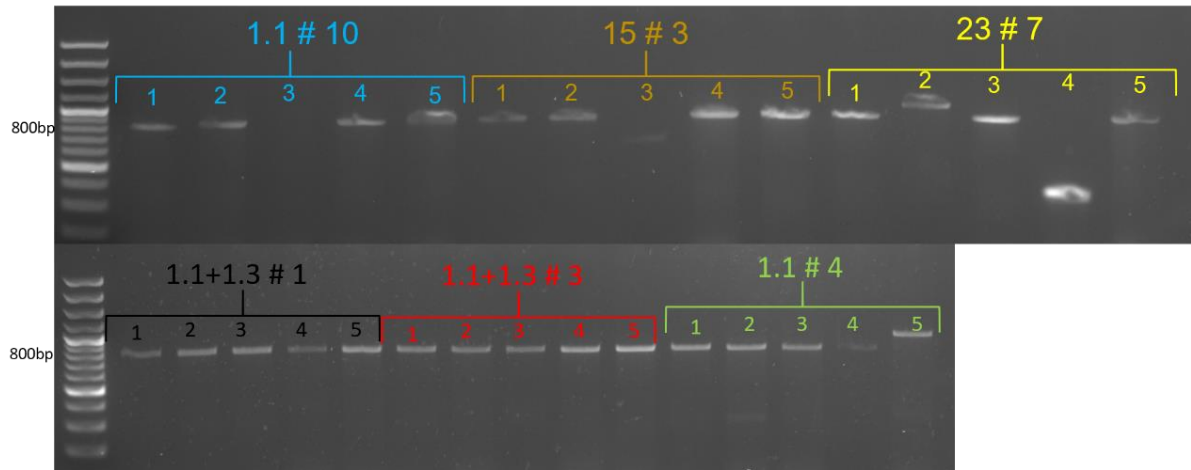


Figure 12. Colony PCR confirming the integration of the *CDH13* insert in the pMiniT 2.0 Vector

4.1.6. Indel mutations in each CRISPRed clone

In the final step, 30 colonies for each clones were picked, the plasmids were isolated and sequenced. The different indels on the different alleles for each clone were identified and listed in Table 10 :

Table 10. Summary of indels on each allele for each CRISPRed clone.

Clones	Allele 1	Allele 2
1.1 + 1.3 #1	2 nucleotide deletion	/
1.1+1.3 #3	1 nucleotide deletion	No indel
1.1 #4	9 nucleotide deletion	1 nucleotide insertion
1.1 #10	1 nucleotide insertion	13 nucleotide deletion
15 #3	4 nucleotide deletion	1 nucleotide insertion
23 #7	1 nucleotide insertion	10 nucleotide insertion

The following clones were used for this study as the heterozygotic and the knockout *CDH13* iPSC lines: 1.1+1.3#3 and C15#3 (Fig. 13). The 1.1+1.3#3 clone was chosen as it was the only *CDH13* heterozygotic deficient cell line we obtained. The C15#3 clone was chosen among the other possible obtained clones since we observed a more stable iPSC growth in culture.

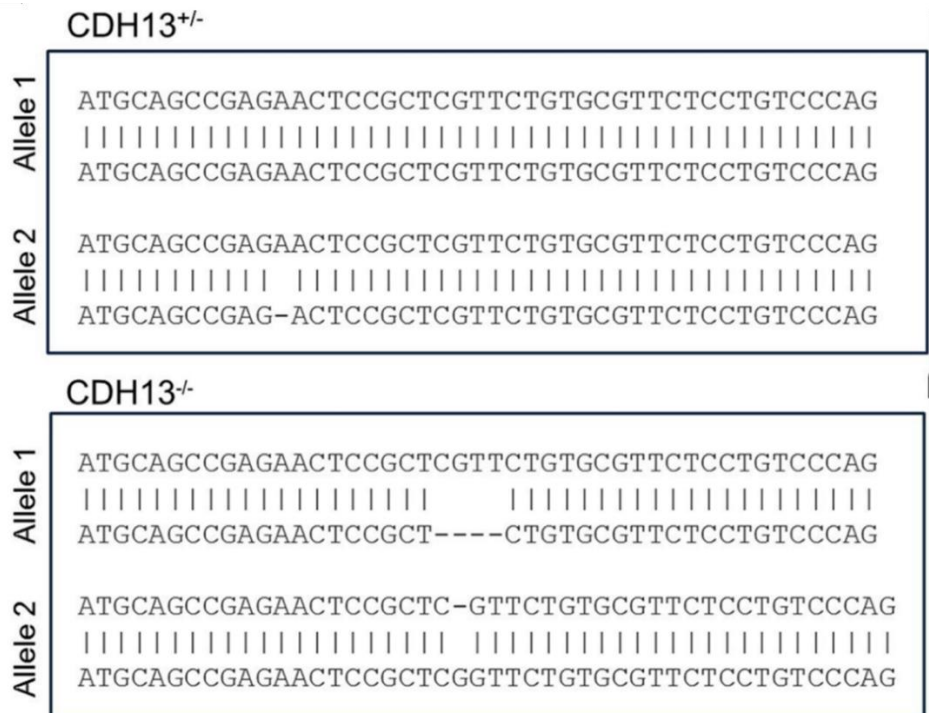


Figure 13. Sequences of *CDH13*^{+/-}: NM_001257.5: c [=]; [13delA] and *CDH13*^{-/-}: NM_001257.5: c.[22_25delGTTTC]; [22_23insG]

4.1.7. Confirmation of *CDH13*^{-/-} at the protein level

The iPSCs were differentiated into their mesodermal state to confirm the modifications of *CDH13* at the protein level (Fig. 14). From the Western blot analysis, we confirmed the clones as the heterozygotic and the knockout *CDH13* iPSC lines: 1.1+1.3#3 and Cl15#3, respectively. From this point onward, these two cell lines will be denominated as *CDH13*^{+/-} and *CDH13*^{-/-} respectively.

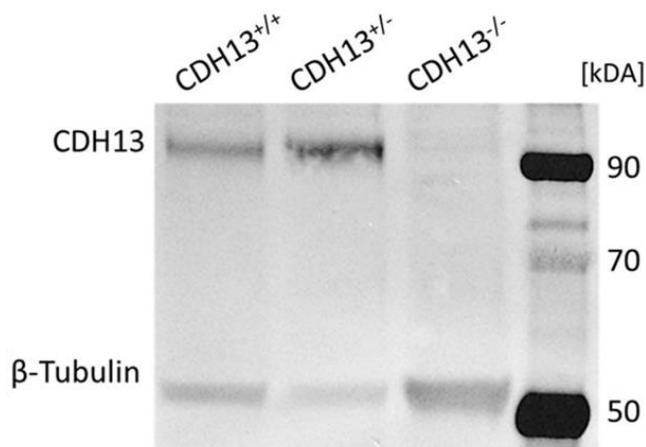


Figure 14. *CDH13* protein expression in *CDH13*^{+/+}, *CDH13*^{+/-} and *CDH13*^{-/-} iPSC lines

4.2. Characterization of generated isogenic cell lines

4.2.1. iPSCs morphology

It is necessary to perform a series of experiments to check that these cells still display all characteristics of pluripotent stem cells since genetic engineering may modify stem cell characteristics. First, the morphology of the pluripotent stem cells was examined across all three cell lines (Fig. 15).

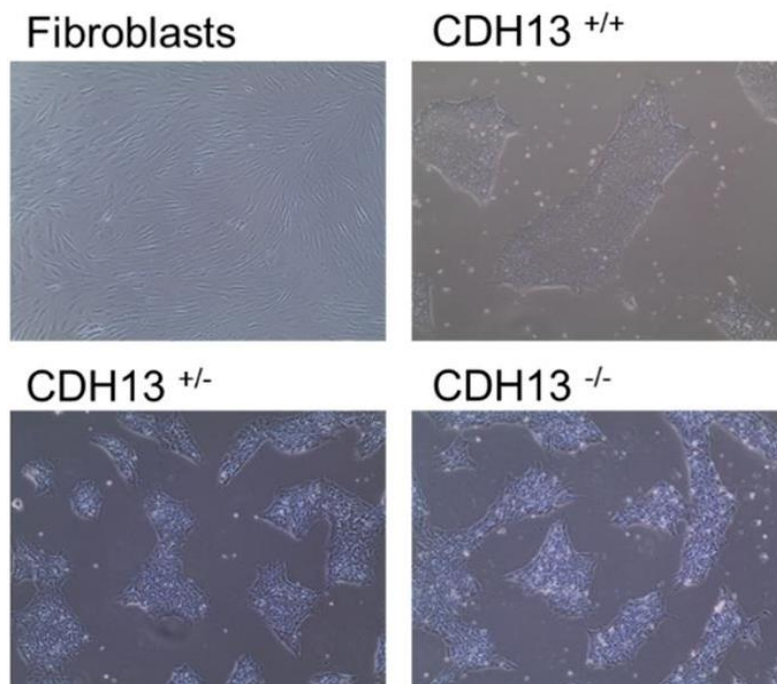


Figure 15. Pluripotent stem cell morphology confirmed in all three-iPSC line

4.2.2. Germ layer differentiation and pluripotency characterization

Following that, the ability of the pluripotent cells to differentiate into the three germ layers was confirmed. This was done by generating embryoid bodies (EBs) which were cultured in suspension in serum-containing medium for seven days. The EBs were differentiated in adherent culture conditions for another three weeks. All three iPSC lines expressed the following germ layer markers: α -SMA (mesoderm), AFP (endoderm) and β -tubulin (ectoderm) (Fig. 16B). Consequently, the expression of specific pluripotency markers was confirmed by immunofluorescence (OCT 3/4, SSEA-4, TRA-1-60) (Fig. 16A) and quantitatively determined by qRT-PCR (NANOG, OCT 3/4, REX 1).

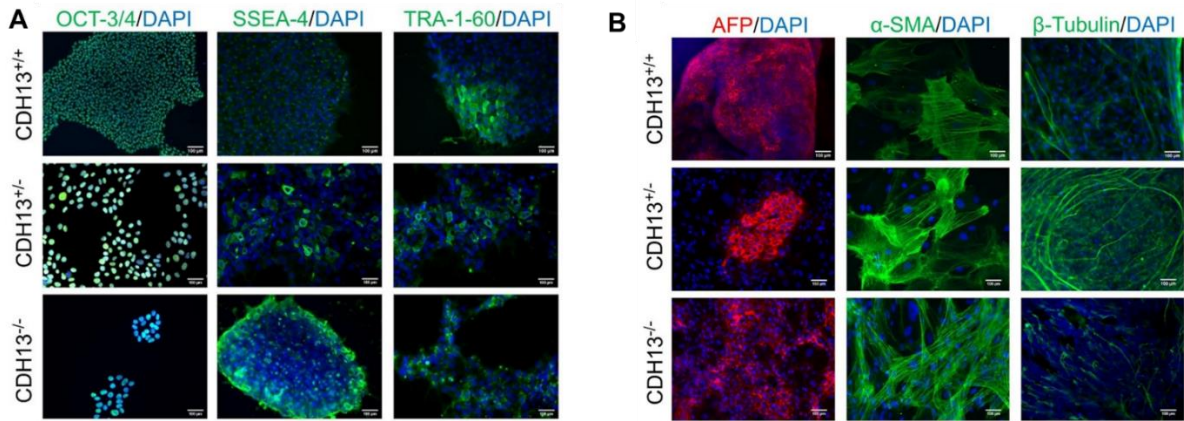


Figure 16. Pluripotency and germ layer markers

A. All three iPSC lines expressed the following pluripotency markers: OCT 3/4, SSEA-4, TRA-1-60. **B.** All three iPSC lines expressed the following germ layer markers: α-SMA (mesoderm), AFP (endoderm) and β-tubulin (ectoderm).

4.2.3. Standard G-banding

When CRISPR/Cas9 genetic editing disrupts the genome, it can cause genetic instability that can lead to chromosomal abnormalities. Standard G-banding revealed no numerical or structural chromosome abnormalities (Fig. 17).

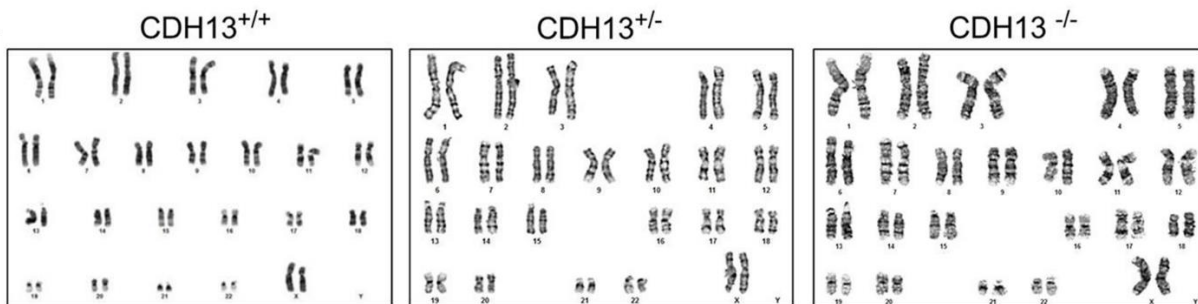


Figure 17. Standard G-banding

Standard G-banding revealed no numerical or structural chromosome abnormalities. The analysis was carried out by the Institute of Human Genetics, University of Würzburg and Creative Bioarray.

4.2.4. Absence of Sendai virus transcripts

Since the *CDH13*^{+/+} iPSC line was generated by reprogramming fibroblasts using the Sendai virus, the absence of Sendai virus-specific transcripts was confirmed by RT-PCR (Fig. 18).

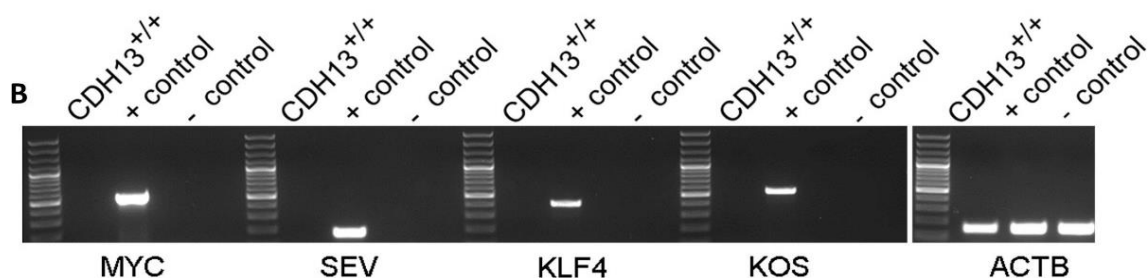


Figure 18. The absence of Sendai virus-specific transcripts was confirmed by RT-PCR

4.2.5. STR

Short tandem repeat (STR) analysis showed that parental fibroblasts and newly created iPSCs shared alleles with a 100% match (Fig. 19).

Client Sample Name	Fibro CJ2	C115_3	1.1 1.3_3
Sample Code	CL00000892	CL00001759	CL00001758
D8S1179	15,15	15,15	15,15
D21S11	29,31.2	29,31.2	29,31.2
D7S820	10,11	10,11	10,11
CSF1PO	11,13	11,13	11,13
D3S1358	15,16	15,16	15,16
TH01	9.3,9.3	9.3,9.3	9.3,9.3
D13S317	8,8	8,8	8,8
D16S539	11,12	11,12	11,12
D2S1338	18,18	18,18	18,18
D19S433	12,13	12,13	12,13
vWA	15,18	15,18	15,18
TPOX	11,12	11,12	11,12
D18S51	12,13	12,13	12,13
AMEL	X,X	X,X	X,X
D5S818	11,13	11,13	11,13
FGA	20,24	20,24	20,24

Figure 19. STR analysis

STR analysis confirmed 100% match between the fibroblasts and the iPSC lines. This analysis was carried out by Eurofins genomics.

4.2.6. Off-target effects

As with any genetic engineering tool, such as CRISPR/Cas9, there is always a potential for unintended genetic modifications outside of the target site. These are called off-target effects. The potential off-target sites are calculated by the “Benchling” software when designing the

sgRNAs. For each sgRNA, the top three potential off target sites were analysed. No off-target effects were identified in our newly generated cell lines (Fig. 20).

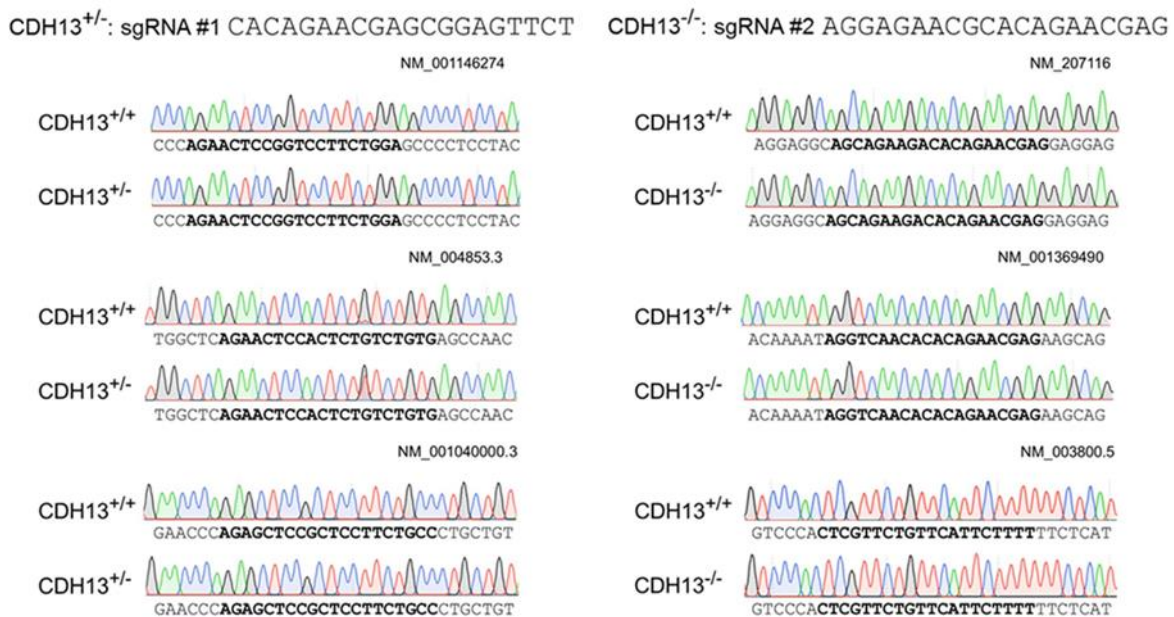


Figure 20. Possible off-target effects in each sgRNA

In conclusion, we generated *CDH13*-deficient iPSC cell lines using CRISPR/Cas9 technology passing all the characterization tests confirming their stable stem cell identity.

The next experiments investigated whether and how different *CDH13* SNP variants affect the E/I balance in neuronal networks.

4.3. Generation of rtTA/Ngn2- and rtTA/Ascl1-positive hiPSCs to model excitatory/inhibitory network activity

In the next experiments, five different iPSC lines, were used to explore how *CDH13* affects the E/I balance. The cell lines used were: *CDH13*^{A/A}, *CDH13*^{G/G} (= *CDH13*^{+/+}), *CDH13*^{A/G}, *CDH13*^{+/-} and *CDH13*^{-/-}. *CDH13*^{A/A}, *CDH13*^{G/G} and *CDH13*^{A/G} are allelic variants of SNP rs2199430.

The *CDH13*^{G/G} line was used as the control line in the generation of the isogenic lines which is why its iPSC characterization was carried out in the previous chapter (*CDH13*^{+/+} = *CDH13*^{G/G}). The characterization of the *CDH13*^{A/A} and *CDH13*^{A/G} iPSC lines are found in Supplementary figure 1 and Supplementary figure 2.

4.3.1. Verification of *CDH13* SNP rs2199430 variants in iPSC lines

The *CDH13*^{AA}, *CDH13*^{GG} (= *CDH13*^{+/+}) and *CDH13*^{AG} iPSC lines were sequenced to confirm the genotype of SNP rs2199430, located on chromosome 16 in intron 1 GRCh38.p14 at position 82803101. The chromatograms confirm the *CDH13* genotype of the SNP for each iPSC cell line (Fig. 21)

After gDNA amplification, the reverse primer was sent with the amplified gDNA of the cell lines to LGC genomics for sequencing. The obtained sequence using the reverse primer (3'-5') can be seen in Figures 21A1, A3, B1, B3, C1, C3. The reverse complement was obtained and used to confirm the genotypes of each cell line which can be seen Figures 21A2, B2, C2. In the reverse complement for *CDH13*^{AA} (Figs. 21A2, A3), the nucleotide at position 82803101 was an adenine (A). In the reverse complement for *CDH13*^{GG} (Figs. 21B2, B3), the nucleotide at position 82803101 was a guanine (G). In the reverse complement for *CDH13*^{AG} (Figs. 21C2, C3), the nucleotide at position 82803101 was an adenine (A), but when looking at the chromatogram, both thymidine and cytosine are present at position 82803101 indicating the presence of both adenine and guanine nucleotides respectively in the cell line.

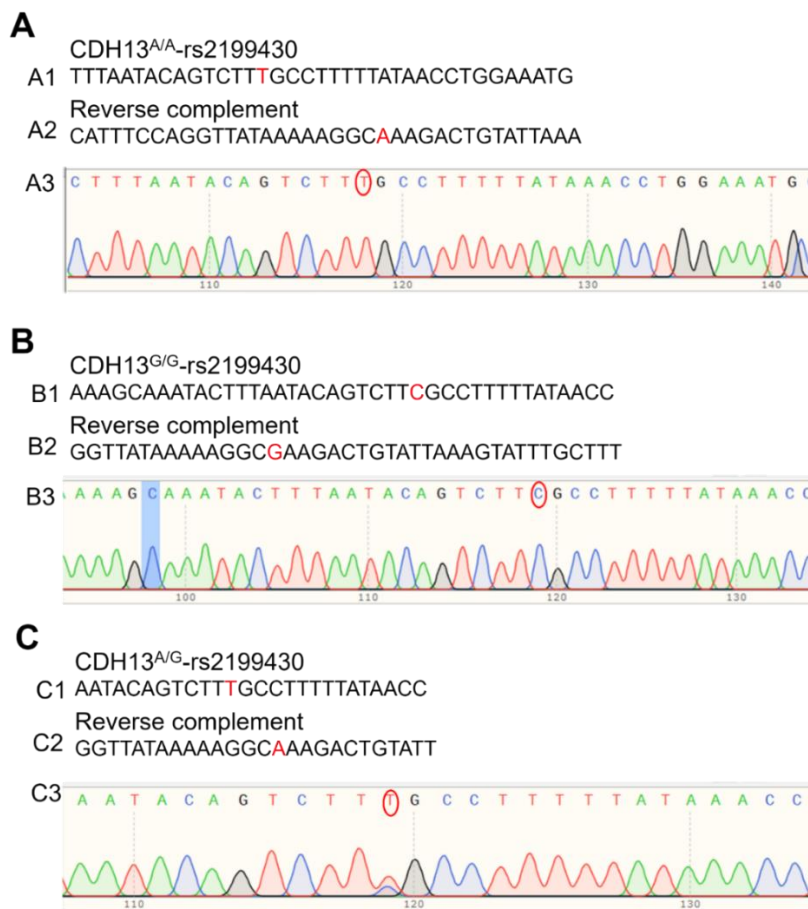


Figure 21. Genotyping of SNP rs2199430

Genotyping of SNP rs2199430 to confirm the *CDH13*^{AA} (A) *CDH13*^{GG} (B) and *CDH13*^{AG} (C) genotypes of the iPSC lines. In the latter, the chromatogram indicates the presence of a cytosine and a thymidine.

4.3.2. Generation of rtTa/Ngn2- and rtTa/Ascl1-positive iPSCs

Next, these iPSCs lines were transduced with lentivirus containing the rtTANgn2 and Ascl1 vectors to allow direct neuronal differentiation upon supplementation with doxycycline and forskolin. After transduction of the iPSCs, cell selection was done using puromycin and G4218 to ensure only cells with the integrated vectors were kept in culture. This was also confirmed by PCR. First, each cell line was activated by induction of the iPSCs. The rtTa/Ngn2-iPSCs were induced by supplementation of doxycycline (Fig. 22) whereas the rtTa/Ascl1-iPSCs were induced by supplementation of doxycycline and forskolin (Fig. 23). The activation lasted for four days.

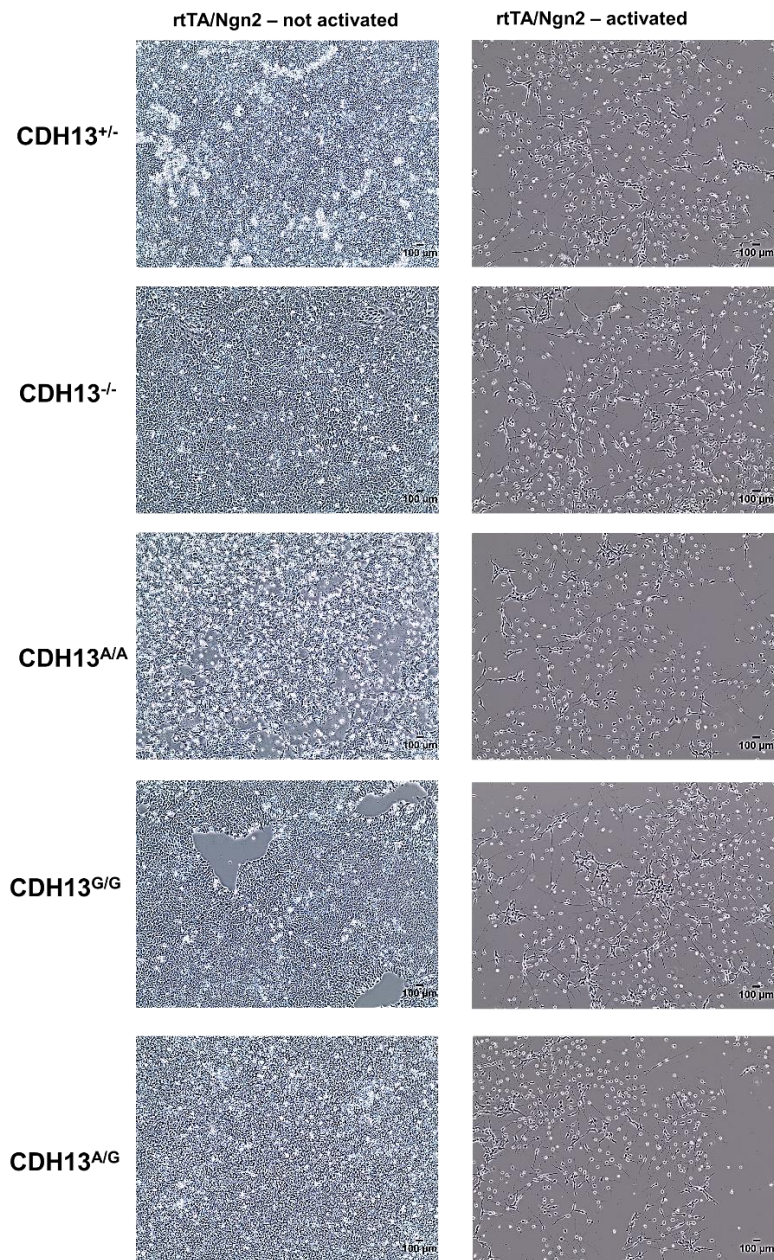


Figure 22. rtTA/Ngn2 positive iPSCs showing morphological changes when induced with supplementation of doxycycline

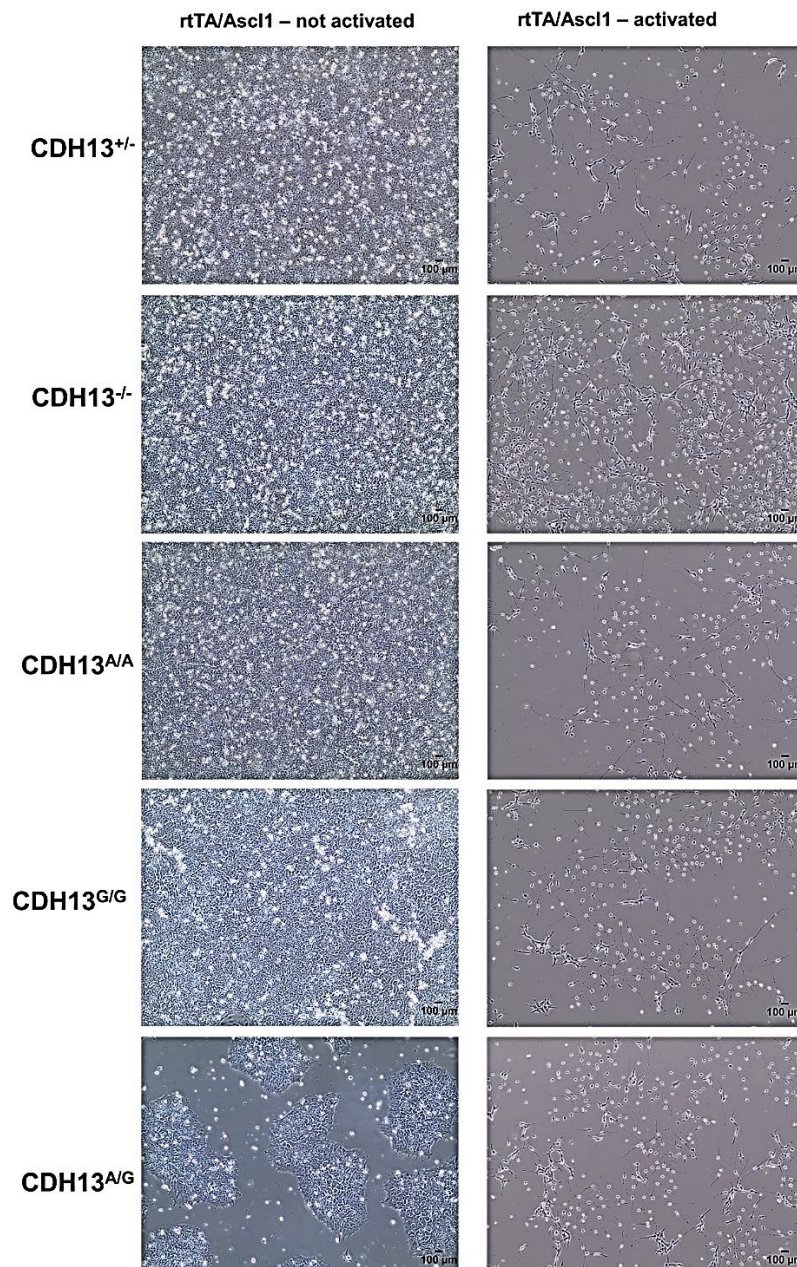
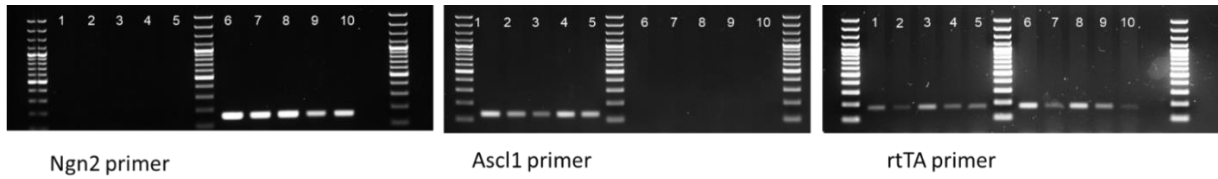


Figure 23. rtTA/Ascl1 positive iPSCs showing morphological changes when induced with doxycycline/forskolin

After that, the cells of each transduced clone collected and centrifuged to obtain a pellet. This pellet was washed with PBS and transferred to anEppi. Genomic DNA was isolated from the pellet using the PureLink Genomic DNA kit and the PCR reaction was carried. The PCR product, which was analyzed using a 2% agarose gel, confirmed the presence of the rtTa and Ngn2 vectors in the transduced rtTa/Ngn2 iPSCs and the presence of the rtTa and Ascl1 vectors in the transduced rtTa/Ascl1 iPSCs (Fig. 24).



1	CDH13 ^{G/G} rtTA/Ascl1	6	CDH13 ^{G/G} rtTA/Ngn2
2	CDH13 ^{A/G} rtTA/Ascl1	7	CDH13 ^{A/G} rtTA/Ngn2
3	CDH13 ^{A/A} rtTA/Ascl1	8	CDH13 ^{A/A} rtTA/Ngn2
4	CDH13 ^{-/-} rtTA/Ascl1	9	CDH13 ^{-/-} rtTA/Ngn2
5	CDH13 ^{+/-} rtTA/Ascl1	10	CDH13 ^{+/-} rtTA/Ngn2

Figure 24. Presence of rtTA, Ascl1 and Ngn2 vectors in transduced iPSC lines

4.3.3. Characterization of rtTa/Ngn2- and rtTa/Ascl1-positive iPSCs

Since the rtTa/Ngn2- and rtTa/Ascl1-positive iPSCs were generated using an integrative vector delivery system (lentivirus), the newly generated cell lines must be assessed for their pluripotency and differentiation potential (Figs. 25 and 26).

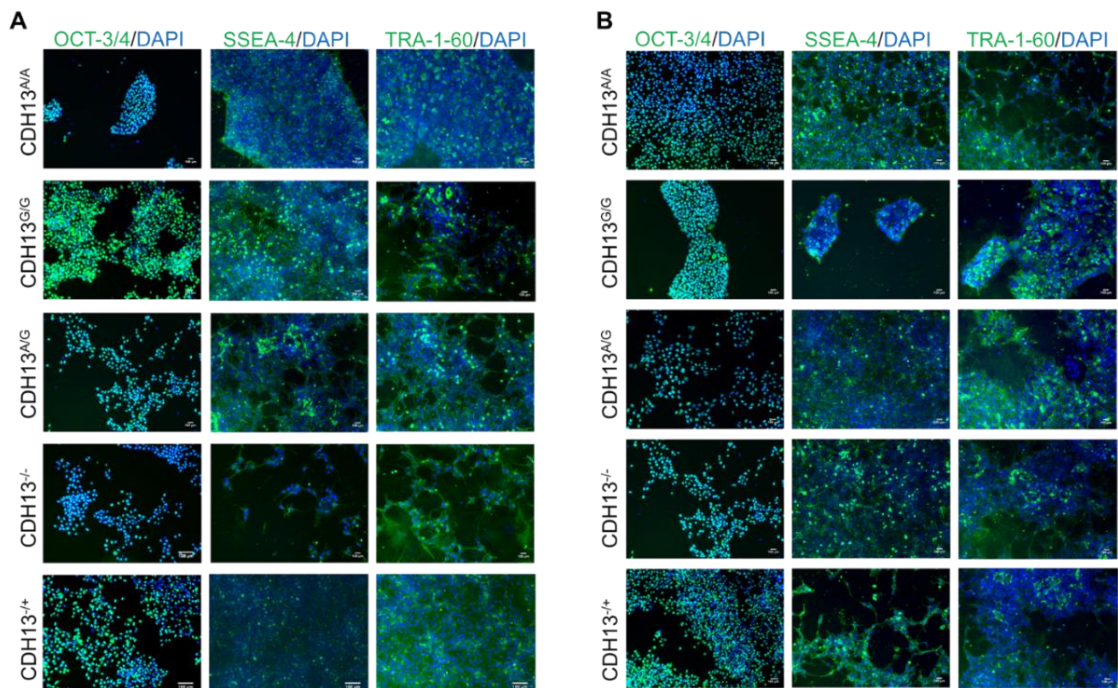


Figure 25. Pluripotency markers

Pluripotency markers (TRA-1-60, SSEA-4 and OCT-3/4, DAPI) in **A.** rtTA/Ascl1- **B.** rtTA/Ngn2 positive iPSCs.

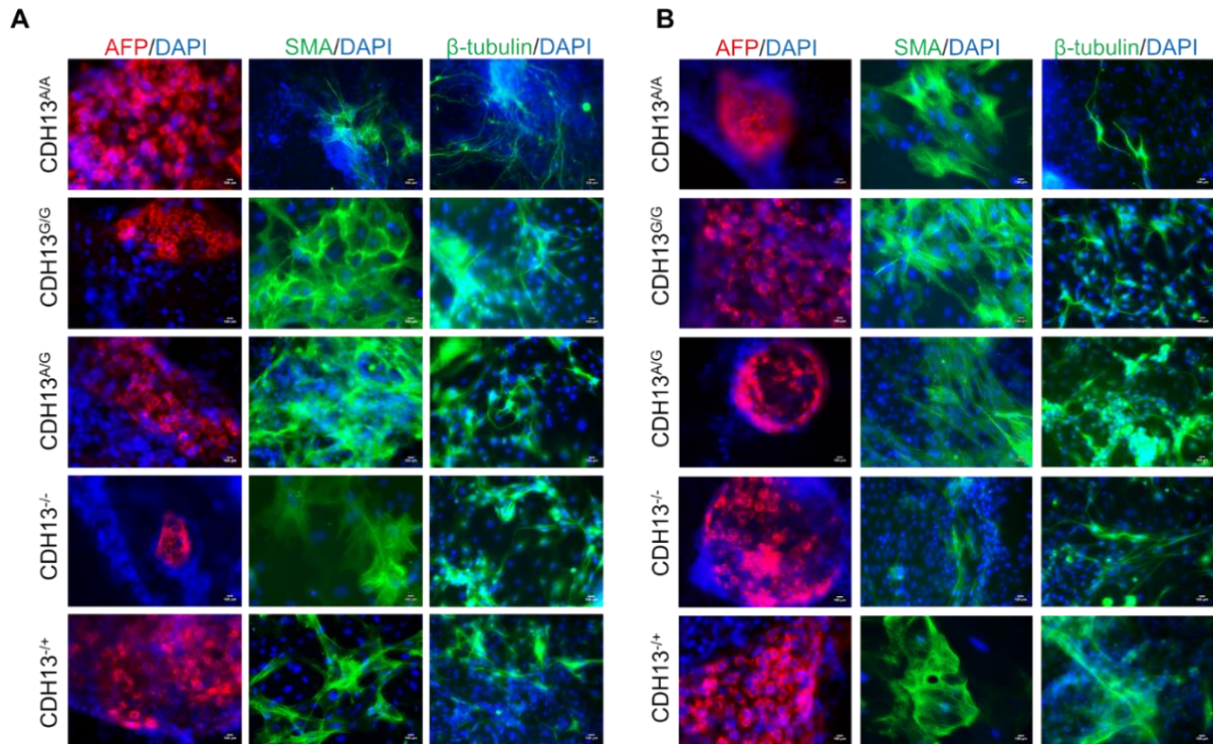


Figure 26. Germlayer markers

Germlayer markers (mesoderm: α -SMA; endoderm: AFP; ectoderm: β -tubulin, DAPI.) in **A.** rtTA/Ascl1- **B.** rtTA/Ngn2 positive iPSCs.

Taken together, we successfully generated rtTa/Ngn2- and rtTa/Ascl1-positive iPSCs which can be differentiated into glutamatergic and GABAergic neurons respectively, when activated with the correct supplement molecules.

4.4. Qualitative characterization of glutamatergic neurons

To investigate *CDH13*'s role in maintaining E/I balance in human neurons, we first verified the identity of pure glutamatergic neuronal cultures derived from the *CDH13*^{G/G} (*CDH13*^{A/A} and *CDH13*^{A/G} neuronal cultures shown in Supplementary figure 3 and Supplementary figure 4). The cultures were qualitatively characterized by using specific markers (Table 11, Fig. 27).

Table 11. Markers to qualitative confirm glutamatergic neuron culture.

Marker	Specificity
<i>VGLUT2</i> (Vesicular glutamate transporter 2)	Glutamatergic neurons
<i>CDH13</i>	/
<i>β-tubulin</i>	Neurons
<i>VGAT</i> (Vesicular GABA transporter)	GABAergic neurons
<i>GAD67</i> (Glutamate decarboxylase 67)	GABAergic neurons

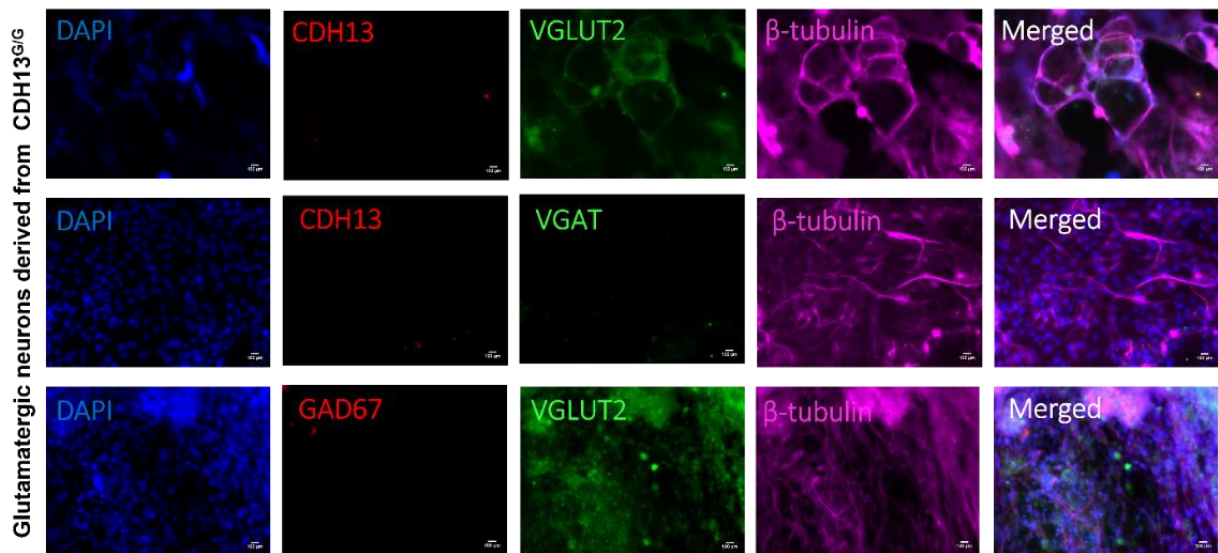


Figure 27. Qualitative staining in the pure glutamatergic neuron culture derived from the $CDH13^{G/G}$ iPSC line

The following specific markers were used: VGLUT2, $CDH13$, β -tubulin, VGAT, GAD67, and nuclei stained with DAPI. Scale bar: 100 μ m.

The glutamatergic neuron cultures demonstrated VGLUT2 expression confirming their identity. In these cultures, $CDH13$ was not expressed in line with previous studies (Mossink et al., 2022).

4.5. Qualitative characterization of GABAergic neurons

In order to investigate $CDH13$'s role in maintaining E/I balance in human neurons, we also verified the identity of pure GABAergic neuronal cultures derived from the $CDH13^{G/G}$ and $CDH13^{-/-}$. ($CDH13^{A/A}$, $CDH13^{A/G}$ and $CDH13^{+/-}$ neuronal cultures shown in Supplementary figure 5-7). The cultures were qualitatively characterized by using specific markers (Table 12, Figs. 28 and 29).

Table 12. Markers to qualitative confirm GABAergic neuron culture.

Marker	Specificity
VGLUT2 (Vesicular glutamate transporter 2)	Glutamatergic neurons
$CDH13$	/
β -tubulin	Neurons
VGAT (Vesicular GABA transporter)	GABAergic neurons
GAD67 (Glutamate decarboxylase 67)	GABAergic neurons
PV	Parvalbumin-positive neurons

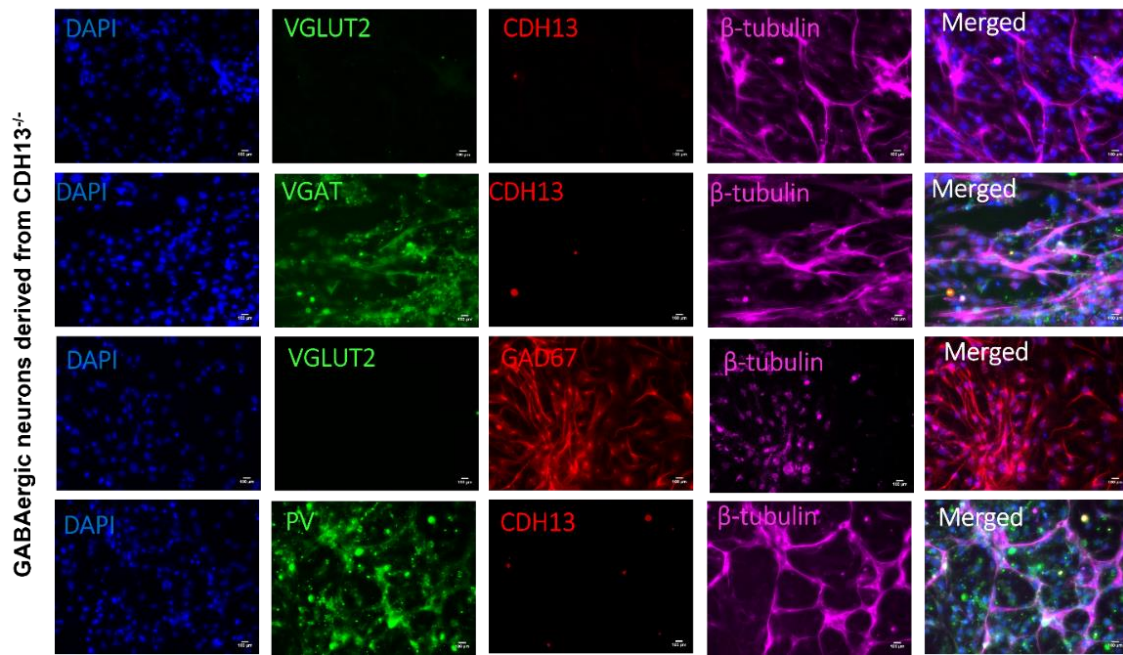


Figure 28. Qualitative staining in the pure GABAergic culture derived from the *CDH13*^{-/-} iPSC line

The following specific markers were used: VGLUT2, *CDH13*, β-tubulin, VGAT, GAD67, PV and nuclei stained with DAPI. Scale bar: 100 μm.

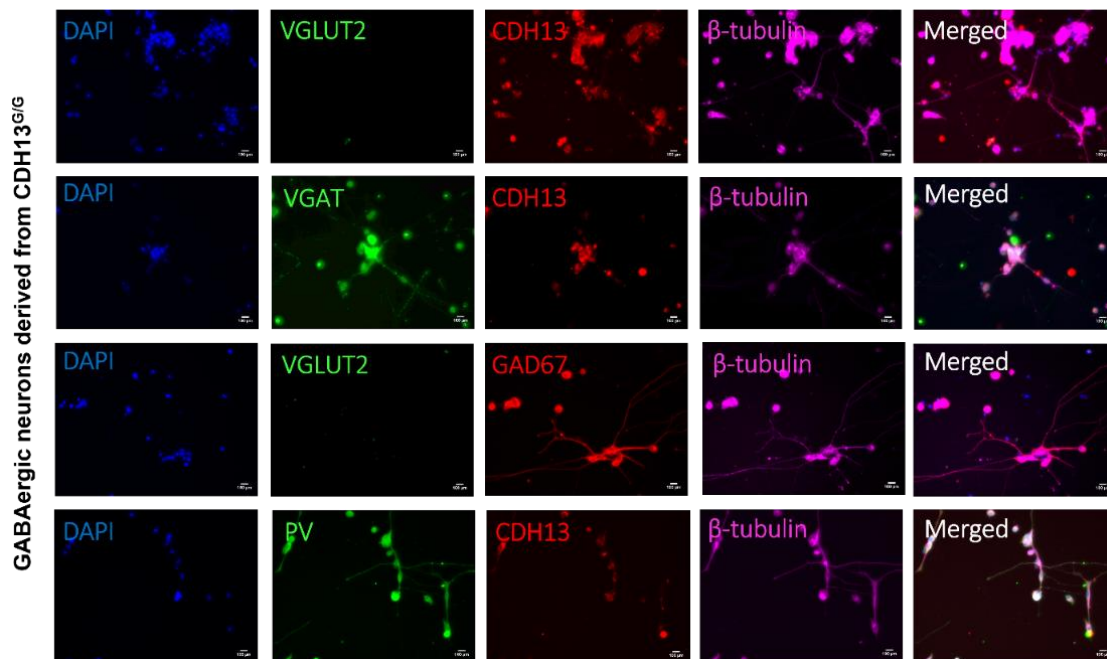


Figure 29. Qualitative staining in the pure GABAergic neuron culture derived from the *CDH13*^{G/G} iPSC line

The following specific markers were used: VGLUT2, *CDH13*, β-tubulin, VGAT, GAD67, PV and nuclei stained with DAPI. Scale bar: 100 μm.

The GABAergic neuron cultures demonstrated GAD67, PV and VGAT expression confirming their identity. In these cultures, *CDH13* expression was in line with previous studies where

$CDH13^{A/A}$, $CDH13^{A/G}$ and $CDH13^{+/-}$ and $CDH13^{G/G}$ showed positive $CDH13$ expression whereas in the $CDH13^{-/-}$ GABAergic cultures, $CDH13$ was as expected not expressed (Mossink et al., 2022; Rivero et al., 2013; Vitale et al., 2021).

4.6. Qualitative characterization of co-cultures

After the glutamatergic and GABAergic cultures from each cell line were characterized and its identity confirmed, we were able to continue investigating $CDH13$'s role in maintaining E/I balance. We co-cultured glutamatergic and GABAergic neurons in a 65:35 ratio, respectively, to form a neuronal network in which the GABAergic inhibitory function was fully functional (Mossink et al., 2022). The composition of the co-cultures is depicted in Table 13. The identity of the $CDH13^{G/G}$ and $CDH13^{-/-}$ co-cultures was also qualitatively confirmed (Table 14, Fig. 30 and 31). The co-culture derived from the $CDH13^{A/A}$, $CDH13^{A/G}$ and $CDH13^{+/-}$ are shown in Supplementary figure 8-10.

Table 13. Composition of glutamatergic/GABAergic neuron co-cultures.

Co-culture	iPSC lines differentiated into GABAergic neurons	iPSC lines differentiated into glutamatergic neurons
$CDH13^{G/G}$	$CDH13^{G/G}$	$CDH13^{G/G}$
$CDH13^{A/A}$	$CDH13^{A/A}$	$CDH13^{A/A}$
$CDH13^{A/G}$	$CDH13^{A/G}$	$CDH13^{A/G}$
$CDH13^{-/-}$	$CDH13^{-/-}$	$CDH13^{+/+}$ (= $CDH13^{G/G}$)
$CDH13^{+/-}$	$CDH13^{+/-}$	$CDH13^{+/+}$ (= $CDH13^{G/G}$)

Table 14. Markers to qualitative confirm glutamatergic/GABAergic neuron co-culture.

Marker	Specificity
VGLUT2 (Vesicular glutamate transporter 2)	Glutamatergic neurons
$CDH13$	/
β -tubulin	Neurons
VGAT (Vesicular GABA transporter)	GABAergic neurons
GAD67 (Glutamate decarboxylase 67)	GABAergic neurons
PV	Parvalbumin-positive neurons
Gephyrin	GABAergic synapses
PSD95	Glutamatergic synapses

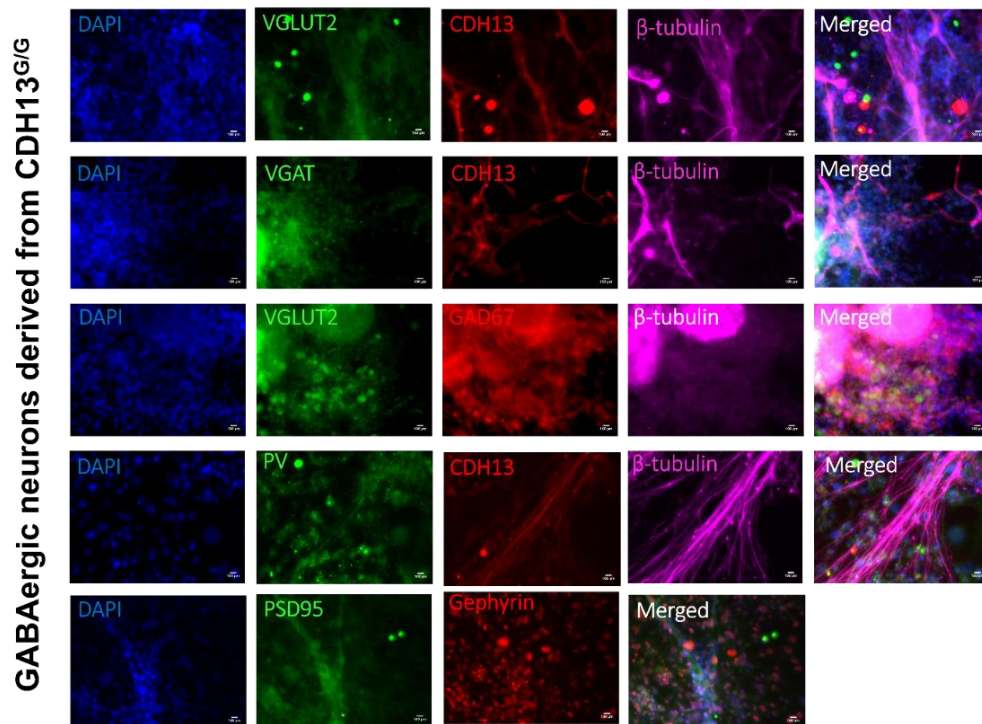


Figure 30. Qualitative staining in the co-culture derived from the $CDH13^{G/G}$ iPSC line
 The following specific markers were used: VGLUT2, $CDH13$, β -tubulin, VGAT, GAD67, PV, Gephyrin, PSD95 and nuclei stained with DAPI. Scale bar 100 μ m.

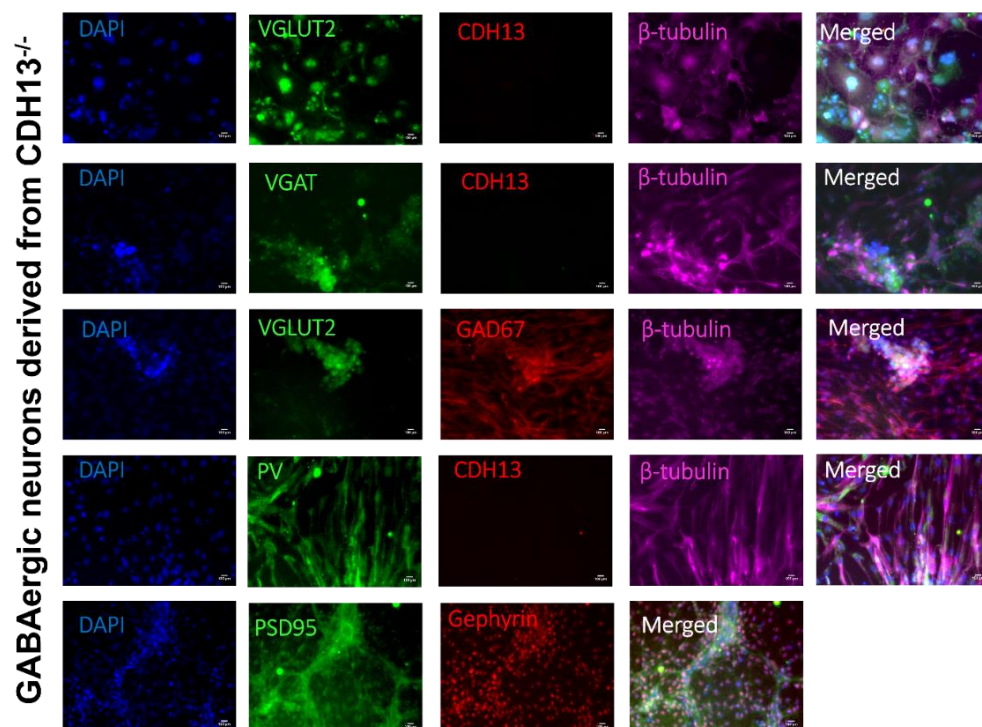


Figure 31. Qualitative staining in the co-culture derived from the $CDH13^{-/-}$ iPSC line
 The following specific markers were used VGLUT2, $CDH13$, β -tubulin, VGAT, GAD67, PV, Gephyrin, PSD95 and nuclei stained with DAPI. Scale bar 100 μ m.

The co-cultures demonstrated GAD67, PV, VGAT and VGLUT2 expression confirming their identity. In these cultures, *CDH13* was expressed in all the cultures apart from *CDH13*^{-/-}. Moreover, PSD95 and gephyrin expression confirmed synapse formation occurring in the cultures.

4.7. Network activity measurement of co-cultures

Because the activity of neural networks in E/I networks is affected by GABAergic modulation, we assessed whether *CDH13* deficiency in GABAergic neurons would affect network activity at DIV 49. The investigated parameters were network burst duration (NBD), network burst rate (NBR), average burst shape and spike detection.

By comparing *CDH13*^{+/+} and *CDH13*^{-/-} networks there were higher numbers of bursts and network bursts in the *CDH13*^{+/+} vs. *CDH13*^{-/-} networks over a 60 s-period in the raster plots (Fig. 32A, B). Additionally, there was a significantly reduced NBD in *CDH13*^{+/+} vs. *CDH13*^{-/-} networks ($p=0.00004$) (Figure 32C), an altered average burst shape ($p=0.146$) (Figure 32D). We also observed a significantly reduced NBR in *CDH13*^{-/-} networks compared to *CDH13*^{+/+} ($p=0.528$) (Supplementary figure 11A). The representative heatmap diagrams combines various parameters in a timescale of 1 s. Even though more bursts were detected in *CDH13*^{-/-} networks ($n=56$ vs. 39), the number of detected spikes within a single network burst was reduced in *CDH13*^{-/-} ($n=48$ vs. 53) (Fig. 32E, F). These latter parameter results confirm the increased inhibitory action found in *CDH13*^{-/-} networks.

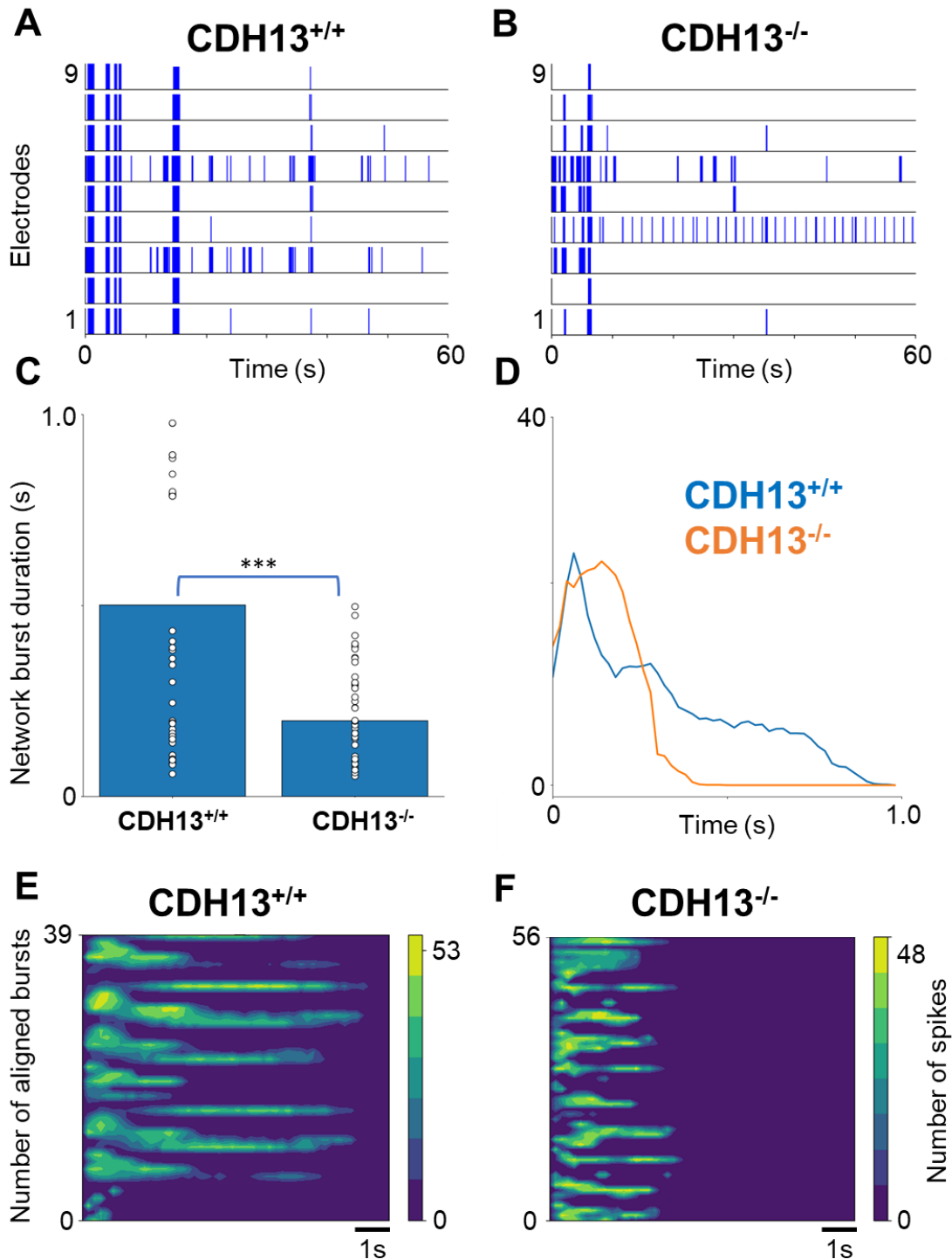


Figure 32. Comparison of *CDH13*^{+/+} and *CDH13*^{-/-} E/I networks

A, B Representative raster plots showing 60 s of electrophysiological activity recorded from E/I 65:35 cultures at DIV 49 from each electrode on the MEA chip (1-9). **C** Quantification of the average network burst duration in E/I 65:35 networks (*CDH13*^{+/+} *n* = 14, *CDH13*^{-/-} *n* = 12 individual wells from two neuronal preparations). Mann–Whitney test with Bonferroni correction was performed). **D** Average network burst shape from E/I 65:35 networks at DIV 49 (*CDH13*^{+/+} *n* = 14, *CDH13*^{-/-} *n* = 12 individual wells from two neuronal preparations), *p* = 0.146. Multiple t-test on bins were performed using the Holm–Sidak method). All data represent means ± SEM ****p* < 0.001. **E, F** Total network burst alignment from recording of E/I 65:35 networks at DIV 49 with a time scale of 1 s, color code represents # spikes. DIV: days in vitro.

By comparing *CDH13^{+/+}* and *CDH13^{+/-}* networks (Fig. 33) there were higher numbers of bursts and network bursts in the *CDH13^{+/+}* vs. *CDH13^{+/-}* networks over a 60 s period in the raster plots (Fig. 33A, B). Additionally, a significantly reduced NBD in *CDH13^{+/+}* vs. *CDH13^{+/-}* networks ($p=0.0007$) (Fig. 33C), an altered average burst shape ($p=0.08e-6$) (Fig. 33D). We also observed a significant reduced NBR in *CDH13^{+/-}* networks compared to *CDH13^{+/+}* ($p=0.921$) (Supplementary figure 11B). The representative heatmap diagrams combines various parameters in a timescale of 1s. A higher number of detected network bursts were found in the *CDH13^{+/+}* networks ($n=39$ vs. 27), whereas the number of detected spikes within a network burst is reduced in *CDH13^{+/-}* ($n=53$ vs. 45) compared to *CDH13^{+/+}* (Fig. 33E, F). The NBD and altered burst shape parameter results confirm the increased inhibitory action found in the *CDH13^{+/-}* networks.

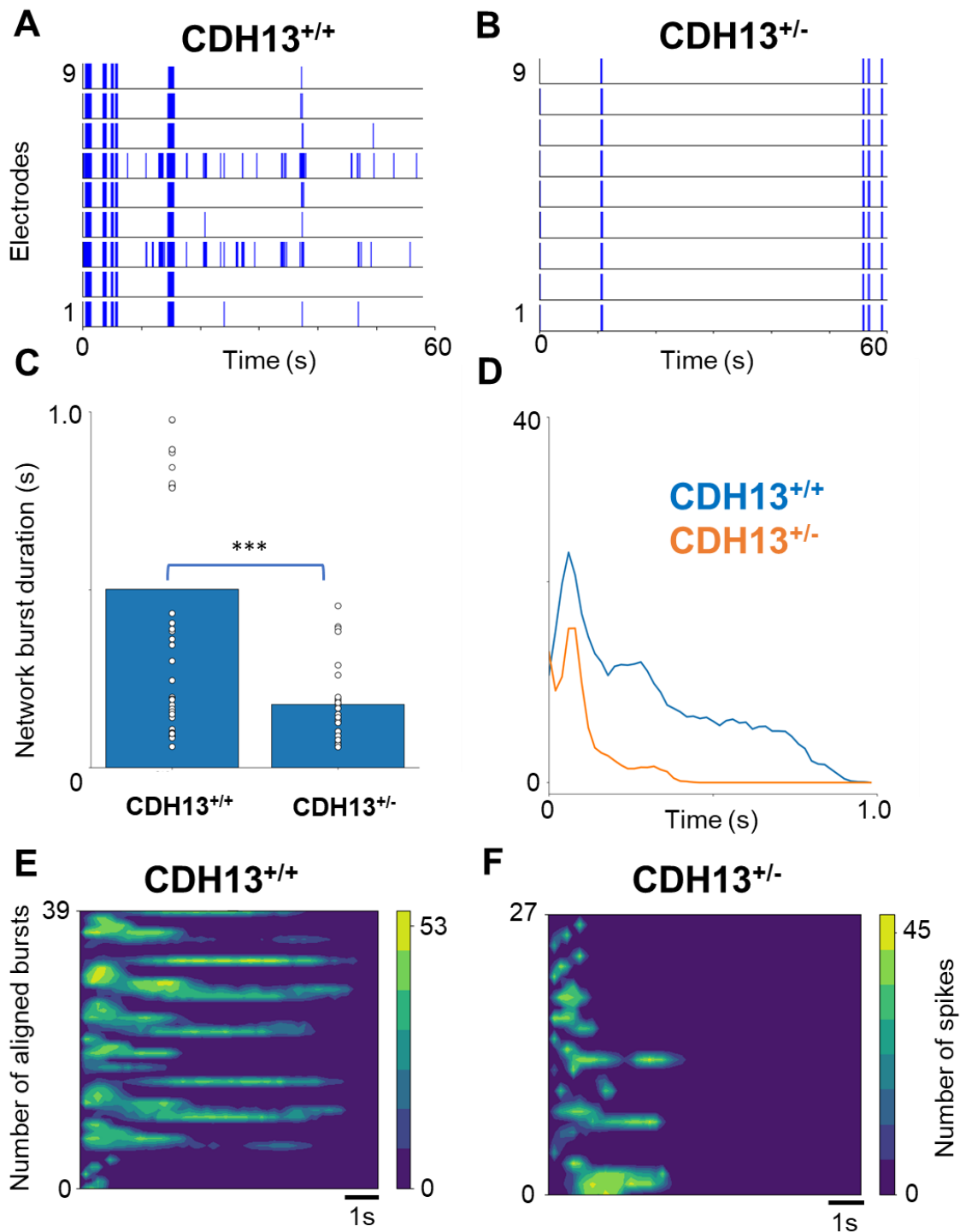


Figure 33. Comparison of *CDH13*^{+/+} and *CDH13*^{+/-} E/I networks

A, B Representative raster plots showing 60 s of electrophysiological activity recorded from E/I 65:35 cultures at DIV 49 from each electrode on the MEA chip (1-9). **C** Quantification of the average network burst duration in E/I 65:35 networks (*CDH13*^{+/+} n = 14, *CDH13*^{+/-} n = 9 individual wells from two neuronal preparations. Mann–Whitney test with Bonferroni correction was performed). **D** Average network burst shape from E/I 65:35 networks at DIV 49 (*CDH13*^{+/+} n = 14, *CDH13*^{+/-} n = 9 individual wells from two neuronal preparations), p = 0.08e-6. Multiple t-test on bins were performed using the Holm–Sidak method. All data represent means ± SEM ***p<0.001. **E, F** Total network burst alignment from recording of E/I 65:35 networks at DIV 49 with a time scale of 1 s, colour code represents # spikes. DIV: days in vitro.

By comparing $CDH13^{G/G}$, $CDH13^{A/G}$, $CDH13^{A/A}$, networks (Fig. 34) there was a higher number of bursts and network bursts in the $CDH13^{A/G}$ networks over a 60 s period in Figure 34A, B and C. Additionally, a significantly reduced NBD was detected in $CDH13^{G/G}$ vs. $CDH13^{A/A}$ networks ($p=0.0487$) as well as $CDH13^{G/G}$ vs. $CDH13^{A/G}$ ($p=0.00035e-30$) and $CDH13^{G/G}$ vs. $CDH13^{A/G}$ ($p=0.0004e-30$) in Figure 34D. Moreover, an altered average burst shape was detected in Figure 34E ($CDH13^{G/G}$ vs. $CDH13^{A/A}$ $p=0.194$; $CDH13^{A/A}$ vs. $CDH13^{A/G}$ $p=0.048$; $CDH13^{G/G}$ vs. $CDH13^{A/G}$ $p=0.503$). We also observed a significant reduced NBR in $CDH13^{G/G}$ networks compared to $CDH13^{A/A}$ and $CDH13^{A/G}$ ($CDH13^{A/A}$ vs. $CDH13^{A/G}$ $p=0.090$; $CDH13^{A/A}$ vs. $CDH13^{G/G}$ $p=0.021$; $CDH13^{G/G}$ vs. $CDH13^{A/G}$ $p=0.0005$) (Supplementary figure 11C). The representative heatmap diagrams combines varies parameters in a timescale of 1 s. A higher number of detected network bursts were found in the $CDH13^{A/G}$ networks ($n=305$) compared to $CDH13^{A/A}$ ($n=43$) and $CDH13^{G/G}$ ($n=39$) networks, while the number of detected spikes within a network burst was reduced in $CDH13^{A/G}$ ($n=40$) compared to $CDH13^{A/A}$ ($n=47$) and $CDH13^{G/G}$ ($n=53$) networks (Figure 34F, G, H).

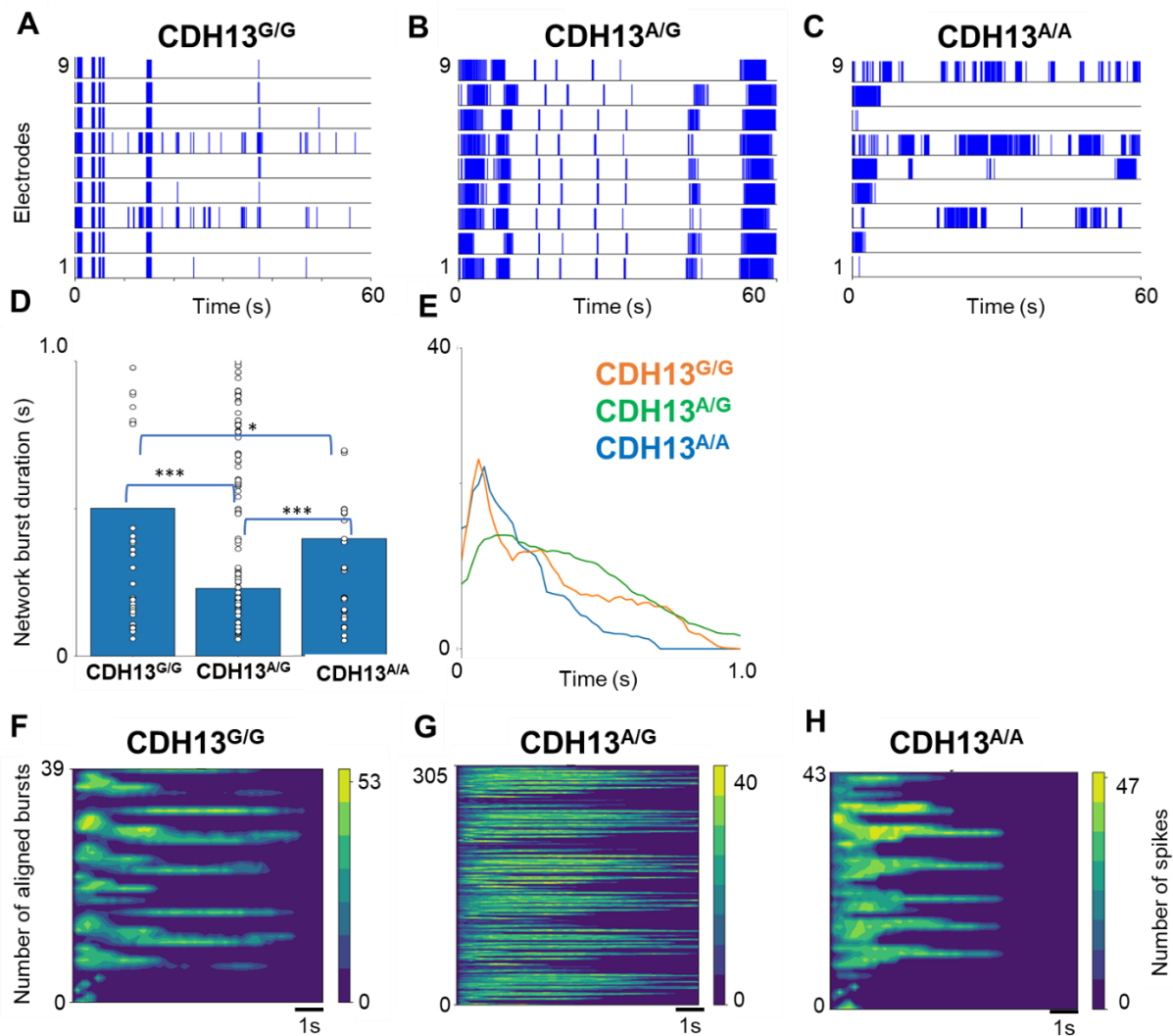


Figure 34. Comparison of $CDH13^{G/G}$, $CDH13^{A/G}$, $CDH13^{A/A}$ E/I networks

A, B, C Representative raster plots showing 60 s of electrophysiological activity recorded from E/I 65:35 cultures at DIV 49 from each electrode on the MEA chip (1-9).. **D** Quantification of the average network burst duration of E/I $CDH13^{G/G}$, $CDH13^{A/G}$ and $CDH13^{A/A}$ networks ($CDH13^{G/G}$ n = 14, $CDH13^{A/G}$ n = 6, $CDH13^{A/A}$ n = 14, individual wells from two neuronal preparations; $CDH13^{G/G}$ only one neuronal preparation). Kruskal–Wallis Two-way ANOVA was performed and, corrected using the Dunn’s method). **E** Average network burst shape from E/I 65:35 networks at DIV 49 ($CDH13^{A/A}$ n = 14, $CDH13^{A/G}$ n = 6, $CDH13^{G/G}$ n = 14, individual wells from two neuronal preparations ($CDH13^{A/G}$ only one neuronal preparation)). $CDH13^{G/G}$ vs. $CDH13^{A/A}$ p=0.194 $CDH13^{A/A}$ vs. $CDH13^{A/G}$ p=0.048, $CDH13^{G/G}$ vs. $CDH13^{A/G}$ p=0.503. Multiple t-test on bins using Holm–Sidak method. All data represent means \pm SEM *p>0.01, ***p<0.001. **F, G, H** Total network burst alignment from recording of E/I 65:35 networks at DIV 49, colour code represents # spikes. DIV: days in vitro.

5. Discussion

iPSC approaches have been revolutionizing how basic research on neurodevelopmental and mental disorders is conducted: through ectopic expression of pluripotency-associated transcription factors in somatic cells, a novel, human-generated model has been introduced. In culture, iPSCs can proliferate indefinitely and differentiated into any cell type present in humans, given the specific molecular cues (Halevy et al., 2015; Mariani et al., 2015). This is why in the present study human iPSCs had been generated from dermal fibroblasts of healthy volunteers carrying different genotypes of *CDH13* SNP rs199430: *CDH13*^{G/G}, *CDH13*^{A/G} and *CDH13*^{A/A}. Variation in several linked *CDH13* SNPs has shown to affect *CDH13* expression in human post-mortem cerebral cortex samples (Drgonova et al., 2016): an approximately 80% higher *CDH13* mRNA expression was detected in samples derived from carriers of the GG genotype of SNP rs2199430. Recently, SNP rs2199430 has been demonstrated to not only have a functional effect at the molecular level but also to intermediate phenotypes related to ADHD. The Big Five personality traits as well as task performance and electroencephalographic (EEG) event-related potentials were measured to associate this SNP to personality traits and its impact on neural processing during working memory tasks, respectively. The study found significant association between agreeableness (minor G allele homozygotes scored lower than A allele carriers) and a heterosis effect in the ADHD group for task performance/EEG measurements (Ziegler et al., 2021), confirming brain functional effects of common gene variation in the *CDH13* gene.

Although the advantage of using iPSCs are evident, one of the challenges associated with iPSC-based disease modelling is differentiating between *in vitro* phenotypes developed because of the specific causative mutations and phenotypes moderated by the individual's genetic background. Advances in genome-editing technology made it possible to introduce genetic mutations directly into human iPSCs to create disease models, with the un-edited cells serving as isogenic controls (Bellin et al., 2013; Ding et al., 2013; Horii et al., 2013; Y. Wang et al., 2014). Artificially engineered nucleases are used to create specific DBSs at designated locations within the genome. By repairing DBSs via the cell's endogenous DNA repair systems (HDR and NHEJ), locus-specific mutations are produced which are caused by nucleotide insertions or deletions. Mutations induce frameshifts, which at best eliminate the gene expression at the proteomic level.

Following the aims of the thesis, we successfully show how *CDH13* destabilizes the E/I balance when knocked out in iPSCs (Geertjens et al., 2022; Mossink et al., 2022; Vitale et al., 2021) and additionally find differential effects of *CDH13* SNP variants in GABAergic neurons in neuronal activity.

5.1. Generation of isogenic cell lines by using CRISPR/Cas9 with a gene dose-dependent deficiency of *CDH13* (*CDH13^{-/-}* and *CDH13^{+/-}*)

In this work, a set of isogenic cell lines using iPSCs carrying the *CDH13* GG genotype was generated, as it showed higher mRNA expression in post-mortem cortex samples compared to the other genotypes of SNP rs2199430 (Drgonova et al., 2016). This cell line was considered the “wildtype” for the genomic editing approach and is designated *CDH13^{+/+}* in this section. The CRISPR/Cas9 technology was used to generate *CDH13* gene-dose dependent deficiency isogenic cell lines (Vitale et al., 2021). We targeted exon 1 of *CDH13*'s open reading frame to ensure *CDH13*'s translation (i.e., protein expression) would be affected by nucleotide frameshift. For this region, two distinct sgRNAs were designed. On-target efficiency and off-target activity depend upon the sequence of target-specific sgRNA (Uniyal et al., 2019). sgRNAs should share sufficient homology with the ~20-nucleotide target sequence which in turn must meet two conditions: the target sequence must be unique within the genome and resides directly adjacent to a Cas9 protospacer adjacent motif (PAM). The appropriate sgRNAs were ligated into the commercially available pSpCas9(BB)-2A-Puro (PX459) V2.0 plasmid (Ran et al., 2013) and the fully functional sgRNAs were then nucleofected in the *CDH13^{+/+}* iPSCs. Nucleofection is more efficient than other forms of transfection because a combination of optimized electrical parameters and cell-type specific solutions can transfer plasmids directly into the nucleus. Because of this independency from cell proliferation, plasmid expression is accelerated. When sgRNAs are nucleofected, they are directly transferred into the nucleus, where transcription takes place. After that the mRNA is translocated out of the nucleus into the cytoplasm where translation of the guideRNA (gRNA) and Cas9 protein takes place. In the cytoplasm they form a ribonucleoprotein (RNP) complex which is translocated back into the nucleus via nuclear localisation signal encoded in the Cas9 plasmid where genome editing occurs. Despite the accelerated expression of sgRNA, it is not possible to determine when it is transcribed and translated to begin the puromycin selection process in the iPSCs.

Therefore, we decided to carry out a parallel control experiment, in which we nucleofected the iPSCs with a GFP plasmid. We orientated ourselves with the GFP expression: when the GFP expression was confirmed under the fluorescent microscope, resulting from translation of the plasmid, we deduced that the sgRNA plasmid also underwent the translation process. This indicated that the puromycin selection process could be initiated. The puromycin selection lasted until the GFP expression in the control experiment was over. The colony which survived the selection were considered to have been successfully nucleofected. The knockout of the targeted gene must be checked on the proteomic level, such as Western blot. By this method it was confirmed that the gene is non-functional. The major challenge we faced, was that *CDH13* was not expressed in iPSCs, so the cells had to be differentiated into a cell type, where the expression of *CDH13* could be observed in the *CDH13^{+/+}*. Therefore, we used a trilineage differentiation kit, which differentiated the iPSCs into the three germ layers (meso-, ecto-, endoderm), thereby establishing *CDH13* expression in the mesodermal cells. As a result, we differentiated CRISPRed cell lines into the mesodermal lineage and performed Western blot analysis to start the exclusion criteria for a gene knockout: CRISPRed cell lines which were positive for *CDH13* expression were screened and excluded from further analysis, except one cell line that showed a higher expression level than the positive control and thus attracted our attention for more in-depth analysis. Several CRISPRed cell lines were checked for allele-

specific mutations. Taking advantage of the PCR cloning method, the alleles of each CRISPRed cell line were separated and sequenced. The data confirmed that a complete knockout ($CDH13^{-/-}$), but also a heterozygous knockout ($CDH13^{+/-}$) was generated associated with the cell line with a higher $CDH13$ expression level compared to the positive control.

To check that the failed protein translation of the knockout cell line was associated with the disruption of the $CDH13$ genetic sequence, PCR cloning was performed to detect $CDH13$ -specific modifications. In addition to that, potential off-target effects were also checked, to exclude the possibility of unspecific genetic alterations in nearby targeting sites. Since this was not the case, confirmed that the failed translation of $CDH13$ originates in the altered genetic sequence which in turn alters the transcription process. iPSCs generated through genetic engineering carry the risk of losing their pluripotency and germlayer differentiation capacity as well as altering the karyotype (Rayner et al., 2019). We confirmed that this was not the case in our cell lines. Taken together, a set of isogenic cell lines, free from undesired genetic alterations, with a gene dose-dependent deficiency of $CDH13$ was generated which facilitates investigation of $CDH13$ in neuronal plasticity and communication and, in particular, its function at inhibitory synapses involved in E/I balance.

5.2. Differentiation into glutamatergic and GABAergic neurons and their co-culture for excitatory/inhibitory network assessment

Differentiating cortical neuronal cultures derived from iPSCs can be done in distinct ways, the easiest being using commercially available kits. Another common way is using a combination of small molecules (Autar et al., 2022; Qi et al., 2017) which inhibit several signalling pathways, involving SMAD (Chambers et al., 2009), Wnt/ β (Nicoleau et al., 2013), BMP (Neely et al., 2012), SHH (Cao et al., 2017), FGF (Sun et al., 1999) and Notch (Dovey et al., 2001). These procedures, however, are usually slow and display a high level of variability. For this reason, a protocol which produced iPSC-derived glutamatergic and GABAergic neurons by enforced expression of transcription using Ngn2 and Ascl1, respectively, was employed (Frega et al., 2017; Mossink et al., 2022) both in combination rtTA, which yield mature neurons already after three weeks with a 100% conversion efficiency upon induction. The advantage is that by generating stably transduced hiPSC cells with either Ngn2 or Ascl1 vectors, complete control over the seeding number of neurons is maintained. Consistency of the cell density is critical in generating neuronal networks on MEA chips, since it determines the functionality of the network as well as contributing to tight contact between the neurons and the electrodes on the MEA chip (Wang et al., 2012).

The pure glutamatergic and GABAergic cultures were qualitatively characterized by immunocytochemistry. Glutamatergic cultures derived from $CDH13^{G/G}$, $CDH13^{A/G}$ and $CDH13^{A/A}$ iPSC lines were positive for the glutamatergic neuron markers VGAT and GAD67, while confirming the absence of GABAergic neurons, as well as the absence of $CDH13$ in line with a previous study (Mossink et al., 2022). The GABAergic cultures derived from the corresponding iPSC lines confirmed the expression of GAD67, VGAT and PV, whereas no glutamatergic neurons were detected. In these cultures, $CDH13$ expression was observed, confirming earlier findings (Mossink et al., 2022; Rivero et al., 2015; Rivero et al., 2013). In the GABAergic culture derived from $CDH13^{-/-}$, the GABAergic markers were detected, while $CDH13$ was not expressed (Mossink et al., 2022). Once the glutamatergic and GABAergic

cultures were qualitatively validated, they were co-cultured in a pre-determined 65:35 ratio. These co-cultures were also qualitatively characterized and, in addition, we confirmed the formation of synapses using the PSD95 and gephyrin markers, which were expressed adjacent to each other. It would be of interest to assess genotype dependency by quantifying expression levels of *CDH13* in GABAergic neurons in pure and co-cultures. Furthermore, the expression of other neuron and glia subtypes, should be investigated. To have a better understanding of the localisation of *CDH13*, PSD95 and gephyrin, high-resolution microscopy such as dSTORM or SIM should be used in follow-up studies.

In conclusion, we successfully generated transduced iPSCs which, when induced with specific molecules, differentiate directly into glutamatergic and GABAergic neurons. This allows control over neuron density and "scalability" of each neuron subtype in this neuronal co-culture system. In future studies, astrocytes derived from iPSCs may be used instead of the freshly prepared ones from mouse pups to avoid a mix different cell types from different species within a culture set-up.

5.3. Neuronal network activity analysis

Since the neuronal network activity of E/I networks varies with the degree of GABAergic modulation (Mossink et al., 2022), the effects *CDH13* deficiency as well as *CDH13* genotypes in GABAergic neurons on network activity was evaluated. Network activity was measured at day 49 of differentiation, since this was the time point at which the inhibitory system was found to be fully functional and mature (Mossink et al., 2022). We observed reduced NBD and NBR together with altered burst shape and less detected spikes within *CDH13*^{-/-} and *CDH13*^{+/-} neuronal networks. These characteristics are a hallmark of mature inhibitory activity caused primarily by a reduction in intra-burst activity (Baltz et al., 2010; Jimbo et al., 2000; Teppola et al., 2019) which prevent depolarization of excitatory neurons, i.e., NMDA receptor activation (Suresh et al., 2016). Interestingly, unlike the *CDH13*^{-/-} networks which showed more network bursts and less spikes compared to the *CDH13*^{+/+}; the *CDH13*^{+/-} networks did not.

We also showed distinct network activity traces within the allelic SNP variants of *CDH13*. *CDH13*^{A/A} and *CDH13*^{A/G} networks showed similarities with the *CDH13*-deficient networks by showing a significant reduction in NBD and a reduced number of detected spikes within a network compared to *CDH13*^{G/G}. Furthermore, *CDH13*^{A/A} and *CDH13*^{A/G} networks showed a higher number of network bursts but decreased number of spikes within the burst, compared to the *CDH13*^{G/G}, similar to the complete knockout cell line but not the heterozygous. Surprisingly, there was a significant increase in NBR of the *CDH13*^{A/A} and *CDH13*^{A/G} compared to *CDH13*^{G/G} networks. *CDH13*^{A/G} networks exhibited significant differences in both parameters compared to the other networks suggesting molecular heterosis effects. This heterosis effect was also evident in a recent finding a study with ADHD patients heterozygous for the rs2199430 SNP (Ziegler et al., 2021). Heterosis effects have been reported in both animals and humans (Comings & MacMurray, 2000) some examples including α -CAMKII (Chen et al., 1994), MBP (Ebato et al., 1983), SLC6A4 (Little et al., 1998). This indicates that at the cellular level, signalling pathways and channels which determine the length and frequency of the network burst may differ between the allelic variants. The differential effects of intronic *CDH13* SNP variants on network activity traces may be the indication of critical role of introns in gene

expression regulation, splicing, exon shuffling and alternative splicing resulting in genotype-phenotype associations (Gorlova et al., 2014; Nair et al., 2021; Yang et al., 2013).

In conclusion, the findings add to previous evidence that *CDH13* is a key negative regulator in E/I balance. Its deficiency increases inhibition at the network level (Mossink et al., 2022), which is consistent with synaptic phenotypes observed in hippocampal CA1 neurons of *CDH13* null mutant (*CDH13*^{-/-}) mice (Rivero et al., 2015). Moreover, we showed that *CDH13*^{+/-} co-cultures exhibited the same neuronal activity as *CDH13*-deficient cultures as well as showing that SNP variation influences network activity. Most likely, *CDH13* interacts with molecules responsible for inhibitory synaptic strength regulation. ITGβ1 and ITGβ3 are novel interaction partners which have been found to interact with *CDH13* (Mossink et al., 2022), though with differential roles as they regulate excitatory and inhibitory input, respectively. This implies that *CDH13* is essential for both excitatory and inhibitory synapses indicating its relevance to maintain E/I balance. These results should be replicated and ultimately validated with an independent sample of isogenic cells.

6. Conclusion and outlook

iPSCs have revolutionized science in a way where research is carried out in a more human-like model and is enabling us to model disease in a patient-specific manner allowing progress towards personalised medicine. Moreover, to understand the functional impact of gene variation causing disease, genetic engineering made it possible to generate isogenic cell lines reducing genetic variability.

There are points of debate regarding best practice procedures for the use of iPSCs despite the advancements and considerations which must be kept in mind when working with them. For example, what are the implications of reprogramming of iPSCs. if by doing so, the epigenetic memory of the cells is erased? This can of course be bypassed, by transdifferentiating fibroblasts into the desired cell type by either a lentivirus-mediated approach or mRNA delivery, the latter being safer, as it does not integrate into the genome. Another controversy in iPSC research is the efficacy of 2D modelling, since this type of modelling misses essential interactions of 3D structures, which recapitulate a realistic *in vivo* environment. Therefore, 3D modelling has been proposed to overcome this inaccuracy of an *in vitro* environment. This intrigued us to start exploring this field as a side project (Appendix-CD). Transcriptomic and proteomic characterizations analysis should be included in future studies to complete the whole neuronal network characterization in differential *CDH13* genotypes exposing potential therapeutic targets to reinstate E/I balance in neurodevelopmental and mental disorders.

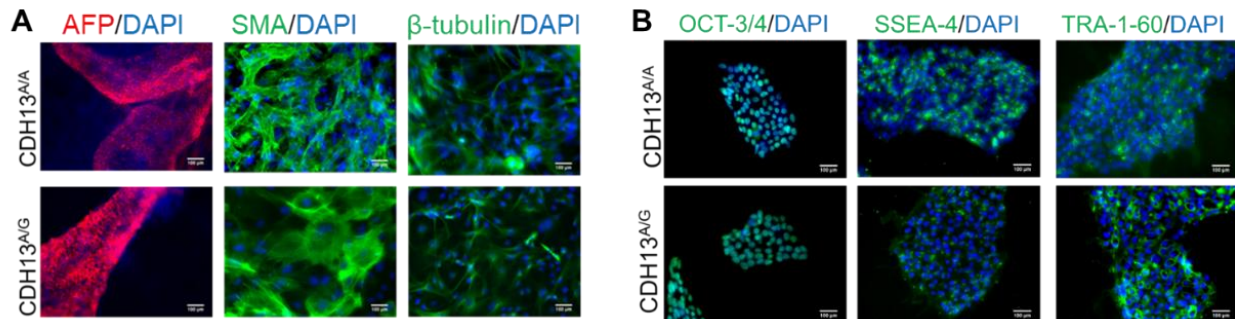
Patients diagnosed with neuropsychiatric disorders who have previously been shown to display disrupted E/I balance, such as ASD and schizophrenia, will benefit from future findings based on our work. To first further validate our findings, patient-specific network activity can be analysed by generating patient-specific iPSCs and a corresponding set of isogenic cell lines which will in turn be used for neuronal co-cultivation. In this way we can see whether our findings conducted with only healthy cell lines match the findings of the isogenic cell line derived from the patient. Once this is confirmed and differences in network activity signatures

between healthy and patient derived iPSCs can indeed be identified, one can start speculating on how to reinstate the E/I balance. One way could involve the transplantation of healthy neurons back into the patient's brain, although this requires extensive controlled clinical trials. A faster way to perhaps implement our findings is to try to reinstate the E/I balance first *in vitro* directly on the MEA chip by either positively or negatively stimulating the network via the MEA system and then performing transcranial direct current stimulation (tDCS) directly to the patient. tDCS is a type of neuromodulation by which brain cells are activated through electrical signals. This stimulation works by either depolarizing or hyperpolarizing neurons. When neuronal excitability needs to be increased, a positive (anodal) stimulation is delivered causing depolarization, whereas neuronal excitability is decreased when a negative (cathodal) stimulation is delivered causing hyperpolarization (Nitsche et al., 2008; Nitsche & Paulus, 2000).

In spite of the fact that it sounds like these applications may be implemented in the distant future, we have witnessed the ability of scientific advancement to accelerate during times of crisis. Ultimately, this a positive sign to trust research, but understudied areas of research such as mental disorders should be given greater prominence within the scientific community as well as more public attention in order to end stigma associated with them.

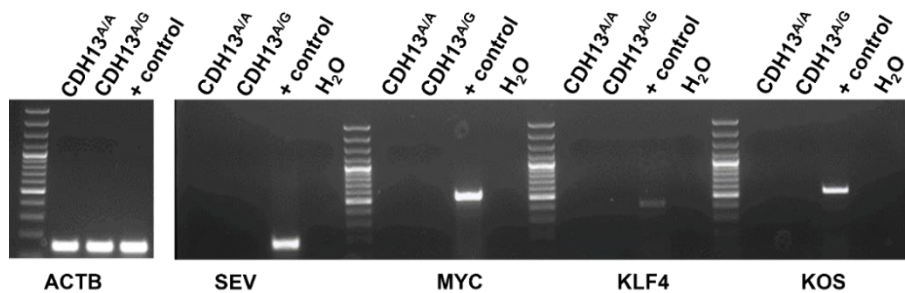
7. Supplementary files

7.1. Supplementary files: iPSC characterization of $CDH13^{A/A}$ and $CDH13^{A/G}$



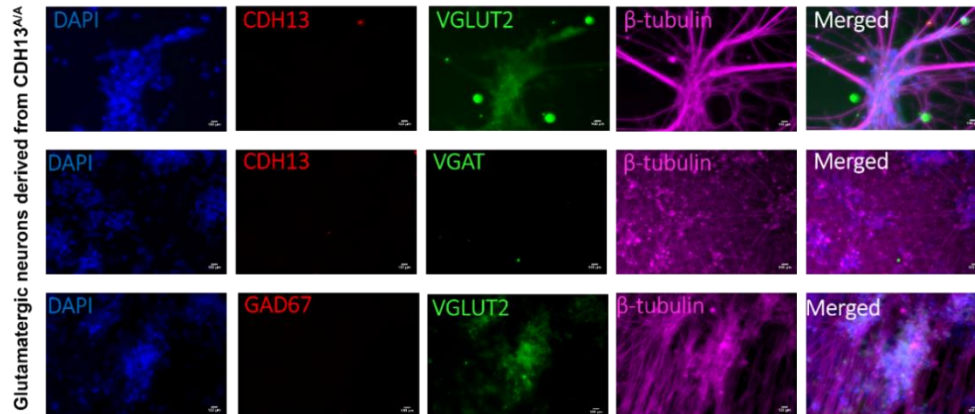
Supplementary figure 1. Germ layer and pluripotency markers

Characterization of $CDH13^{A/A}$ and $CDH13^{A/G}$: **A** iPSCs were differentiated into cells of all three germ layers mesoderm: α -SMA; endoderm: AFP; ectoderm: β -tubulin; nuclei stained with DAPI. **B** The expression of specific pluripotency markers was confirmed via immunofluorescence (OCT 3/4, SSEA-4, TRA-1-60).



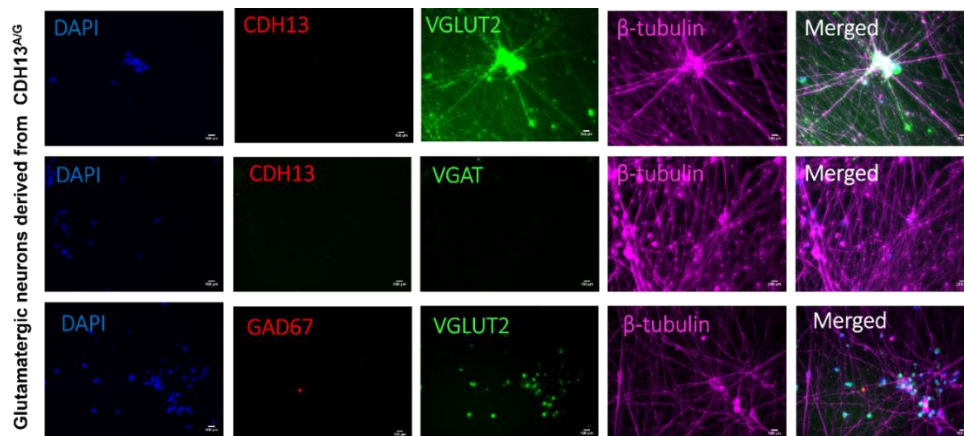
Supplementary figure 2. The absence of Sendai virus-specific transcripts was confirmed by RT-PCR

7.2. Supplementary files: Qualitative characterization of glutamatergic neurons



Supplementary figure 3. Qualitative staining in the pure glutamatergic neuron culture derived from the CDH13^{A/A} iPSC line

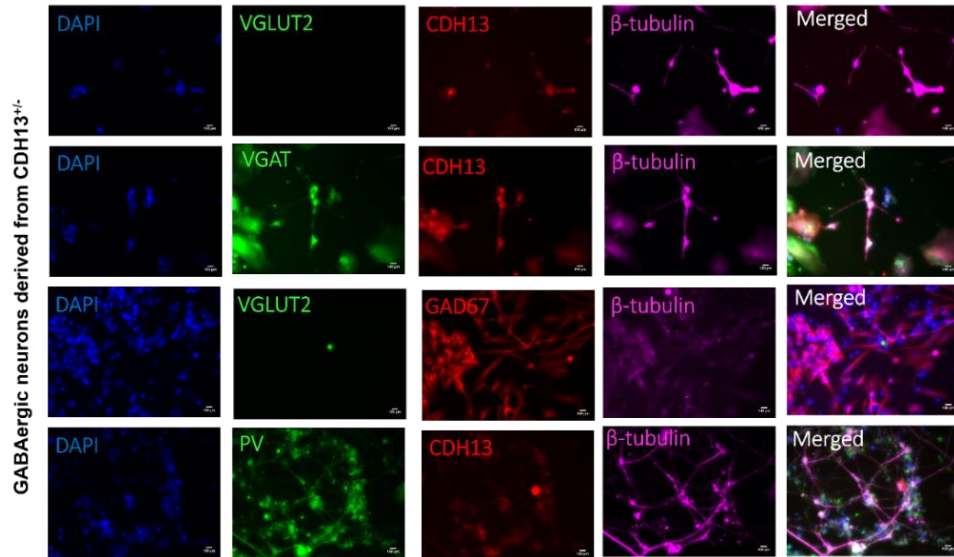
The following specific markers were used: VGLUT2, CDH13, β -tubulin, VGAT, GAD67, and nuclei stained with DAPI. Scale bar 100 μ m.



Supplementary figure 4. Qualitative staining in the pure glutamatergic neuron culture derived from the CDH13^{A/G} iPSC line

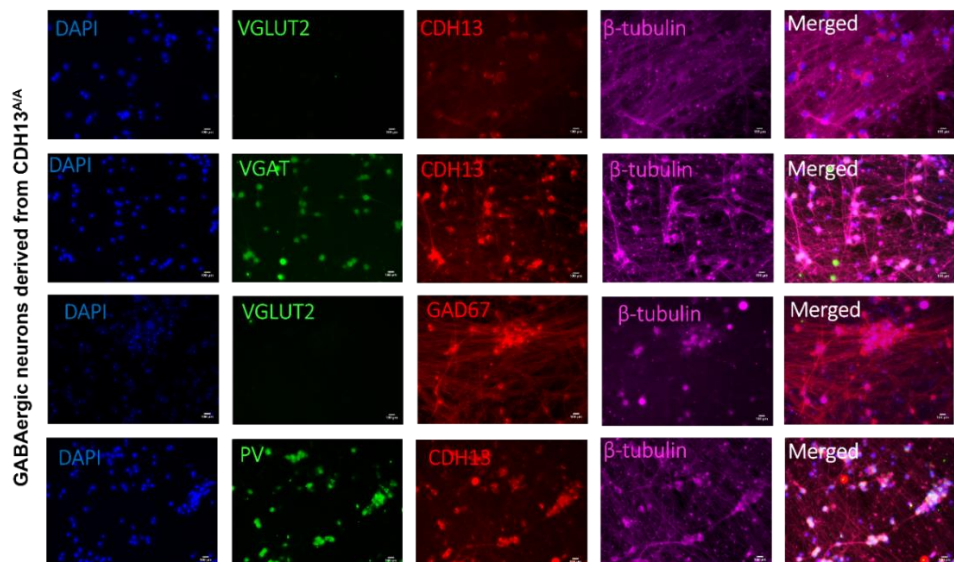
The following specific markers were used: VGLUT2, CDH13, β -tubulin, VGAT, GAD67, and nuclei stained with DAPI. Scale bar: 100 μ m.

7.3. Supplementary files: Qualitative characterization of GABAergic neurons



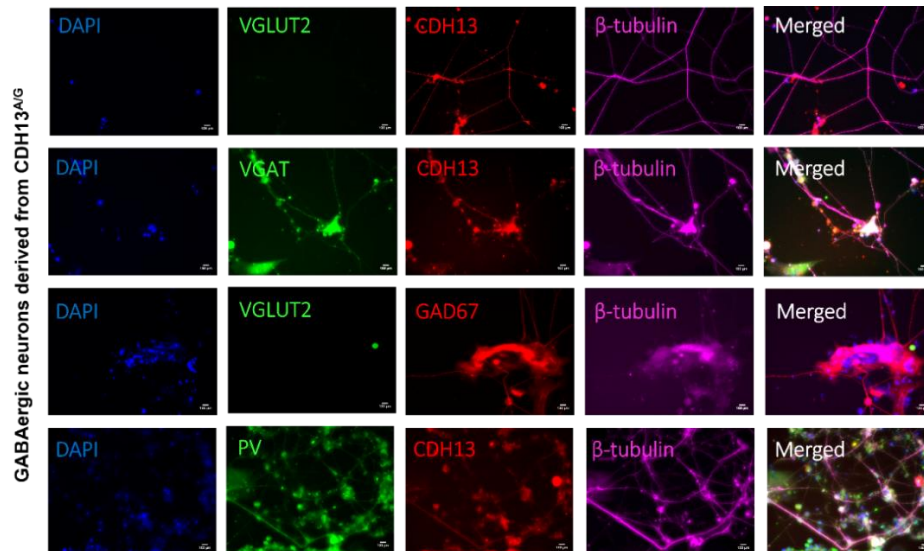
Supplementary figure 5. Qualitative staining in the pure GABAergic neuron culture derived from the *CDH13*^{+/-} iPSC line

The following specific markers were used: VGLUT2, CDH13, β -tubulin, VGAT, GAD67, PV and nuclei stained with DAPI. Scale bar: 100 μ m.



Supplementary figure 6. Qualitative staining in the pure GABAergic neuron culture derived from the *CDH13*^{+A} iPSC line

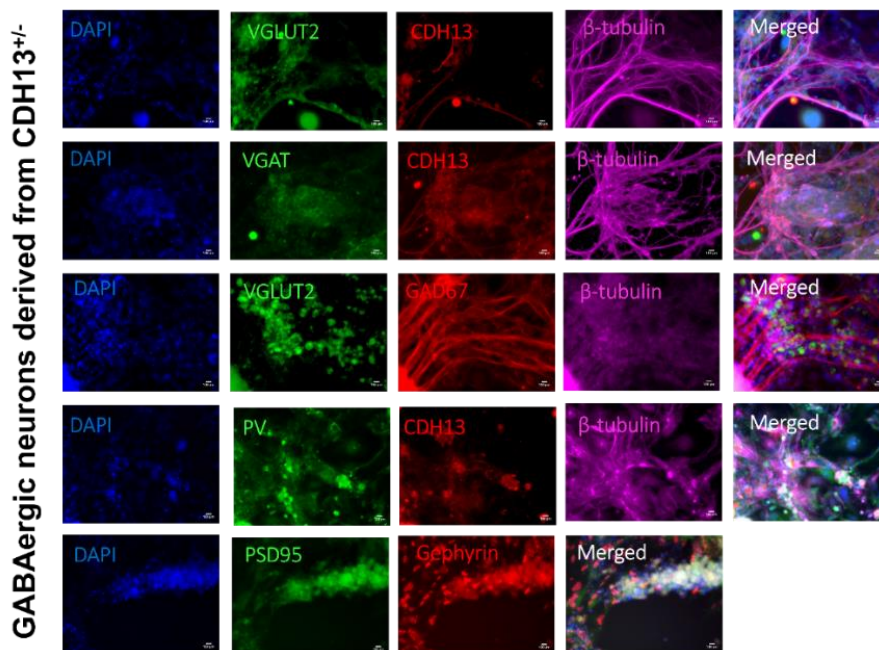
The following specific markers were used: VGLUT2, CDH13, β -tubulin, VGAT, GAD67, PV and nuclei stained with DAPI. Scale bar: 100 μ m.



Supplementary figure 7. Qualitative staining in the pure GABAergic neuron culture derived from the *CDH13*^{ΔG} iPSC line

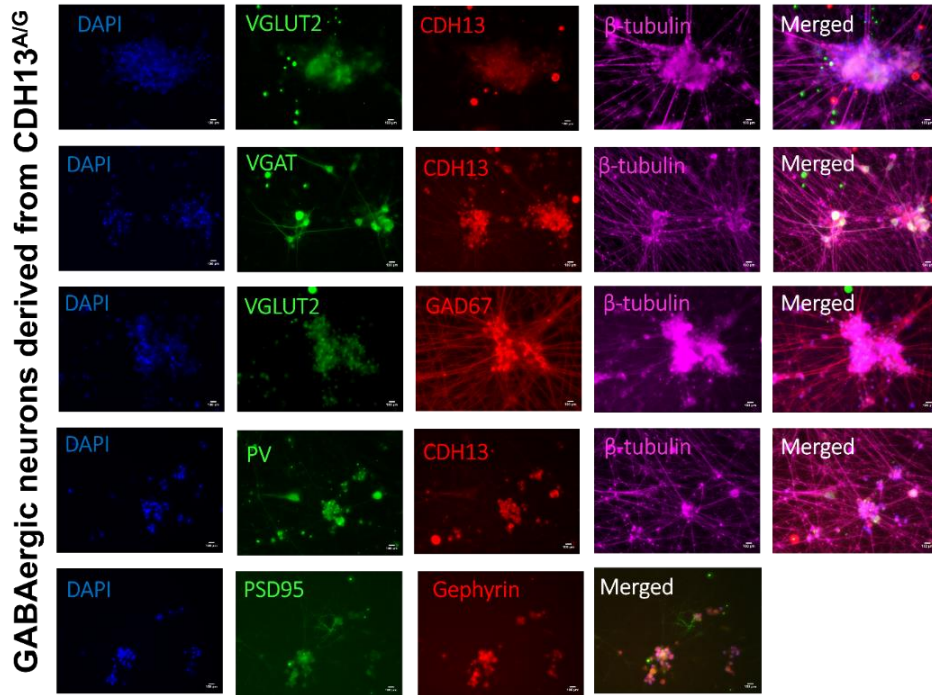
The following specific markers were used: VGLUT2, CDH13, β-tubulin, VGAT, GAD67, PV and nuclei stained with DAPI. Scale bar: 100 μm.

7.4. Supplementary files: Qualitative characterization of co-culture neurons



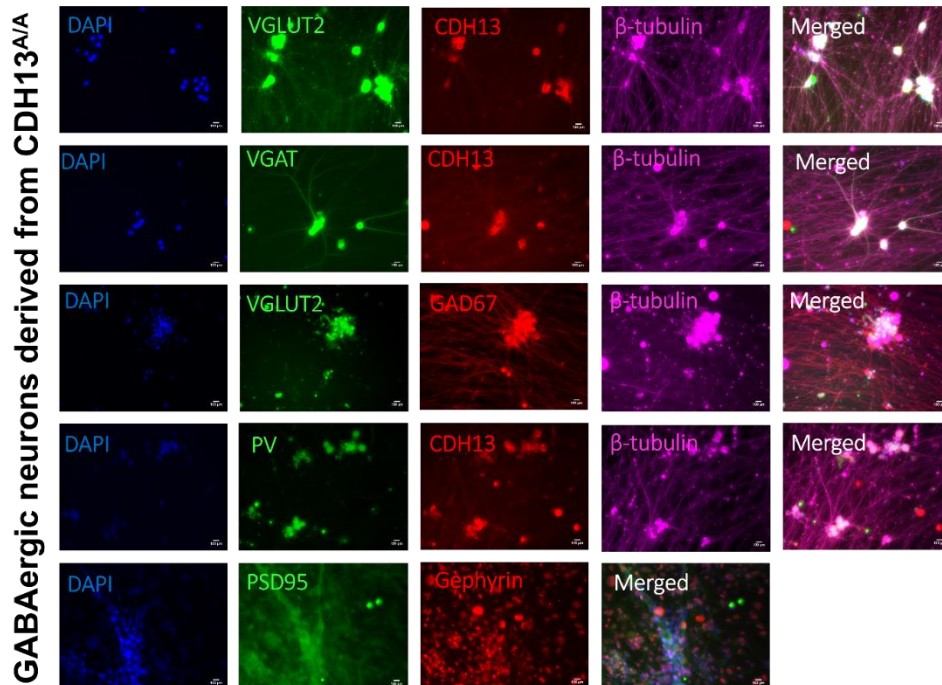
Supplementary figure 8. Qualitative staining in the co-culture derived from the *CDH13*^{-/-} iPSC line

The following specific markers were used: VGLUT2, CDH13, β-tubulin, VGAT, GAD67, PV, Gephyrin, PSD95 and nuclei stained with DAPI. Scale bar 100 μm.



Supplementary figure 9. Qualitative staining in the co-culture derived from the CDH13^{ΔG} iPSC line

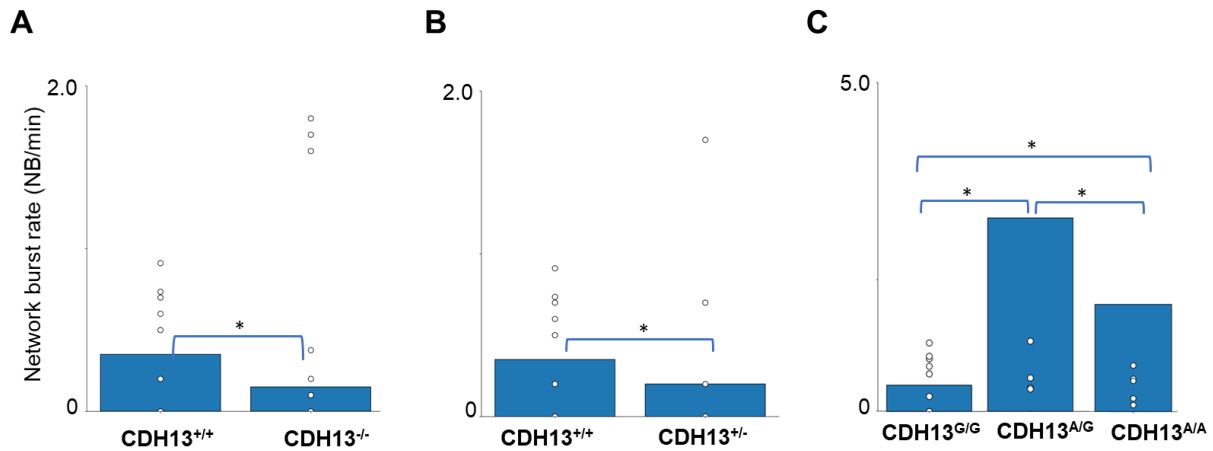
The following specific markers were used: VGLUT2, CDH13, β -tubulin, VGAT, GAD67, PV, Gephyrin, PSD95 and nuclei stained with DAPI. Scale bar 100 μ m.



Supplementary figure 10. Qualitative staining in the co-culture derived from the CDH13^{ΔA} iPSC line

The following specific markers were used: VGLUT2, CDH13, β -tubulin, VGAT, GAD67, PV, Gephyrin, and nuclei stained with DAPI. Scale bar 100 μ m.

7.5 Supplementary file: Network burst rate



Supplementary figure 11. Network burst rate of co-culture networks

Quantification of the average network burst rate in E/I 65:35 networks **A** $CDH13^{+/+}$ $n = 14$, $CDH13^{-/-}$ $n = 12$ individual wells from two neuronal preparations. **B** $CDH13^{+/+}$ $n = 14$, $CDH13^{+/-}$ $n = 9$ individual wells from two neuronal preparations. **C** $CDH13^{G/G}$ $n = 14$, $CDH13^{A/G}$ $n = 6$, $CDH13^{A/A}$ $n = 14$ individual wells from two neuronal preparations ($CDH13^{A/G}$ only one neuronal preparation). Mann–Whitney test with Bonferroni correction was performed. All data represent means \pm SEM. * $p > 0.01$.

7.6 Supplementary file: MEA statistics

		DIV	Mean	SEM	n	p-value
NBD (ms)	$CDH13^{+/+}$ ($CDH13^{G/G}$)	49	0.501	0.028	14	$CDH13^{+/+}$ vs. $CDH13^{-/-}$ =0.00004 (Fig. 32C)
	$CDH13^{A/A}$	49	0.397	0.013	14	
	$CDH13^{A/G}$	49	0.229	0.006	6	$CDH13^{+/+}$ vs. $CDH13^{+/-}$ =0.0007 (Fig. 33C)
	$CDH13^{-/-}$	49	0.198	0.008	12	
	$CDH13^{+/-}$	49	0.177	0.011	9	
						$CDH13^{G/G}$ vs. $CDH13^{A/A}$ =0.0487 (Fig. 34D)
						$CDH13^{G/G}$ vs. $CDH13^{A/G}$ =0.00035e-30 (Fig. 34D)
						$CDH13^{A/G}$ vs. $CDH13^{A/A}$ =0.00041 e-30 (Fig. 34D)
NBR (burst/min)						

	<i>CDH13</i> ^{+/+} (<i>CDH13</i> ^{G/G})	49	0.346	0.093	14	<i>CDH13</i> ^{+/+} vs. <i>CDH13</i> ^{-/-} =0.528 (Suppl. fig 11A)
	<i>CDH13</i> ^{A/A}	49	14.5	12	14	
	<i>CDH13</i> ^{-/-}	49	1.619	1.095	12	<i>CDH13</i> ^{+/+} vs. <i>CDH13</i> ^{+/-} =0.921 (Suppl. fig 11B)
	<i>CDH13</i> ^{+/-}	49	0.388	0.189	9	<i>CDH13</i> ^{A/A} vs. <i>CDH13</i> ^{A/G} = 0.090 (Suppl. fig 11C) <i>CDH13</i> ^{A/A} vs. <i>CDH13</i> ^{G/G} =0.021 (Suppl. fig 11C) <i>CDH13</i> ^{G/G} vs. <i>CDH13</i> ^{A/G} =0.0005 (Suppl. fig 11C)
	<i>CDH13</i> ^{A/G}	49	5.216	0.332	6	

Supplementary table 1. Statistics from figures 32-34 and supplementary figure 11

All data represent means ± SEM. *p > 0.01; **p > 0.001; ***p < 0.001. MEA parameters from *CDH13*^{+/+} vs *CDH13*^{-/-} and *CDH13*^{+/+} vs *CDH13*^{+/-} were compared using Mann-Whitney ranked sum test with post-hoc Bonferroni correction. Kruskal Wallis ANOVA with Dunn's correction for multiple testing was used to compare between *CDH13*^{A/A} vs *CDH13*^{A/G} vs *CDH13*^{G/G}. NBD = Network burst duration, NBR = Network Burst Rate, n = number of wells, DIV = Days in vitro.

7.7. Supplementary file: Cell lines

Cell line	Name	Detail	Unique stem cell lines identifier
Human fibroblast cell lines	CJ1	Control cell line carrying AA variant of <i>CDH13</i> SNP rs2199430	
	CJ2	Control cell line carrying GG variant of <i>CDH13</i> SNP rs2199430	
	CJ3	Control cell line carrying AG variant of <i>CDH13</i> SNP rs2199430	
Human iPS cell lines	CJ1Ci6	Control cell line carrying AA variant of <i>CDH13</i> SNP rs2199430	
	CJ2Ci2	Control cell line carrying GG variant of	

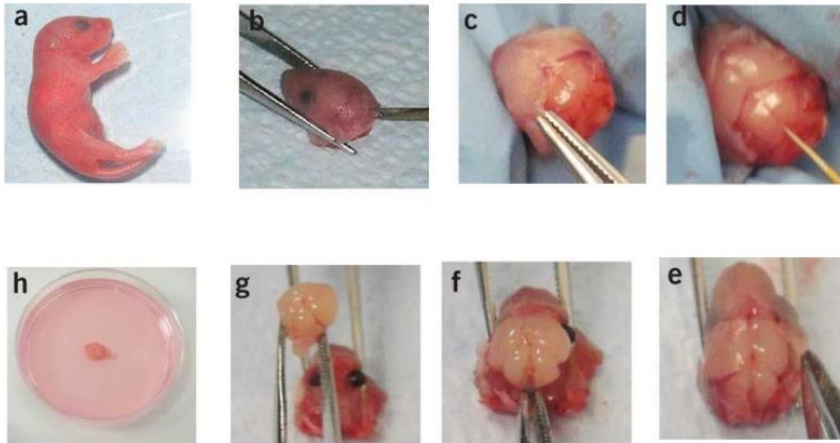
		<i>CDH13</i> SNP rs2199430	UKWMPi002-A
	CJ3CL2	Control cell line carrying AG variant of <i>CDH13</i> SNP rs2199430	
	<i>CDH13</i> ^{-/-}	NM_001257.5: c.[22_25delGTTTC]; [22_23insG]	UKWMPi002-A-2
	<i>CDH13</i> ^{+/+}	NM_001257.5: c. [=]; [13delA]	UKWMPi002-A-1
rtTA/Ngn2-positive iPC lines	<i>CDH13</i> AA rtTA/Ngn2	Integration of rtTA/Ngn2 transgenes into <i>CDH13</i> AA to generate glutamatergic neurons	
	<i>CDH13</i> GG rtTA/Ngn2	Integration of rtTA/Ngn2 transgenes into <i>CDH13</i> GG to generate glutamatergic neurons	
	<i>CDH13</i> AG rtTA/Ngn2	Integration of rtTA/Ngn2 transgenes into <i>CDH13</i> AG to generate glutamatergic neurons	
	<i>CDH13</i> ^{-/-} rtTA/Ngn2	Integration of rtTA/Ngn2 transgenes into <i>CDH13</i> ^{-/-} to generate glutamatergic neurons	
	<i>CDH13</i> ^{+/+} rtTA/Ngn2	Integration of rtTA/Ngn2 transgenes into <i>CDH13</i> ^{+/+} to generate glutamatergic neurons	
rtTa/Ascl1-positive iPC lines	<i>CDH13</i> AA rtTa/Ascl1	Integration of rtTa/Ascl1 transgenes into <i>CDH13</i> AA to generate GABAergic neurons	
	<i>CDH13</i> GG rtTa/Ascl1	Integration of rtTa/Ascl1 transgenes into <i>CDH13</i> GG to	

		generate GABAergic neurons	
	<i>CDH13</i> AG rtTa/Ascl1	Integration of rtTA/Ascl1 transgenes into <i>CDH13</i> AG to generate GABAergic neurons	
	<i>CDH13</i> ^{-/-} rtTa/Ascl1	Integration of rtTA/Ascl1 transgenes into <i>CDH13</i> ^{-/-} to generate GABAergic neurons	
	<i>CDH13</i> ^{+/+} rtTa/Ascl1	Integration of rtTA/Ascl1 transgenes into <i>CDH13</i> ^{+/+} to generate GABAergic neurons	
HEK 293T cells	Human Embryo Kidney Culture	Used for generating Lentivirus	
HELAs	Immortal cell line used in scientific research (Henrietta Lacks)	Used for Western blot and qPCR optimization	
SH-SY5Y	Thrice-subcloned cell line derived from SK-N-SH neuroblastoma cell line.	Used for Western blot and qPCR optimization	
Competent <i>E.coli</i> cells	Escherichia coli	Transformation	New England Biolabs Inc., USA

Supplementary table 2. Cell lines used

7.8. Supplementary file: Astrocyte isolation

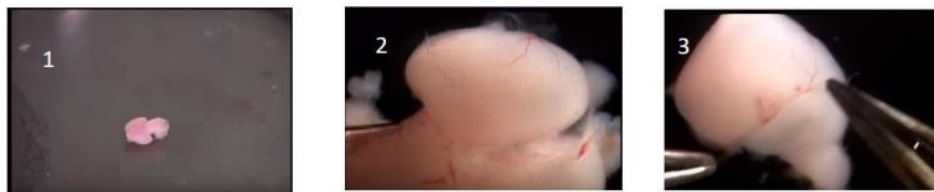
Brain removal



Supplementary figure 12. Stepwise picture showing how the brain was removed

a, b Pups were decapitated, and the head was removed by using a fine scissors. A midline incision at the skin surface close to the hindbrain region was made. **c** The incision was followed to the extreme rostral region. **d** A small incision at the base of the skull was made and it was followed along the midline. **e** The two halves of the skull were separated to reveal the brain. **f** The forceps were gently placed underneath the brain and separated from the underlying tissue. **g, h** The intact brain was gently removed and quickly place it into dissection medium (Beaudoin et al., 2012).

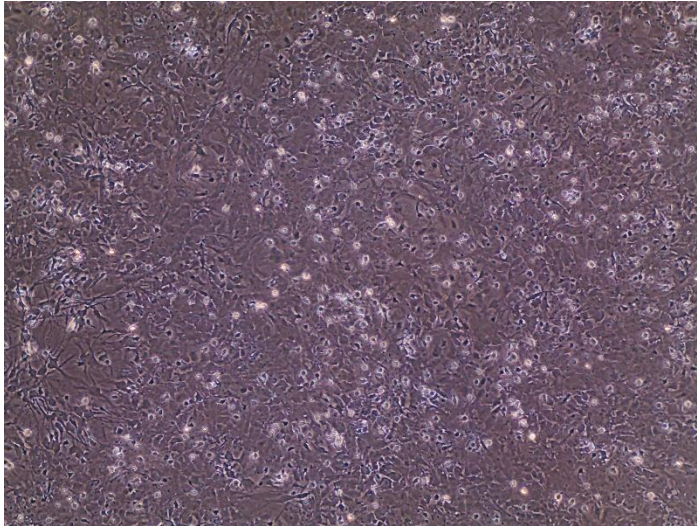
Removal of Meninges



Supplementary figure 13. Stepwise picture showing how the brain was dissected

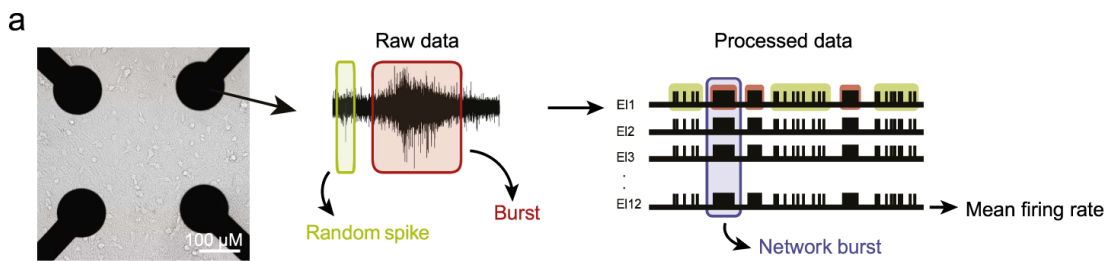
1 The isolated brain is between 0-1cm in size **2** it was placed under a light microscope for the following steps to ensure high work precision. **3** The brain was cleaned by removing the meninges (blood vessels) as these interfere with the astrocytic culture (<https://www.youtube.com/watch?v=eHDapIC6QvY> .This video was made by the Fritschy Lab at the University of Zurich).

Astrocyte culture should form a confluent tessellated monolayer



Supplementary figure 14. Morphology of healthy astrocytic culture

7.9. Supplementary file: Schematic representation of spontaneous electric activity patterns measured on MEAs



Supplementary figure 15 Schematic representation of spontaneous electric activity patterns measured on Mea

Figure taken from (Mossink et al., 2022)

8. Materials

8.1. Cell culture

8.1.1. Cell culture media

Table 15. Cell culture media.

Media	Manufacturer
DMEM/F12	Thermo Fisher Scientific, Waltham, MA, USA
Neurobasal™ Medium	Thermo Fisher Scientific, Waltham, MA, USA
KnockOut™ DMEM/F-12	Thermo Fisher Scientific, Waltham, MA, USA
KnockOut™ DMEM	Thermo Fisher Scientific, Waltham, MA, USA
DMEM, high glucose, GlutaMAX™ Supplement, pyruvate	Thermo Fisher Scientific, Waltham, MA, USA
StemMACS™ iPS-Brew XF, human	Miltenyi Biotec, Bergisch Gladbach Germany
E8 medium	Stemcell Technologies
Neurobasal™ Plus Medium	Life Technologies, Carlsbad, CA, USA
StemMacs™ Trilineage Differentiation kit	Miltenyi Biotec, Bergisch Gladbach, Germany
P3 Primary Cell 4D-Nucleofector™ X Kit L	Lonza Bioscience, Basel, Switzerland
Jetprime® Transfection Kit	Polyplus, Strasbourg, France

8.1.2. Cell culture reagents and supplements

Table 16. Cell culture reagents and supplements

Reagent/Supplement	Manufacturer
Corning® Matrigel® hESCQualified Matrix, *LDEVfree, 5 ml	Corning, NY, USA
Corning® Matrigel® Growth Factor Reduced (GFR) Basement Membrane Matrix, *LDEVfree, 10 ml	Corning, NY, USA
TrypLE™ Express Enzyme (1X), phenol red	Thermo Fisher Scientific, Waltham, MA, USA
GlutaMAX™ Supplement	Thermo Fisher Scientific, Waltham, MA, USA

MEM NEAA, Non Essential Amino Acid Solution (100x) w/o: L-Glutamine	PAN-Biotech, Aidenbach, Germany
2-Mercaptoethanol (50 mM)	Thermo Fisher Scientific, Waltham, MA, USA
Accutase cell detachment solution	Merck Millipore, Darmstadt, Germany
Trypsin-EDTA (0.05%), phenol red	Thermo Fisher Scientific, Waltham, MA, USA
N6,2'-ODibutyryladenine 3',5'- cyclic monophosphate sodium salt (cAMP)	Sigma-Aldrich, St. Louis, MO, USA
StemMACS™ Y27632 (Rock inhibitor)	Miltenyi Biotec, Germany
N-2 Supplement (100X)	Thermo Fisher Scientific, Waltham, MA, USA
B-27™ Supplement (50X), minus vitamin A	Thermo Fisher Scientific, Waltham, MA, USA
B-27™ Supplement (50X), serum free	Thermo Fisher Scientific, Waltham, MA, USA
DPBS, no calcium, no magnesium	Thermo Fisher Scientific, Waltham, MA, USA
Human Recombinant Laminin-511	BioLamina, Sundbyberg, Sweden
Bovine Serum Albumin solution (7.5% in DPBS, sterile-filtered, BioXtra, suitable for cell culture)	Sigma-Aldrich, St. Louis, MO, USA
Fetal bovine serum, qualified, heat inactivated	Thermo Fisher Scientific, Waltham, MA, USA
Poly-L-ornithine solution (mol wt 30,000-70,000, 0.01%, sterile-filtered, BioReagent, suitable for cell culture)	Sigma-Aldrich, St. Louis, MO, USA
L-Ascorbic acid	Sigma-Aldrich, St. Louis, MO, USA
KnockOut™ Serum Replacement	Thermo Fisher Scientific, Waltham, MA, USA
Paraformaldehyde (PFA) Solution 4% (Roti®-Histofix 4 %)	Carl Roth, Karlsruhe, Germany
Trypan Blue solution	Sigma-Aldrich, St. Louis, MO, USA
Triton™ X-100	Sigma-Aldrich, St. Louis, MO, USA
Distilled water (cell culture grade, endotoxin-screened)	Thermo Fisher Scientific, Waltham, MA, USA
Ibidi Mounting Medium	Ibidi, Martinsried, Germany
D-(+)-Glucose solution	Sigma-Aldrich, St. Louis, MO, USA

N-2 Supplement (100X)	Life Technologies, Carlsbad, CA, USA
Basement Membrane Matrix	Life Technologies, Carlsbad, CA, USA
Cell Freezing Medium, serum-free	Sigma-Aldrich, St. Louis, MO, USA
Cryo-Gel – embedding solution	Leica Biosystems, Nussloch, Germany
DMSO (Dimethyl sulfoxide)	Thermo Fisher Scientific, Waltham, MA, USA

8.1.3. Cell culture small molecules and growth factors

Table 17. Small molecules and growth factors.

Small molecule/Growth factor	Manufacturer
CHIR 99021	Axon Medchem, Groningen, The Netherlands
StemMACS™ SB431542	Miltenyi Biotec, Bergisch Gladbach, Germany
Recombinant human/mouse/rat BDNF	Peprtech, Hamburg, Germany
Recombinant human GDNF	Peprtech, Hamburg, Germany
Recombinant human FGF-4	Peprtech, Hamburg, Germany
DMH-1	Tocris Bioscience, Bristol, United Kingdom
RI Y27632	Miltenyi Biotec, Bergisch Gladbach, Germany
Doxycyclin	Sigma-Aldrich, St. Louis, MO, USA
NT-3, human recombinant	Creative Biolabs, NY, USA
Forskolin	Sigma-Aldrich, St. Louis, MO, USA

8.2. Lentivirus reagents

Table 18. Lentivirus reagents.

Name	Manufacturer
psPAX2 lentiviral packaging vector	Addgene, Watertown, MA, USA
pMD2.G lentiviral packaging vector	Addgene, Watertown, MA, USA
Lenti-X™ Concentrator	Takara Bioscience, San Jose, CA, USA
Puromycin	InvivoGen, San Diego, CA, USA

G418	Sigma-Aldrich, St. Louis, MO, USA
Polybrene	Sigma-Aldrich, St. Louis, MO, USA
Primocin (0.1 µg/ml)	InvivoGen, San Diego, USA
Transfer vectors	
pLVX-EF1α-(Tet-On-Advanced)-IRES-G418(R)	Department of Cognitive Neuroscience, Radboudumc, Nijmegen, The Netherlands
pLVX-(TRE-thight) Ngn2-PGK-Puromycin(R)	Department of Cognitive Neuroscience, Radboudumc, Nijmegen, The Netherlands
pLVX- (TRE-thight) - Ascl1-PGK-Puromycin (R)	Department of Cognitive Neuroscience, Radboudumc, Nijmegen, The Netherlands

8.3. Genome editing using CRISPR/Cas9

8.3.1. Kits

Table 19. Kits.

Kit	Manufacturer	Catalogue#
P3 Primary Cell 4D-Nucleofector™ X Kit L	Lonza Bioscience, Basel, Switzerland	V4XP-4024
GeneArt™ Genomic Cleavage Detection Kit	Thermo Fisher Scientific, Waltham, MA, USA	A24372
NEB® PCR Cloning Kit	New England Biolabs, Ipswich, MA, USA	E1202S

8.4. Primary and secondary antibodies

8.4.1. Primary antibodies

Table 20. Primary antibodies.

Name	Manufacturer	Host	Dilution
Anti-OCT-3/4	Santa Cruz Biotechnology Inc, Santa Cruz, Dallas, TX, USA	Mouse	1:50
Anti TRA-1-60	Santa Cruz Biotechnology Inc, Santa Cruz, Dallas, TX, USA	Mouse	1:50
Anti-SSEA-4	Thermo Fisher Scientific, Waltham, MA, USA	Mouse	1:200
Anti-AFP	Dako, Santa Clara, CA, USA	Rabbit	1:400

Anti-SMA	Abcam, Cambridge, United Kingdom	Mouse	1:200
Anti-Pax6	Sigma-Aldrich, St. Louis, MO, USA	Rabbit	1:400
Anti-Sox2	Sigma-Aldrich, St. Louis, MO, USA	Mouse	1:300
Anti-Otx2	Merck Millipore, Darmstadt, Germany	Rabbit	1:500
Anti- β III Tubulin	Promega, Madison, WI, United States	Mouse	1:1000
Human <i>CDH13</i>	R&D Systems, Minneapolis, United States	Goat	1:200
PSD95	Merck Millipore, Darmstadt, Germany	Mouse	1:500
DAPI	Thermo Fisher Scientific, Waltham, MA, USA		300 nM
VGLUT2	Synaptic Systems, Göttingen, Germany		Rabbit 1:500
VGAT	Synaptic Systems, Göttingen, Germany	Rabbit	1:500
Gephyrin	Synaptic Systems, Göttingen, Germany	Mouse	1:500
GAD67	Merck Millipore, Darmstadt, Germany	Mouse	1:50

8.4.2. Secondary antibodies

Table 21. Secondary antibodies

Name	Manufacturer	Host	Dilution
Donkey anti- Mouse IgG (H+L) ReadyProbes™ Secondary Antibody, Alexa Fluor 488	Thermo Fisher Scientific, Waltham, MA, USA	IgG (H&L)	1:400
Donkey anti- Rabbit IgG	Thermo Fisher Scientific, Waltham, MA, USA	IgG (H&L)	1:400
Highly Cross- Adsorbed Secondary Antibody (H+L), Alexa Fluor 555	Thermo Fisher Scientific, Waltham, MA, USA	IgG (H&L)	1:400
Donkey anti-Mouse IgG (H+L) Highly Cross Adsorbed Secondary Antibody, Alexa Fluor Plus 555	Thermo Fisher Scientific, Waltham, MA, USA	IgG (H&L)	1:400
IRDye® 680RD Goat anti-Rabbit IgG (H + L), 0.5 mg	LI-COR®, Bad Homburg, Germany	IgG (H&L)	1:5000
IRDye® 800CW Goat anti-Mouse IgG (H + L), 0.5	LI-COR®, Bad Homburg, Germany	IgG (H&L)	1:5000

mg			
----	--	--	--

8.5. Technical equipment

Table 22. Technical equipment.

Equipment	Manufacturer
Motorized inverted system microscope IX81 X-Cite fluorescence illuminator, XM10 camera	Olympus, Hamburg, Germany
EVOS™ XL Core Configured Microscope with Mechanical Stage	Novus Biologicals, Nordenstadt, Germany
Nucleofector	Lonza Bioscience, Basel, Switzerland, Switzerland
Microelectrode System	Multi channel Systems MCS GmbH, Reutlingen, Germany

8.6. Software

Table 23. Softwares.

Software	Manufacturer
Python3.9	
Multi Channel Experimenter	Multi channel Systems MCS GmbH, Reutlingen, Germany
Multi Channel Analyzer	Multi channel Systems MCS GmbH, Reutlingen, Germany
Multi Channel Data Manager	Multi channel Systems MCS GmbH, Reutlingen, Germany

Appendix

1. List of tables

Table 1. Primers used to sequence exon 1 of <i>CDH13</i>	28
Table 2. sgRNAs used to generate the <i>CDH13</i> knockout (sgRNA #2) and heterozygous (sgRNA #1) iPSC lines.	28
Table 3. Primers used to confirm insertion of sgRNA.....	29
Table 4. Accession number and off-target sequences.	31
Table 5. Primers used to check the off-target sequences.	31
Table 6. Primers used to quantitatively determine pluripotency markers.	32
Table 7. Primers used to confirm absence of CytoTune™ 2.0 reprogramming transgenes...33	
Table 8. Primers for SNP rs2199430 verification.	34
Table 9. Primers used to confirm the presence of rtTA, Ngn2 and ASCL1.....	35
Table 10. Summary of indels on each allele for each CRISPRed clone.....	45
Table 11. Markers to qualitative confirm glutamatergic neuron culture.	56

Table 12. Markers to qualitative confirm GABAergic neuron culture.	57
Table 13. Composition of glutamatergic/GABAergic neuron co-cultures.	59
Table 14. Markers to qualitative confirm glutamatergic/GABAergic neuron co-culture.	59
Table 15. Cell culture media.	84
Table 16. Cell culture reagents and supplements	84
Table 17. Small molecules and growth factors.	86
Table 18. Lentivirus reagents.	86
Table 19. Kits.	87
Table 20. Primary antibodies.	87
Table 21. Secondary antibodies	88
Table 22. Technical equipment.	89
Table 23. Softwares.	89

2. List of figures

Figure 1. Structural domains of <i>CDH13</i>	15
Figure 2. Translocation and processing of <i>CDH13</i>	16
Figure 3. Amino acid sequence of <i>CDH13</i>	17
Figure 4. CRISPR/Cas9 mode of action	21
Figure 5. The physiology of a balanced E/I synapse.	23
Figure 6. Chandelier and Basket neurons acting on Pyramidal cell	24
Figure 7. Start of the open reading frame (NM_001257.5).	41
Figure 8. Colonies start to grow 5 days post nucleofection and monitored up to 10 days	42
Figure 9. Exemplary noisy chromatogram of a CRISPRed colony	43
Figure 10. Growth of colonies in a 96-well format for 14 days.	43
Figure 11. Amplification of CRISPRed clones.	44
Figure 12. Colony PCR confirming the integration of the <i>CDH13</i> insert in the pMiniT 2.0 Vector.	45
Figure 13. Sequences of <i>CDH13</i> ^{+/-} : NM_001257.5: c [=]; [13delA] and <i>CDH13</i> ^{-/-} : NM_001257.5: c.[22_25delGTTTC]; [22_23insG]	46
Figure 14. <i>CDH13</i> protein expression in <i>CDH13</i> ^{+/+} , <i>CDH13</i> ^{+/-} and <i>CDH13</i> ^{-/-} iPSC lines	46
Figure 15. Pluripotent stem cell morphology confirmed in all three-iPSC line	47
Figure 16. Pluripotency and germ layer markers	48
Figure 17. Standard G-banding	48
Figure 18. The absence of Sendai virus-specific transcripts was confirmed by RT-PCR	49
Figure 19. STR analysis	49
Figure 20. Possible off-target effects in each sgRNA.	50
Figure 21. Genotyping of SNP rs2199430	51
Figure 22. rt/TA/NGn2 positive iPSCs showing morphological changes when induced with supplementation of doxycycline.	53
Figure 23. rt/TA/Ascl1 positive iPSCs showing morphological changes when induced with doxycycline/forskolin	54
Figure 24. Presence of rtTA, Ascl1 and Ngn2 vectors in transduced iPSC lines	55
Figure 25. Pluripotency markers	55
Figure 26. Germlayer markers.	56
Figure 27. Qualitative staining in the pure glutamatergic neuron culture derived from the <i>CDH13</i> ^{G/G} iPSC line	57
Figure 28. Qualitative staining in the pure GABAergic culture derived from the <i>CDH13</i> ^{-/-} iPSC line	58

Figure 29. Qualitative staining in the pure GABAergic neuron culture derived from the <i>CDH13</i> ^{G/G} iPSC line	58
Figure 30. Qualitative staining in the co-culture derived from the <i>CDH13</i> ^{G/G} iPSC line.....	60
Figure 31. Qualitative staining in the co-culture derived from the <i>CDH13</i> ^{-/-} iPSC line.....	60
Figure 32. Comparison of <i>CDH13</i> ^{+/+} and <i>CDH13</i> ^{-/-} E/I networks	62
Figure 33. Comparison of <i>CDH13</i> ^{+/+} and <i>CDH13</i> ^{+/-} E/I networks.....	64
Figure 34. Comparison of <i>CDH13</i> ^{G/G} , <i>CDH13</i> ^{A/G} , <i>CDH13</i> ^{A/A} E/I networks.....	66

3. List of supplementary figures

Supplementary figure 1. Germ layer and pluripotency markers	73
Supplementary figure 2. The absence of Sendai virus-specific transcripts was confirmed by RT-PCR.....	73
Supplementary figure 3. Qualitative staining in the pure glutamatergic neuron culture derived from the <i>CDH13</i> ^{A/A} iPSC line.....	74
Supplementary figure 4. Qualitative staining in the pure glutamatergic neuron culture derived from the <i>CDH13</i> ^{A/G} iPSC line	74
Supplementary figure 5. Qualitative staining in the pure GABAergic neuron culture derived from the <i>CDH13</i> ^{+/-} iPSC line	75
Supplementary figure 6. Qualitative staining in the pure GABAergic neuron culture derived from the <i>CDH13</i> ^{A/A} iPSC line.....	75
Supplementary figure 7. Qualitative staining in the pure GABAergic neuron culture derived from the <i>CDH13</i> ^{A/G} iPSC line	76
Supplementary figure 8. Qualitative staining in the co-culture derived from the <i>CDH13</i> ^{+/-} iPSC line	76
Supplementary figure 9. Qualitative staining in the co-culture derived from the <i>CDH13</i> ^{A/G} iPSC line	77
Supplementary figure 10. Qualitative staining in the co-culture derived from the <i>CDH13</i> ^{A/A} iPSC line	77
Supplementary figure 11. Network burst rate of co-culture networks	78
Supplementary figure 12. Stepwise picture showing how the brain was removed.....	82
Supplementary figure 13. Stepwise picture showing how the brain was dissected	82
Supplementary figure 14. Morphology of healthy astrocytic culture	83
Supplementary figure 15 Schematic representation of spontaneous electric activity patterns measured on Mea	83

4. List of supplementary tables

Supplementary table 1. Statistics from figures 32-34 and supplementary figure 11	79
Supplementary table 2. Cell lines used.....	81

References

- Ahn, J. Y. (2014). Neuroprotection signaling of nuclear akt in neuronal cells. *Exp Neurobiol*, 23(3), 200-206. <https://doi.org/10.5607/en.2014.23.3.200>
- Aloy, E. M., Weinmann, O., Pot, C., Kasper, H., Dodd, D. A., Rüllicke, T., Rossi, F., & Schwab, M. E. (2006). Synaptic destabilization by neuronal Nogo-A. *Brain Cell Biol*, 35(2-3), 137-156. <https://doi.org/10.1007/s11068-007-9014-3>
- Anders, C., Niewoehner, O., Duerst, A., & Jinek, M. (2014). Structural basis of PAM-dependent target DNA recognition by the Cas9 endonuclease. *Nature*, 513(7519), 569-573. <https://doi.org/10.1038/nature13579>
- Andreyeva, A., Nieweg, K., Horstmann, K., Klapper, S., Müller-Schiffmann, A., Korth, C., & Gottmann, K. (2012). C-terminal fragment of N-cadherin accelerates synapse destabilization by amyloid- β . *Brain*, 135(Pt 7), 2140-2154. <https://doi.org/10.1093/brain/aws120>
- Arias-Vásquez, A., Altink, M. E., Rommelse, N. N., Slaats-Willemse, D. I., Buschgens, C. J., Fliers, E. A., Faraone, S. V., Sergeant, J. A., Oosterlaan, J., Franke, B., & Buitelaar, J. K. (2011). CDH13 is associated with working memory performance in attention deficit/hyperactivity disorder. *Genes Brain Behav*, 10(8), 844-851. <https://doi.org/10.1111/j.1601-183X.2011.00724.x>
- Autar, K., Guo, X., Rumsey, J. W., Long, C. J., Akanda, N., Jackson, M., Narasimhan, N. S., Caneus, J., Morgan, D., & Hickman, J. J. (2022). A functional hiPSC-cortical neuron differentiation and maturation model and its application to neurological disorders. *Stem Cell Reports*, 17(1), 96-109. <https://doi.org/10.1016/j.stemcr.2021.11.009>
- Baltz, T., de Lima, A. D., & Voigt, T. (2010). Contribution of GABAergic interneurons to the development of spontaneous activity patterns in cultured neocortical networks. *Front Cell Neurosci*, 4, 15. <https://doi.org/10.3389/fncel.2010.00015>
- Barrangou, R., & Doudna, J. A. (2016). Applications of CRISPR technologies in research and beyond. *Nat Biotechnol*, 34(9), 933-941. <https://doi.org/10.1038/nbt.3659>
- Bartos, M., Vida, I., & Jonas, P. (2007). Synaptic mechanisms of synchronized gamma oscillations in inhibitory interneuron networks. *Nat Rev Neurosci*, 8(1), 45-56. <https://doi.org/10.1038/nrn2044>
- Bassett, A. R. (2017). Editing the genome of hiPSC with CRISPR/Cas9: disease models. *Mamm Genome*, 28(7-8), 348-364. <https://doi.org/10.1007/s00335-017-9684-9>
- Beaudoin, G. M., 3rd, Lee, S. H., Singh, D., Yuan, Y., Ng, Y. G., Reichardt, L. F., & Arikath, J. (2012). Culturing pyramidal neurons from the early postnatal mouse hippocampus and cortex. *Nat Protoc*, 7(9), 1741-1754. <https://doi.org/10.1038/nprot.2012.099>
- Becker, S., & Boch, J. (2021). TALE and TALEN genome editing technologies. *Gene and Genome Editing*, 2, 100007. <https://doi.org/https://doi.org/10.1016/j.ggedit.2021.100007>
- Beierlein, M., Gibson, J. R., & Connors, B. W. (2000). A network of electrically coupled interneurons drives synchronized inhibition in neocortex. *Nat Neurosci*, 3(9), 904-910. <https://doi.org/10.1038/78809>
- Bellin, M., Casini, S., Davis, R. P., D'Aniello, C., Haas, J., Ward-van Oostwaard, D., Tertoolen, L. G., Jung, C. B., Elliott, D. A., Welling, A., Laugwitz, K. L., Moretti, A., & Mummery, C. L. (2013). Isogenic human pluripotent stem cell pairs reveal the role of a KCNH2 mutation in long-QT syndrome. *Embo j*, 32(24), 3161-3175. <https://doi.org/10.1038/emboj.2013.240>
- Bennett, E. P., Petersen, B. L., Johansen, I. E., Niu, Y., Yang, Z., Chamberlain, C. A., Met, Ö., Wandall, H. H., & Frödin, M. (2020). INDEL detection, the 'Achilles heel' of precise genome editing: a survey of methods for accurate profiling of gene editing induced indels. *Nucleic Acids Res*, 48(21), 11958-11981. <https://doi.org/10.1093/nar/gkaa975>

- Bhaya, D., Davison, M., & Barrangou, R. (2011). CRISPR-Cas systems in bacteria and archaea: versatile small RNAs for adaptive defense and regulation. *Annu Rev Genet*, *45*, 273-297. <https://doi.org/10.1146/annurev-genet-110410-132430>
- Cao, S. Y., Hu, Y., Chen, C., Yuan, F., Xu, M., Li, Q., Fang, K. H., Chen, Y., & Liu, Y. (2017). Enhanced derivation of human pluripotent stem cell-derived cortical glutamatergic neurons by a small molecule. *Sci Rep*, *7*(1), 3282. <https://doi.org/10.1038/s41598-017-03519-w>
- Carroll, D. (2008). Progress and prospects: zinc-finger nucleases as gene therapy agents. *Gene Ther*, *15*(22), 1463-1468. <https://doi.org/10.1038/gt.2008.145>
- Cencic, R., Miura, H., Malina, A., Robert, F., Ethier, S., Schmeing, T. M., Dostie, J., & Pelletier, J. (2014). Protospacer adjacent motif (PAM)-distal sequences engage CRISPR Cas9 DNA target cleavage. *PLoS One*, *9*(10), e109213. <https://doi.org/10.1371/journal.pone.0109213>
- Chambers, S. M., Fasano, C. A., Papapetrou, E. P., Tomishima, M., Sadelain, M., & Studer, L. (2009). Highly efficient neural conversion of human ES and iPS cells by dual inhibition of SMAD signaling. *Nat Biotechnol*, *27*(3), 275-280. <https://doi.org/10.1038/nbt.1529>
- Chen, C., Rainnie, D. G., Greene, R. W., & Tonegawa, S. (1994). Abnormal fear response and aggressive behavior in mutant mice deficient for alpha-calcium-calmodulin kinase II. *Science*, *266*(5183), 291-294. <https://doi.org/10.1126/science.7939668>
- Chen, C. P., Posy, S., Ben-Shaul, A., Shapiro, L., & Honig, B. H. (2005). Specificity of cell-cell adhesion by classical cadherins: Critical role for low-affinity dimerization through beta-strand swapping. *Proc Natl Acad Sci U S A*, *102*(24), 8531-8536. <https://doi.org/10.1073/pnas.0503319102>
- Ciatto, C., Bahna, F., Zampieri, N., VanSteenhouse, H. C., Katsamba, P. S., Ahlsen, G., Harrison, O. J., Brasch, J., Jin, X., Posy, S., Vendome, J., Ranscht, B., Jessell, T. M., Honig, B., & Shapiro, L. (2010). T-cadherin structures reveal a novel adhesive binding mechanism. *Nat Struct Mol Biol*, *17*(3), 339-347. <https://doi.org/10.1038/nsmb.1781>
- Comings, D. E., & MacMurray, J. P. (2000). Molecular heterosis: a review. *Mol Genet Metab*, *71*(1-2), 19-31. <https://doi.org/10.1006/mgme.2000.3015>
- Cong, L., Ran, F. A., Cox, D., Lin, S., Barretto, R., Habib, N., Hsu, P. D., Wu, X., Jiang, W., Marraffini, L. A., & Zhang, F. (2013). Multiplex genome engineering using CRISPR/Cas systems. *Science*, *339*(6121), 819-823. <https://doi.org/10.1126/science.1231143>
- Culotta, L., & Penzes, P. (2020). Exploring the mechanisms underlying excitation/inhibition imbalance in human iPSC-derived models of ASD. *Mol Autism*, *11*(1), 32. <https://doi.org/10.1186/s13229-020-00339-0>
- Dames, S. A., Bang, E., Haüssinger, D., Ahrens, T., Engel, J., & Grzesiek, S. (2008). Insights into the low adhesive capacity of human T-cadherin from the NMR structure of its N-terminal extracellular domain. *J Biol Chem*, *283*(34), 23485-23495. <https://doi.org/10.1074/jbc.M708335200>
- de Curtis, I. (2008). Functions of Rac GTPases during neuronal development. *Dev Neurosci*, *30*(1-3), 47-58. <https://doi.org/10.1159/000109851>
- de Curtis, I. (2019). The Rac3 GTPase in Neuronal Development, Neurodevelopmental Disorders, and Cancer. *Cells*, *8*(9). <https://doi.org/10.3390/cells8091063>
- Deltcheva, E., Chylinski, K., Sharma, C. M., Gonzales, K., Chao, Y., Pirzada, Z. A., Eckert, M. R., Vogel, J., & Charpentier, E. (2011). CRISPR RNA maturation by trans-encoded small RNA and host factor RNase III. *Nature*, *471*(7340), 602-607. <https://doi.org/10.1038/nature09886>
- Ding, Q., Lee, Y. K., Schaefer, E. A., Peters, D. T., Veres, A., Kim, K., Kuperwasser, N., Motola, D. L., Meissner, T. B., Hendriks, W. T., Trevisan, M., Gupta, R. M., Moisan, A., Banks, E., Friesen, M., Schinzel, R. T., Xia, F., Tang, A., Xia, Y., Figueroa, E., Wann, A., Ahfeldt, T., Daheron, L., Zhang, F., Rubin, L. L., Peng, L. F., Chung, R. T., Musunuru, K., & Cowan, C. A. (2013). A TALEN genome-editing system for

- generating human stem cell-based disease models. *Cell Stem Cell*, 12(2), 238-251. <https://doi.org/10.1016/j.stem.2012.11.011>
- Dovey, H. F., John, V., Anderson, J. P., Chen, L. Z., de Saint Andrieu, P., Fang, L. Y., Freedman, S. B., Folmer, B., Goldbach, E., Holsztynska, E. J., Hu, K. L., Johnson-Wood, K. L., Kennedy, S. L., Kholodenko, D., Knops, J. E., Latimer, L. H., Lee, M., Liao, Z., Lieberburg, I. M., Motter, R. N., Mutter, L. C., Nietz, J., Quinn, K. P., Sacchi, K. L., Seubert, P. A., Shopp, G. M., Thorsett, E. D., Tung, J. S., Wu, J., Yang, S., Yin, C. T., Schenk, D. B., May, P. C., Altstiel, L. D., Bender, M. H., Boggs, L. N., Britton, T. C., Clemens, J. C., Czilli, D. L., Dieckman-McGinty, D. K., Droste, J. J., Fuson, K. S., Gitter, B. D., Hyslop, P. A., Johnstone, E. M., Li, W. Y., Little, S. P., Mabry, T. E., Miller, F. D., & Audia, J. E. (2001). Functional gamma-secretase inhibitors reduce beta-amyloid peptide levels in brain. *J Neurochem*, 76(1), 173-181. <https://doi.org/10.1046/j.1471-4159.2001.00012.x>
- Drgon, T., Montoya, I., Johnson, C., Liu, Q. R., Walther, D., Hamer, D., & Uhl, G. R. (2009). Genome-wide association for nicotine dependence and smoking cessation success in NIH research volunteers. *Mol Med*, 15(1-2), 21-27. <https://doi.org/10.2119/molmed.2008.00096>
- Drgonova, J., Walther, D., Hartstein, G. L., Bukhari, M. O., Baumann, M. H., Katz, J., Hall, F. S., Arnold, E. R., Flax, S., Riley, A., Rivero-Martin, O., Lesch, K. P., Troncoso, J., Ranscht, B., & Uhl, G. R. (2016). Cadherin 13: human cis-regulation and selectively-altered addiction phenotypes and cerebral cortical dopamine in knockout mice. *Mol Med*, 22, 537-547. <https://doi.org/10.2119/molmed.2015.00170>
- Ebato, H., Seyfried, T. N., & Yu, R. K. (1983). Biochemical study of heterosis for brain myelin content in mice. *J Neurochem*, 40(2), 440-446. <https://doi.org/10.1111/j.1471-4159.1983.tb11302.x>
- Eichler, S. A., & Meier, J. C. (2008). E-I balance and human diseases - from molecules to networking. *Front Mol Neurosci*, 1, 2. <https://doi.org/10.3389/neuro.02.002.2008>
- Elitt, M. S., Barbar, L., & Tesar, P. J. (2018). Drug screening for human genetic diseases using iPSC models. *Hum Mol Genet*, 27(R2), R89-r98. <https://doi.org/10.1093/hmg/ddy186>
- Elston, G. N. (2003). Cortex, cognition and the cell: new insights into the pyramidal neuron and prefrontal function. *Cereb Cortex*, 13(11), 1124-1138. <https://doi.org/10.1093/cercor/bhg093>
- Farhy-Tselnicker, I., & Allen, N. J. (2018). Astrocytes, neurons, synapses: a tripartite view on cortical circuit development. *Neural Dev*, 13(1), 7. <https://doi.org/10.1186/s13064-018-0104-y>
- Flahou, C., Morishima, T., Takizawa, H., & Sugimoto, N. (2021). Fit-For-All iPSC-Derived Cell Therapies and Their Evaluation in Humanized Mice With NK Cell Immunity. *Front Immunol*, 12, 662360. <https://doi.org/10.3389/fimmu.2021.662360>
- Forero, A., Ku, H. P., Malpartida, A. B., Wäldchen, S., Alhama-Riba, J., Kulka, C., Aboagye, B., Norton, W. H. J., Young, A. M. J., Ding, Y. Q., Blum, R., Sauer, M., Rivero, O., & Lesch, K. P. (2020). Serotonin (5-HT) neuron-specific inactivation of Cadherin-13 impacts 5-HT system formation and cognitive function. *Neuropharmacology*, 168, 108018. <https://doi.org/10.1016/j.neuropharm.2020.108018>
- Forero, A., Rivero, O., Wäldchen, S., Ku, H. P., Kiser, D. P., Gärtner, Y., Pennington, L. S., Waider, J., Gaspar, P., Jansch, C., Edenhofer, F., Resink, T. J., Blum, R., Sauer, M., & Lesch, K. P. (2017). Cadherin-13 Deficiency Increases Dorsal Raphe 5-HT Neuron Density and Prefrontal Cortex Innervation in the Mouse Brain. *Front Cell Neurosci*, 11, 307. <https://doi.org/10.3389/fncel.2017.00307>
- Franke, B., Neale, B. M., & Faraone, S. V. (2009). Genome-wide association studies in ADHD. *Hum Genet*, 126(1), 13-50. <https://doi.org/10.1007/s00439-009-0663-4>
- Fredette, B. J., Miller, J., & Ranscht, B. (1996). Inhibition of motor axon growth by T-cadherin substrata. *Development*, 122(10), 3163-3171. <https://doi.org/10.1242/dev.122.10.3163>

- Fredette, B. J., & Ranscht, B. (1994). T-cadherin expression delineates specific regions of the developing motor axon-hindlimb projection pathway. *J Neurosci*, *14*(12), 7331-7346. <https://doi.org/10.1523/jneurosci.14-12-07331.1994>
- Frega, M., van Gestel, S. H., Linda, K., van der Raadt, J., Keller, J., Van Rhijn, J. R., Schubert, D., Albers, C. A., & Nadif Kasri, N. (2017). Rapid Neuronal Differentiation of Induced Pluripotent Stem Cells for Measuring Network Activity on Micro-electrode Arrays. *J Vis Exp*(119). <https://doi.org/10.3791/54900>
- Freund, T. F., & Katona, I. (2007). Perisomatic inhibition. *Neuron*, *56*(1), 33-42. <https://doi.org/10.1016/j.neuron.2007.09.012>
- Fritschy, J. M., & Brünig, I. (2003). Formation and plasticity of GABAergic synapses: physiological mechanisms and pathophysiological implications. *Pharmacol Ther*, *98*(3), 299-323. [https://doi.org/10.1016/s0163-7258\(03\)00037-8](https://doi.org/10.1016/s0163-7258(03)00037-8)
- Fu, Y., Foden, J. A., Khayter, C., Maeder, M. L., Reyon, D., Joung, J. K., & Sander, J. D. (2013). High-frequency off-target mutagenesis induced by CRISPR-Cas nucleases in human cells. *Nat Biotechnol*, *31*(9), 822-826. <https://doi.org/10.1038/nbt.2623>
- Fusaki, N., Ban, H., Nishiyama, A., Saeki, K., & Hasegawa, M. (2009). Efficient induction of transgene-free human pluripotent stem cells using a vector based on Sendai virus, an RNA virus that does not integrate into the host genome. *Proc Jpn Acad Ser B Phys Biol Sci*, *85*(8), 348-362. <https://doi.org/10.2183/pjab.85.348>
- Gao, R., & Penzes, P. (2015). Common mechanisms of excitatory and inhibitory imbalance in schizophrenia and autism spectrum disorders. *Curr Mol Med*, *15*(2), 146-167. <https://doi.org/10.2174/1566524015666150303003028>
- Gatto, C. L., & Broadie, K. (2010). Genetic controls balancing excitatory and inhibitory synaptogenesis in neurodevelopmental disorder models. *Front Synaptic Neurosci*, *2*, 4. <https://doi.org/10.3389/fnsyn.2010.00004>
- Geertjens, L., van Voorst, T. W., Bouman, A., van Boven, M. A., Kleefstra, T., Verhage, M., Linkenkaer-Hansen, K., Nadif Kasri, N., Cornelisse, L. N., & Bruining, H. (2022). Following Excitation/Inhibition Ratio Homeostasis from Synapse to EEG in Monogenetic Neurodevelopmental Disorders. *Genes (Basel)*, *13*(2). <https://doi.org/10.3390/genes13020390>
- Gerber, L. D., Kodukula, K., & Udenfriend, S. (1992). Phosphatidylinositol glycan (PI-G) anchored membrane proteins. Amino acid requirements adjacent to the site of cleavage and PI-G attachment in the COOH-terminal signal peptide. *J Biol Chem*, *267*(17), 12168-12173.
- Ghaffari, L. T., Starr, A., Nelson, A. T., & Sattler, R. (2018). Representing Diversity in the Dish: Using Patient-Derived in Vitro Models to Recreate the Heterogeneity of Neurological Disease. *Front Neurosci*, *12*, 56. <https://doi.org/10.3389/fnins.2018.00056>
- González-Burgos, G., Krimer, L. S., Povysheva, N. V., Barrionuevo, G., & Lewis, D. A. (2005). Functional properties of fast spiking interneurons and their synaptic connections with pyramidal cells in primate dorsolateral prefrontal cortex. *J Neurophysiol*, *93*(2), 942-953. <https://doi.org/10.1152/jn.00787.2004>
- Gorlova, O., Fedorov, A., Logothetis, C., Amos, C., & Gorlov, I. (2014). Genes with a large intronic burden show greater evolutionary conservation on the protein level. *BMC Evol Biol*, *14*(1), 50. <https://doi.org/10.1186/1471-2148-14-50>
- Govek, E. E., Newey, S. E., & Van Aelst, L. (2005). The role of the Rho GTPases in neuronal development. *Genes Dev*, *19*(1), 1-49. <https://doi.org/10.1101/gad.1256405>
- Guhr, A., Kobold, S., Seltmann, S., Seiler Wulczyn, A. E. M., Kurtz, A., & Löser, P. (2018). Recent Trends in Research with Human Pluripotent Stem Cells: Impact of Research and Use of Cell Lines in Experimental Research and Clinical Trials. *Stem Cell Reports*, *11*(2), 485-496. <https://doi.org/10.1016/j.stemcr.2018.06.012>
- Gulyás, A. I., Megias, M., Emri, Z., & Freund, T. F. (1999). Total number and ratio of excitatory and inhibitory synapses converging onto single interneurons of different

- types in the CA1 area of the rat hippocampus. *J Neurosci*, 19(22), 10082-10097. <https://doi.org/10.1523/jneurosci.19-22-10082.1999>
- Gumbiner, B. M. (2005). Regulation of cadherin-mediated adhesion in morphogenesis. *Nat Rev Mol Cell Biol*, 6(8), 622-634. <https://doi.org/10.1038/nrm1699>
- Halevy, T., Czech, C., & Benvenisty, N. (2015). Molecular mechanisms regulating the defects in fragile X syndrome neurons derived from human pluripotent stem cells. *Stem Cell Reports*, 4(1), 37-46. <https://doi.org/10.1016/j.stemcr.2014.10.015>
- Harrison, O. J., Bahna, F., Katsamba, P. S., Jin, X., Brasch, J., Vendome, J., Ahlsen, G., Carroll, K. J., Price, S. R., Honig, B., & Shapiro, L. (2010). Two-step adhesive binding by classical cadherins. *Nat Struct Mol Biol*, 17(3), 348-357. <https://doi.org/10.1038/nsmb.1784>
- He, Y., Xu, T., Zhang, W., & Zuo, X. N. (2016). Lifespan anxiety is reflected in human amygdala cortical connectivity. *Hum Brain Mapp*, 37(3), 1178-1193. <https://doi.org/10.1002/hbm.23094>
- Hirano, S., & Takeichi, M. (2012). Cadherins in brain morphogenesis and wiring. *Physiol Rev*, 92(2), 597-634. <https://doi.org/10.1152/physrev.00014.2011>
- Horii, T., Tamura, D., Morita, S., Kimura, M., & Hatada, I. (2013). Generation of an ICF syndrome model by efficient genome editing of human induced pluripotent stem cells using the CRISPR system. *Int J Mol Sci*, 14(10), 19774-19781. <https://doi.org/10.3390/ijms141019774>
- Howard, D. M., Adams, M. J., Clarke, T. K., Hafferty, J. D., Gibson, J., Shirali, M., Coleman, J. R. I., Hagenars, S. P., Ward, J., Wigmore, E. M., Alloza, C., Shen, X., Barbu, M. C., Xu, E. Y., Whalley, H. C., Marioni, R. E., Porteous, D. J., Davies, G., Deary, I. J., Hemani, G., Berger, K., Teismann, H., Rawal, R., Arold, V., Baune, B. T., Dannlowski, U., Domschke, K., Tian, C., Hinds, D. A., Trzaskowski, M., Byrne, E. M., Ripke, S., Smith, D. J., Sullivan, P. F., Wray, N. R., Breen, G., Lewis, C. M., & McIntosh, A. M. (2019). Genome-wide meta-analysis of depression identifies 102 independent variants and highlights the importance of the prefrontal brain regions. *Nat Neurosci*, 22(3), 343-352. <https://doi.org/10.1038/s41593-018-0326-7>
- Hsu, P. D., Scott, D. A., Weinstein, J. A., Ran, F. A., Konermann, S., Agarwala, V., Li, Y., Fine, E. J., Wu, X., Shalem, O., Cradick, T. J., Marraffini, L. A., Bao, G., & Zhang, F. (2013). DNA targeting specificity of RNA-guided Cas9 nucleases. *Nat Biotechnol*, 31(9), 827-832. <https://doi.org/10.1038/nbt.2647>
- Huntley, G. W., Gil, O., & Bozdagi, O. (2002). The cadherin family of cell adhesion molecules: multiple roles in synaptic plasticity. *Neuroscientist*, 8(3), 221-233. <https://doi.org/10.1177/1073858402008003008>
- Jang, S., Lee, H., & Kim, E. (2017). Synaptic adhesion molecules and excitatory synaptic transmission. *Curr Opin Neurobiol*, 45, 45-50. <https://doi.org/10.1016/j.conb.2017.03.005>
- Jimbo, Y., Kawana, A., Parodi, P., & Torre, V. (2000). The dynamics of a neuronal culture of dissociated cortical neurons of neonatal rats. *Biol Cybern*, 83(1), 1-20. <https://doi.org/10.1007/pl00007970>
- Jinek, M., Chylinski, K., Fonfara, I., Hauer, M., Doudna, J. A., & Charpentier, E. (2012). A programmable dual-RNA-guided DNA endonuclease in adaptive bacterial immunity. *Science*, 337(6096), 816-821. <https://doi.org/10.1126/science.1225829>
- Johnson, C., Drgon, T., Walther, D., & Uhl, G. R. (2011). Genomic regions identified by overlapping clusters of nominally-positive SNPs from genome-wide studies of alcohol and illegal substance dependence. *PLoS One*, 6(7), e19210. <https://doi.org/10.1371/journal.pone.0019210>
- Joshi, M. B., Ivanov, D., Philippova, M., Erne, P., & Resink, T. J. (2007). Integrin-linked kinase is an essential mediator for T-cadherin-dependent signaling via Akt and GSK3beta in endothelial cells. *Faseb j*, 21(12), 3083-3095. <https://doi.org/10.1096/fj.06-7723com>

- Joshi, M. B., Philippova, M., Ivanov, D., Allenspach, R., Erne, P., & Resink, T. J. (2005). T-cadherin protects endothelial cells from oxidative stress-induced apoptosis. *FASEB J*, *19*(12), 1737-1739. <https://doi.org/10.1096/fj.05-3834fje>
- Kawaguchi, Y. (1995). Physiological subgroups of nonpyramidal cells with specific morphological characteristics in layer II/III of rat frontal cortex. *J Neurosci*, *15*(4), 2638-2655. <https://doi.org/10.1523/jneurosci.15-04-02638.1995>
- Kilpinen, H., Goncalves, A., Leha, A., Afzal, V., Alasoo, K., Ashford, S., Bala, S., Bensaddek, D., Casale, F. P., Culley, O. J., Danecek, P., Faulconbridge, A., Harrison, P. W., Kathuria, A., McCarthy, D., McCarthy, S. A., Meleckyte, R., Memari, Y., Moens, N., Soares, F., Mann, A., Streeter, I., Agu, C. A., Alderton, A., Nelson, R., Harper, S., Patel, M., White, A., Patel, S. R., Clarke, L., Halai, R., Kirton, C. M., Kolb-Kokocinski, A., Beales, P., Birney, E., Danovi, D., Lamond, A. I., Ouweland, W. H., Vallier, L., Watt, F. M., Durbin, R., Stegle, O., & Gaffney, D. J. (2017). Common genetic variation drives molecular heterogeneity in human iPSCs. *Nature*, *546*(7658), 370-375. <https://doi.org/10.1038/nature22403>
- Kim, C. (2015). iPSC technology--Powerful hand for disease modeling and therapeutic screen. *BMB Rep*, *48*(5), 256-265. <https://doi.org/10.5483/bmbrep.2015.48.5.100>
- Kim, H. S., Bernitz, J. M., Lee, D. F., & Lemischka, I. R. (2014). Genomic editing tools to model human diseases with isogenic pluripotent stem cells. *Stem Cells Dev*, *23*(22), 2673-2686. <https://doi.org/10.1089/scd.2014.0167>
- Kim, W. S., Shen, G., Liu, C., Kang, N. I., Lee, K. H., Sui, J., & Chung, Y. C. (2020). Altered amygdala-based functional connectivity in individuals with attenuated psychosis syndrome and first-episode schizophrenia. *Sci Rep*, *10*(1), 17711. <https://doi.org/10.1038/s41598-020-74771-w>
- Kinoshita, T. (2020). Biosynthesis and biology of mammalian GPI-anchored proteins. *Open Biol*, *10*(3), 190290. <https://doi.org/10.1098/rsob.190290>
- Lasky-Su, J., Neale, B. M., Franke, B., Anney, R. J., Zhou, K., Maller, J. B., Vasquez, A. A., Chen, W., Asherson, P., Buitelaar, J., Banaschewski, T., Ebstein, R., Gill, M., Miranda, A., Mulas, F., Oades, R. D., Roeyers, H., Rothenberger, A., Sergeant, J., Sonuga-Barke, E., Steinhausen, H. C., Taylor, E., Daly, M., Laird, N., Lange, C., & Faraone, S. V. (2008). Genome-wide association scan of quantitative traits for attention deficit hyperactivity disorder identifies novel associations and confirms candidate gene associations. *Am J Med Genet B Neuropsychiatr Genet*, *147b*(8), 1345-1354. <https://doi.org/10.1002/ajmg.b.30867>
- Lee, S. W. (1996). H-cadherin, a novel cadherin with growth inhibitory functions and diminished expression in human breast cancer. *Nat Med*, *2*(7), 776-782. <https://doi.org/10.1038/nm0796-776>
- Lesch, K. P., Timmesfeld, N., Renner, T. J., Halperin, R., Röser, C., Nguyen, T. T., Craig, D. W., Romanos, J., Heine, M., Meyer, J., Freitag, C., Warnke, A., Romanos, M., Schäfer, H., Walitza, S., Reif, A., Stephan, D. A., & Jacob, C. (2008). Molecular genetics of adult ADHD: converging evidence from genome-wide association and extended pedigree linkage studies. *J Neural Transm (Vienna)*, *115*(11), 1573-1585. <https://doi.org/10.1007/s00702-008-0119-3>
- Lewis, D. A., & Lund, J. S. (1990). Heterogeneity of chandelier neurons in monkey neocortex: corticotropin-releasing factor- and parvalbumin-immunoreactive populations. *J Comp Neurol*, *293*(4), 599-615. <https://doi.org/10.1002/cne.902930406>
- Li, K. T., Liang, J., & Zhou, C. (2021). Gamma Oscillations Facilitate Effective Learning in Excitatory-Inhibitory Balanced Neural Circuits. *Neural Plast*, *2021*, 6668175. <https://doi.org/10.1155/2021/6668175>
- LiCausi, F., & Hartman, N. W. (2018). Role of mTOR Complexes in Neurogenesis. *Int J Mol Sci*, *19*(5). <https://doi.org/10.3390/ijms19051544>
- Little, K. Y., McLaughlin, D. P., Zhang, L., Livermore, C. S., Dalack, G. W., McFinton, P. R., DelProposto, Z. S., Hill, E., Cassin, B. J., Watson, S. J., & Cook, E. H. (1998). Cocaine, ethanol, and genotype effects on human midbrain serotonin transporter

- binding sites and mRNA levels. *Am J Psychiatry*, 155(2), 207-213.
<https://doi.org/10.1176/ajp.155.2.207>
- Liu, G. (2004). Local structural balance and functional interaction of excitatory and inhibitory synapses in hippocampal dendrites. *Nat Neurosci*, 7(4), 373-379.
<https://doi.org/10.1038/nn1206>
- Liu, Z. Q., Mahmood, T., & Yang, P. C. (2014). Western blot: technique, theory and trouble shooting. *N Am J Med Sci*, 6(3), 160. <https://doi.org/10.4103/1947-2714.128482>
- Ma, Y., Zhang, L., & Huang, X. (2014). Genome modification by CRISPR/Cas9. *Febs j*, 281(23), 5186-5193. <https://doi.org/10.1111/febs.13110>
- Mali, P., Aach, J., Stranges, P. B., Esvelt, K. M., Moosburner, M., Kosuri, S., Yang, L., & Church, G. M. (2013). CAS9 transcriptional activators for target specificity screening and paired nickases for cooperative genome engineering. *Nat Biotechnol*, 31(9), 833-838. <https://doi.org/10.1038/nbt.2675>
- Mariani, J., Coppola, G., Zhang, P., Abyzov, A., Provini, L., Tomasini, L., Amenduni, M., Szekely, A., Palejev, D., Wilson, M., Gerstein, M., Grigorenko, E. L., Chawarska, K., Pelphrey, K. A., Howe, J. R., & Vaccarino, F. M. (2015). FOXP1-Dependent Dysregulation of GABA/Glutamate Neuron Differentiation in Autism Spectrum Disorders. *Cell*, 162(2), 375-390. <https://doi.org/10.1016/j.cell.2015.06.034>
- Markram, H., Toledo-Rodriguez, M., Wang, Y., Gupta, A., Silberberg, G., & Wu, C. (2004). Interneurons of the neocortical inhibitory system. *Nat Rev Neurosci*, 5(10), 793-807.
<https://doi.org/10.1038/nrn1519>
- Mavroconstanti, T., Johansson, S., Winge, I., Knappskog, P. M., & Haavik, J. (2013). Functional properties of rare missense variants of human CDH13 found in adult attention deficit/hyperactivity disorder (ADHD) patients. *PLoS One*, 8(8), e71445.
<https://doi.org/10.1371/journal.pone.0071445>
- McDonald, A. J. (1992). Projection neurons of the basolateral amygdala: a correlative Golgi and retrograde tract tracing study. *Brain Res Bull*, 28(2), 179-185.
[https://doi.org/10.1016/0361-9230\(92\)90177-y](https://doi.org/10.1016/0361-9230(92)90177-y)
- Megias, M., Emri, Z., Freund, T. F., & Gulyás, A. I. (2001). Total number and distribution of inhibitory and excitatory synapses on hippocampal CA1 pyramidal cells. *Neuroscience*, 102(3), 527-540. [https://doi.org/10.1016/s0306-4522\(00\)00496-6](https://doi.org/10.1016/s0306-4522(00)00496-6)
- Moreno-Mateos, M. A., Vejnar, C. E., Beaudoin, J. D., Fernandez, J. P., Mis, E. K., Khokha, M. K., & Giraldez, A. J. (2015). CRISPRscan: designing highly efficient sgRNAs for CRISPR-Cas9 targeting in vivo. *Nat Methods*, 12(10), 982-988.
<https://doi.org/10.1038/nmeth.3543>
- Mossink, B., van Rhijn, J. R., Wang, S., Linda, K., Vitale, M. R., Zöller, J. E. M., van Hugte, E. J. H., Bak, J., Verboven, A. H. A., Selten, M., Negwer, M., Latour, B. L., van der Werf, I., Keller, J. M., Klein Gunnewiek, T. M., Schoenmaker, C., Oudakker, A., Anania, A., Jansen, S., Lesch, K. P., Frega, M., van Bokhoven, H., Schubert, D., & Nadif Kasri, N. (2022). Cadherin-13 is a critical regulator of GABAergic modulation in human stem-cell-derived neuronal networks. *Mol Psychiatry*, 27(1), 1-18.
<https://doi.org/10.1038/s41380-021-01117-x>
- Muller, J. F., Mascagni, F., & McDonald, A. J. (2006). Pyramidal cells of the rat basolateral amygdala: synaptology and innervation by parvalbumin-immunoreactive interneurons. *J Comp Neurol*, 494(4), 635-650. <https://doi.org/10.1002/cne.20832>
- Nair, V., Sankaranarayanan, R., & Vasavada, A. R. (2021). Deciphering the association of intronic single nucleotide polymorphisms of crystallin gene family with congenital cataract. *Indian J Ophthalmol*, 69(8), 2064-2070.
https://doi.org/10.4103/ijo.IJO_3062_20
- Neale, B. M., Medland, S., Ripke, S., Anney, R. J., Asherson, P., Buitelaar, J., Franke, B., Gill, M., Kent, L., Holmans, P., Middleton, F., Thapar, A., Lesch, K. P., Faraone, S. V., Daly, M., Nguyen, T. T., Schäfer, H., Steinhausen, H. C., Reif, A., Renner, T. J., Romanos, M., Romanos, J., Warnke, A., Walitza, S., Freitag, C., Meyer, J., Palmason, H., Rothenberger, A., Hawi, Z., Sergeant, J., Roeyers, H., Mick, E., &

- Biederman, J. (2010). Case-control genome-wide association study of attention-deficit/hyperactivity disorder. *J Am Acad Child Adolesc Psychiatry*, 49(9), 906-920. <https://doi.org/10.1016/j.jaac.2010.06.007>
- Neely, M. D., Litt, M. J., Tidball, A. M., Li, G. G., Aboud, A. A., Hopkins, C. R., Chamberlin, R., Hong, C. C., Ess, K. C., & Bowman, A. B. (2012). DMH1, a highly selective small molecule BMP inhibitor promotes neurogenesis of hiPSCs: comparison of PAX6 and SOX1 expression during neural induction. *ACS Chem Neurosci*, 3(6), 482-491. <https://doi.org/10.1021/cn300029t>
- Nicoleau, C., Varela, C., Bonnefond, C., Maury, Y., Bugi, A., Aubry, L., Viegas, P., Bourgois-Rocha, F., Peschanski, M., & Perrier, A. L. (2013). Embryonic stem cells neural differentiation qualifies the role of Wnt/ β -Catenin signals in human telencephalic specification and regionalization. *Stem Cells*, 31(9), 1763-1774. <https://doi.org/10.1002/stem.1462>
- Nitsche, M. A., Cohen, L. G., Wassermann, E. M., Priori, A., Lang, N., Antal, A., Paulus, W., Hummel, F., Boggio, P. S., Fregni, F., & Pascual-Leone, A. (2008). Transcranial direct current stimulation: State of the art 2008. *Brain Stimul*, 1(3), 206-223. <https://doi.org/10.1016/j.brs.2008.06.004>
- Nitsche, M. A., & Paulus, W. (2000). Excitability changes induced in the human motor cortex by weak transcranial direct current stimulation. *J Physiol*, 527 Pt 3(Pt 3), 633-639. <https://doi.org/10.1111/j.1469-7793.2000.t01-1-00633.x>
- Norgaard, S., & Pocock, R. (2019). Rac GTPases: domain-specific functions in neuronal development. *Neural Regen Res*, 14(8), 1367-1368. <https://doi.org/10.4103/1673-5374.253515>
- Otsuka, I., Watanabe, Y., Hishimoto, A., Boku, S., Mouri, K., Shirowa, K., Okazaki, S., Nunokawa, A., Shirakawa, O., Someya, T., & Sora, I. (2015). Association analysis of the Cadherin13 gene with schizophrenia in the Japanese population. *Neuropsychiatr Dis Treat*, 11, 1381-1393. <https://doi.org/10.2147/ndt.S84736>
- Paradis, S., Harrar, D. B., Lin, Y., Koon, A. C., Hauser, J. L., Griffith, E. C., Zhu, L., Brass, L. F., Chen, C., & Greenberg, M. E. (2007). An RNAi-based approach identifies molecules required for glutamatergic and GABAergic synapse development. *Neuron*, 53(2), 217-232. <https://doi.org/10.1016/j.neuron.2006.12.012>
- Parenti, I., Rabaneda, L. G., Schoen, H., & Novarino, G. (2020). Neurodevelopmental Disorders: From Genetics to Functional Pathways. *Trends Neurosci*, 43(8), 608-621. <https://doi.org/10.1016/j.tins.2020.05.004>
- Penzes, P., Cahill, M. E., Jones, K. A., VanLeeuwen, J. E., & Woolfrey, K. M. (2011). Dendritic spine pathology in neuropsychiatric disorders. *Nat Neurosci*, 14(3), 285-293. <https://doi.org/10.1038/nn.2741>
- Philippova, M., Ivanov, D., Joshi, M. B., Kyriakakis, E., Rupp, K., Afonyushkin, T., Bochkov, V., Erne, P., & Resink, T. J. (2008). Identification of proteins associating with glycosylphosphatidylinositol- anchored T-cadherin on the surface of vascular endothelial cells: role for Grp78/BiP in T-cadherin-dependent cell survival. *Mol Cell Biol*, 28(12), 4004-4017. <https://doi.org/10.1128/mcb.00157-08>
- Pokutta, S., Herrenknecht, K., Kemler, R., & Engel, J. (1994). Conformational changes of the recombinant extracellular domain of E-cadherin upon calcium binding. *Eur J Biochem*, 223(3), 1019-1026. <https://doi.org/10.1111/j.1432-1033.1994.tb19080.x>
- Popp, B., Krumbiegel, M., Grosch, J., Sommer, A., Uebe, S., Kohl, Z., Plötz, S., Farrell, M., Trautmann, U., Kraus, C., Ekici, A. B., Asadollahi, R., Regensburger, M., Günther, K., Rauch, A., Edenhofer, F., Winkler, J., Winner, B., & Reis, A. (2018). Need for high-resolution Genetic Analysis in iPSC: Results and Lessons from the ForIPS Consortium. *Sci Rep*, 8(1), 17201. <https://doi.org/10.1038/s41598-018-35506-0>
- Prata, D. P., Costa-Neves, B., Cosme, G., & Vassos, E. (2019). Unravelling the genetic basis of schizophrenia and bipolar disorder with GWAS: A systematic review. *J Psychiatr Res*, 114, 178-207. <https://doi.org/10.1016/j.jpsychires.2019.04.007>

- Qi, Y., Zhang, X. J., Renier, N., Wu, Z., Atkin, T., Sun, Z., Ozair, M. Z., Tchieu, J., Zimmer, B., Fattahi, F., Ganat, Y., Azevedo, R., Zeltner, N., Brivanlou, A. H., Karayiorgou, M., Gogos, J., Tomishima, M., Tessier-Lavigne, M., Shi, S. H., & Studer, L. (2017). Combined small-molecule inhibition accelerates the derivation of functional cortical neurons from human pluripotent stem cells. *Nat Biotechnol*, *35*(2), 154-163. <https://doi.org/10.1038/nbt.3777>
- Ran, F. A., Hsu, P. D., Wright, J., Agarwala, V., Scott, D. A., & Zhang, F. (2013). Genome engineering using the CRISPR-Cas9 system. *Nat Protoc*, *8*(11), 2281-2308. <https://doi.org/10.1038/nprot.2013.143>
- Ranscht, B. (1994). Cadherins and catenins: interactions and functions in embryonic development. *Curr Opin Cell Biol*, *6*(5), 740-746. [https://doi.org/10.1016/0955-0674\(94\)90102-3](https://doi.org/10.1016/0955-0674(94)90102-3)
- Ranscht, B., & Dours-Zimmermann, M. T. (1991). T-cadherin, a novel cadherin cell adhesion molecule in the nervous system lacks the conserved cytoplasmic region. *Neuron*, *7*(3), 391-402. [https://doi.org/10.1016/0896-6273\(91\)90291-7](https://doi.org/10.1016/0896-6273(91)90291-7)
- Rayner, E., Durin, M. A., Thomas, R., Moralli, D., O'Cathail, S. M., Tomlinson, I., Green, C. M., & Lewis, A. (2019). CRISPR-Cas9 Causes Chromosomal Instability and Rearrangements in Cancer Cell Lines, Detectable by Cytogenetic Methods. *Crispr j*, *2*(6), 406-416. <https://doi.org/10.1089/crispr.2019.0006>
- Read, D. E., & Gorman, A. M. (2009). Involvement of Akt in neurite outgrowth. *Cell Mol Life Sci*, *66*(18), 2975-2984. <https://doi.org/10.1007/s00018-009-0057-8>
- Ren, X., Yang, Z., Xu, J., Sun, J., Mao, D., Hu, Y., Yang, S. J., Qiao, H. H., Wang, X., Hu, Q., Deng, P., Liu, L. P., Ji, J. Y., Li, J. B., & Ni, J. Q. (2014). Enhanced specificity and efficiency of the CRISPR/Cas9 system with optimized sgRNA parameters in *Drosophila*. *Cell Rep*, *9*(3), 1151-1162. <https://doi.org/10.1016/j.celrep.2014.09.044>
- Rivero, O., Selten, M. M., Sich, S., Popp, S., Bacmeister, L., Amendola, E., Negwer, M., Schubert, D., Proft, F., Kiser, D., Schmitt, A. G., Gross, C., Kolk, S. M., Strekalova, T., van den Hove, D., Resink, T. J., Nadif Kasri, N., & Lesch, K. P. (2015). Cadherin-13, a risk gene for ADHD and comorbid disorders, impacts GABAergic function in hippocampus and cognition. *Transl Psychiatry*, *5*(10), e655. <https://doi.org/10.1038/tp.2015.152>
- Rivero, O., Sich, S., Popp, S., Schmitt, A., Franke, B., & Lesch, K. P. (2013). Impact of the ADHD-susceptibility gene CDH13 on development and function of brain networks. *Eur Neuropsychopharmacol*, *23*(6), 492-507. <https://doi.org/10.1016/j.euroneuro.2012.06.009>
- Romli, F., Alitheen, N. B., Hamid, M., Ismail, R., & Abd Rahman, N. M. (2013). Current techniques in reprogramming cell potency. *J Cell Biochem*, *114*(6), 1230-1237. <https://doi.org/10.1002/jcb.24477>
- Sakurai, T., Kamiyoshi, A., Kawate, H., Watanabe, S., Sato, M., & Shindo, T. (2020). Production of genetically engineered mice with higher efficiency, lower mosaicism, and multiplexing capability using maternally expressed Cas9. *Sci Rep*, *10*(1), 1091. <https://doi.org/10.1038/s41598-020-57996-7>
- Salatino-Oliveira, A., Genro, J. P., Polanczyk, G., Zeni, C., Schmitz, M., Kieling, C., Anselmi, L., Menezes, A. M., Barros, F. C., Polina, E. R., Mota, N. R., Grevet, E. H., Bau, C. H., Rohde, L. A., & Hutz, M. H. (2015). Cadherin-13 gene is associated with hyperactive/impulsive symptoms in attention/deficit hyperactivity disorder. *Am J Med Genet B Neuropsychiatr Genet*, *168b*(3), 162-169. <https://doi.org/10.1002/ajmg.b.32293>
- Satterthwaite, T. D., Cook, P. A., Bruce, S. E., Conway, C., Mikkelsen, E., Satchell, E., Vandekar, S. N., Durbin, T., Shinohara, R. T., & Sheline, Y. I. (2016). Dimensional depression severity in women with major depression and post-traumatic stress disorder correlates with fronto-amygdalar hypoconnectivity. *Mol Psychiatry*, *21*(7), 894-902. <https://doi.org/10.1038/mp.2015.149>

- Schubert, D., Martens, G. J., & Kolk, S. M. (2015). Molecular underpinnings of prefrontal cortex development in rodents provide insights into the etiology of neurodevelopmental disorders. *Mol Psychiatry*, *20*(7), 795-809. <https://doi.org/10.1038/mp.2014.147>
- Selten, M., van Bokhoven, H., & Nadif Kasri, N. (2018). Inhibitory control of the excitatory/inhibitory balance in psychiatric disorders. *F1000Res*, *7*, 23. <https://doi.org/10.12688/f1000research.12155.1>
- Shepherd, G. M. (2004). The synaptic organization of the brain.
- Shi, Z., Zhang, J., Chen, S., Li, Y., Lei, X., Qiao, H., Zhu, Q., Hu, B., Zhou, Q., & Jiao, J. (2016). Conversion of Fibroblasts to Parvalbumin Neurons by One Transcription Factor, *Ascl1*, and the Chemical Compound Forskolin. *J Biol Chem*, *291*(26), 13560-13570. <https://doi.org/10.1074/jbc.M115.709808>
- Spruston, N. (2008). Pyramidal neurons: dendritic structure and synaptic integration. *Nat Rev Neurosci*, *9*(3), 206-221. <https://doi.org/10.1038/nrn2286>
- Sternberg, S. H., Redding, S., Jinek, M., Greene, E. C., & Doudna, J. A. (2014). DNA interrogation by the CRISPR RNA-guided endonuclease Cas9. *Nature*, *507*(7490), 62-67. <https://doi.org/10.1038/nature13011>
- Sun, L., Tran, N., Liang, C., Tang, F., Rice, A., Schreck, R., Waltz, K., Shawver, L. K., McMahon, G., & Tang, C. (1999). Design, synthesis, and evaluations of substituted 3-[(3- or 4-carboxyethylpyrrol-2-yl)methylidene]indolin-2-ones as inhibitors of VEGF, FGF, and PDGF receptor tyrosine kinases. *J Med Chem*, *42*(25), 5120-5130. <https://doi.org/10.1021/jm9904295>
- Suresh, J., Radojicic, M., Pesce, L. L., Bhansali, A., Wang, J., Tryba, A. K., Marks, J. D., & van Drongelen, W. (2016). Network burst activity in hippocampal neuronal cultures: the role of synaptic and intrinsic currents. *J Neurophysiol*, *115*(6), 3073-3089. <https://doi.org/10.1152/jn.00995.2015>
- Szabadics, J., Lorincz, A., & Tamás, G. (2001). Beta and gamma frequency synchronization by dendritic gabaergic synapses and gap junctions in a network of cortical interneurons. *J Neurosci*, *21*(15), 5824-5831. <https://doi.org/10.1523/jneurosci.21-15-05824.2001>
- Takahashi, K., Tanabe, K., Ohnuki, M., Narita, M., Ichisaka, T., Tomoda, K., & Yamanaka, S. (2007). Induction of pluripotent stem cells from adult human fibroblasts by defined factors. *Cell*, *131*(5), 861-872. <https://doi.org/10.1016/j.cell.2007.11.019>
- Takahashi, K., & Yamanaka, S. (2006). Induction of pluripotent stem cells from mouse embryonic and adult fibroblast cultures by defined factors. *Cell*, *126*(4), 663-676. <https://doi.org/10.1016/j.cell.2006.07.024>
- Takeuchi, T., Misaki, A., Liang, S. B., Tachibana, A., Hayashi, N., Sonobe, H., & Ohtsuki, Y. (2000). Expression of T-cadherin (CDH13, H-Cadherin) in human brain and its characteristics as a negative growth regulator of epidermal growth factor in neuroblastoma cells. *J Neurochem*, *74*(4), 1489-1497. <https://doi.org/10.1046/j.1471-4159.2000.0741489.x>
- Tamás, G., Buhl, E. H., Lörincz, A., & Somogyi, P. (2000). Proximally targeted GABAergic synapses and gap junctions synchronize cortical interneurons. *Nat Neurosci*, *3*(4), 366-371. <https://doi.org/10.1038/73936>
- Teppola, H., Acímović, J., & Linne, M. L. (2019). Unique Features of Network Bursts Emerge From the Complex Interplay of Excitatory and Inhibitory Receptors in Rat Neocortical Networks. *Front Cell Neurosci*, *13*, 377. <https://doi.org/10.3389/fncel.2019.00377>
- Thurtle-Schmidt, D. M., & Lo, T. W. (2018). Molecular biology at the cutting edge: A review on CRISPR/CAS9 gene editing for undergraduates. *Biochem Mol Biol Educ*, *46*(2), 195-205. <https://doi.org/10.1002/bmb.21108>
- Tiihonen, J., Rautiainen, M. R., Ollila, H. M., Repo-Tiihonen, E., Virkkunen, M., Palotie, A., Pietiläinen, O., Kristiansson, K., Joukamaa, M., Lauerma, H., Saarela, J., Tyni, S., Vartiainen, H., Paananen, J., Goldman, D., & Paunio, T. (2015). Genetic background

- of extreme violent behavior. *Mol Psychiatry*, 20(6), 786-792.
<https://doi.org/10.1038/mp.2014.130>
- Townsend, J. A., Wright, D. A., Winfrey, R. J., Fu, F., Maeder, M. L., Joung, J. K., & Voytas, D. F. (2009). High-frequency modification of plant genes using engineered zinc-finger nucleases. *Nature*, 459(7245), 442-445. <https://doi.org/10.1038/nature07845>
- Turrigiano, G. (2011). Too many cooks? Intrinsic and synaptic homeostatic mechanisms in cortical circuit refinement. *Annu Rev Neurosci*, 34, 89-103.
<https://doi.org/10.1146/annurev-neuro-060909-153238>
- Turrigiano, G. G., Leslie, K. R., Desai, N. S., Rutherford, L. C., & Nelson, S. B. (1998). Activity-dependent scaling of quantal amplitude in neocortical neurons. *Nature*, 391(6670), 892-896. <https://doi.org/10.1038/36103>
- Uhl, G. R., Drgon, T., Liu, Q. R., Johnson, C., Walther, D., Komiyama, T., Harano, M., Sekine, Y., Inada, T., Ozaki, N., Iyo, M., Iwata, N., Yamada, M., Sora, I., Chen, C. K., Liu, H. C., Ujike, H., & Lin, S. K. (2008). Genome-wide association for methamphetamine dependence: convergent results from 2 samples. *Arch Gen Psychiatry*, 65(3), 345-355. <https://doi.org/10.1001/archpsyc.65.3.345>
- Uniyal, A. P., Mansotra, K., Yadav, S. K., & Kumar, V. (2019). An overview of designing and selection of sgRNAs for precise genome editing by the CRISPR-Cas9 system in plants. *3 Biotech*, 9(6), 223. <https://doi.org/10.1007/s13205-019-1760-2>
- Urnov, F. D., Rebar, E. J., Holmes, M. C., Zhang, H. S., & Gregory, P. D. (2010). Genome editing with engineered zinc finger nucleases. *Nat Rev Genet*, 11(9), 636-646.
<https://doi.org/10.1038/nrg2842>
- Verweij, N., Eppinga, R. N., Hagemeijer, Y., & van der Harst, P. (2017). Identification of 15 novel risk loci for coronary artery disease and genetic risk of recurrent events, atrial fibrillation and heart failure. *Sci Rep*, 7(1), 2761. <https://doi.org/10.1038/s41598-017-03062-8>
- Vitale, M. R., Zöller, J. E. M., Jansch, C., Janz, A., Edenhofer, F., Klopocki, E., van den Hove, D., Vanmierlo, T., Rivero, O., Nadif Kasri, N., Ziegler, G. C., & Lesch, K. P. (2021). Generation of induced pluripotent stem cell (iPSC) lines carrying a heterozygous (UKWMPi002-A-1) and null mutant knockout (UKWMPi002-A-2) of Cadherin 13 associated with neurodevelopmental disorders using CRISPR/Cas9. *Stem Cell Res*, 51, 102169. <https://doi.org/10.1016/j.scr.2021.102169>
- Volpato, V., Smith, J., Sandor, C., Ried, J. S., Baud, A., Handel, A., Newey, S. E., Wessely, F., Attar, M., Whiteley, E., Chintawar, S., Verheyen, A., Barta, T., Lako, M., Armstrong, L., Muschet, C., Artati, A., Cusulin, C., Christensen, K., Patsch, C., Sharma, E., Nicod, J., Brownjohn, P., Stubbs, V., Heywood, W. E., Gissen, P., De Filippis, R., Janssen, K., Reinhardt, P., Adamski, J., Royaux, I., Peeters, P. J., Terstappen, G. C., Graf, M., Livesey, F. J., Akerman, C. J., Mills, K., Bowden, R., Nicholson, G., Webber, C., Cader, M. Z., & Lakics, V. (2018). Reproducibility of Molecular Phenotypes after Long-Term Differentiation to Human iPSC-Derived Neurons: A Multi-Site Omics Study. *Stem Cell Reports*, 11(4), 897-911.
<https://doi.org/10.1016/j.stemcr.2018.08.013>
- Volpato, V., & Webber, C. (2020). Addressing variability in iPSC-derived models of human disease: guidelines to promote reproducibility. *Dis Model Mech*, 13(1).
<https://doi.org/10.1242/dmm.042317>
- Walmsley, G. G., Hyun, J., McArdle, A., Senarath-Yapa, K., Hu, M. S., Chung, M. T., Wong, V. W., Longaker, M. T., & Wan, D. C. (2014). Induced pluripotent stem cells in regenerative medicine and disease modeling. *Curr Stem Cell Res Ther*, 9(2), 73-81.
<https://doi.org/10.2174/1574888x09666131217004137>
- Wang, L., Riss, M., Buitrago, J. O., & Claverol-Tinturé, E. (2012). Biophysics of microchannel-enabled neuron-electrode interfaces. *J Neural Eng*, 9(2), 026010.
<https://doi.org/10.1088/1741-2560/9/2/026010>

- Wang, T., Wei, J. J., Sabatini, D. M., & Lander, E. S. (2014). Genetic screens in human cells using the CRISPR-Cas9 system. *Science*, *343*(6166), 80-84. <https://doi.org/10.1126/science.1246981>
- Wang, Y., Liang, P., Lan, F., Wu, H., Lisowski, L., Gu, M., Hu, S., Kay, M. A., Urnov, F. D., Shinnawi, R., Gold, J. D., Gepstein, L., & Wu, J. C. (2014). Genome editing of isogenic human induced pluripotent stem cells recapitulates long QT phenotype for drug testing. *J Am Coll Cardiol*, *64*(5), 451-459. <https://doi.org/10.1016/j.jacc.2014.04.057>
- Wargelius, A. (2019). Application of genome editing in aquatic farm animals: Atlantic salmon. *Transgenic Res*, *28*(Suppl 2), 101-105. <https://doi.org/10.1007/s11248-019-00163-0>
- Williams, S., & Boksa, P. (2010). Gamma oscillations and schizophrenia. *J Psychiatry Neurosci*, *35*(2), 75-77. <https://doi.org/10.1503/jpn.100021>
- Woolf, T. M. (1998). Therapeutic repair of mutated nucleic acid sequences. *Nat Biotechnol*, *16*(4), 341-344. <https://doi.org/10.1038/nbt0498-341>
- Wu, X., Scott, D. A., Kriz, A. J., Chiu, A. C., Hsu, P. D., Dadon, D. B., Cheng, A. W., Trevino, A. E., Konermann, S., Chen, S., Jaenisch, R., Zhang, F., & Sharp, P. A. (2014). Genome-wide binding of the CRISPR endonuclease Cas9 in mammalian cells. *Nat Biotechnol*, *32*(7), 670-676. <https://doi.org/10.1038/nbt.2889>
- Yang, Y. F., Zhu, T., & Niu, D. K. (2013). Association of intron loss with high mutation rate in Arabidopsis: implications for genome size evolution. *Genome Biol Evol*, *5*(4), 723-733. <https://doi.org/10.1093/gbe/evt043>
- Yap, A. S., Brieher, W. M., & Gumbiner, B. M. (1997). Molecular and functional analysis of cadherin-based adherens junctions. *Annu Rev Cell Dev Biol*, *13*, 119-146. <https://doi.org/10.1146/annurev.cellbio.13.1.119>
- Zhang, X. H., Tee, L. Y., Wang, X. G., Huang, Q. S., & Yang, S. H. (2015). Off-target Effects in CRISPR/Cas9-mediated Genome Engineering. *Mol Ther Nucleic Acids*, *4*(11), e264. <https://doi.org/10.1038/mtna.2015.37>
- Zhou, K., Dempfle, A., Arcos-Burgos, M., Bakker, S. C., Banaschewski, T., Biederman, J., Buitelaar, J., Castellanos, F. X., Doyle, A., Ebstein, R. P., Ekholm, J., Forabosco, P., Franke, B., Freitag, C., Friedel, S., Gill, M., Hebebrand, J., Hinney, A., Jacob, C., Lesch, K. P., Loo, S. K., Lopera, F., McCracken, J. T., McGough, J. J., Meyer, J., Mick, E., Miranda, A., Muenke, M., Mulas, F., Nelson, S. F., Nguyen, T. T., Oades, R. D., Ogdie, M. N., Palacio, J. D., Pineda, D., Reif, A., Renner, T. J., Roeyers, H., Romanos, M., Rothenberger, A., Schäfer, H., Sergeant, J., Sinke, R. J., Smalley, S. L., Sonuga-Barke, E., Steinhausen, H. C., van der Meulen, E., Walitza, S., Warnke, A., Lewis, C. M., Faraone, S. V., & Asherson, P. (2008). Meta-analysis of genome-wide linkage scans of attention deficit hyperactivity disorder. *Am J Med Genet B Neuropsychiatr Genet*, *147b*(8), 1392-1398. <https://doi.org/10.1002/ajmg.b.30878>
- Ziegler, G. C., Ehlis, A. C., Weber, H., Vitale, M. R., Zöllner, J. E. M., Ku, H. P., Schiele, M. A., Kürbitz, L. I., Romanos, M., Pauli, P., Kalisch, R., Zwanzger, P., Domschke, K., Fallgatter, A. J., Reif, A., & Lesch, K. P. (2021). A Common CDH13 Variant Is Associated with Low Agreeableness and Neural Responses to Working Memory Tasks in ADHD. *Genes (Basel)*, *12*(9). <https://doi.org/10.3390/genes12091356>

Affidavit/Eidesstattliche Erklärung

I hereby confirm that my thesis entitled “Excitatory/inhibitory balance in iPSC-derived glutamatergic/GABAergic neuronal networks: differential Cadherin-13 genotype effects” is the result of my own work. I did not receive any help or support from commercial consultants. All sources and / or materials applied are listed and specified in the thesis.

Furthermore, I confirm that this thesis has not yet been submitted as part of another examination process neither in identical nor in similar form.

Place, Date

Signature

Hiermit erkläre ich an Eides statt, die Dissertation “ Exzitatorisch/inhibitorisches Gleichgewicht in iPSC-abgeleiteten glutamaterg/GABAergen neuronalen Netzwerken: Differentielle Cadherin-13 Genotyp-Effekte“ eigenständig, d.h. insbesondere selbstständig und ohne Hilfe eines kommerziellen Promotionsberaters, angefertigt und keine anderen als die von mir angegebenen Quellen als Hilfsmittel verwendet zu haben.

Ort, Datum

Unterschrift

List of publications

Jansch C, Ziegler GC, Forero A, Gredy S, Wäldchen S, **Vitale MR**, Svirin E, Zöller JEM, Waider J, Günther K, Edenhofer F, Sauer M, Wischmeyer E, Lesch KP (2021) Serotonin-specific neurons differentiated from human iPSCs form distinct subtypes with synaptic protein assembly. *J Neural Transm* 128:225-241
<https://doi.org/10.1007/s00702-021-02303-5>

Vitale MR, Zöller JEM, Jansch C, Janz A, Edenhofer F, Klopocki E, van den Hove D, Vanmierlo T, Rivero O, Nadif Kasri N, Ziegler GC, Lesch KP (2021) Generation of induced pluripotent stem cell (iPSC) lines carrying a heterozygous (UKWMPi002-A-1) and null mutant knockout (UKWMPi002-A-2) of Cadherin 13 associated with neurodevelopmental disorders using CRISPR/Cas9. *Stem Cell Res* 51:102169
<https://doi.org/10.1016/j.scr.2021.102169>.

Ziegler GC, Ehlis AC, Weber H, **Vitale MR**, Zöller JEM, Ku HP, Schiele MA, Kürbitz LI, Romanos M, Pauli P, Kalisch R, Zwanzger P, Domschke K, Fallgatter AJ, Reif A, Lesch KP (2021) A common *CDH13* variant is associated with low agreeableness and neural responses to working memory tasks in ADHD. *Genes (Basel)* 12:1356
<https://doi.org/10.3390/genes12091356>

Ziegler GC, Radtke F, **Vitale MR**, Preuße A, Klopocki E, Herms S, Lesch KP (2021) Generation of multiple human iPSC lines from peripheral blood mononuclear cells of two SLC2A3 deletion and two SLC2A3 duplication carriers. *Stem Cell Res* 56:102526
<https://doi.org/10.1016/j.scr.2021.102526>

Mossink B, van Rhijn JR, Wang S, Linda K, **Vitale MR**, *et.al.* (2021) Cadherin-13 is a critical regulator of GABAergic modulation in human stem-cell-derived neuronal networks *Molecular Psychiatry* 27, 1–18
<https://doi.org/10.1038/s41380-021-01117-x>

Vitale MR, Vitale A, Nadif Kasri N, Lesch KP (manuscript in preparation) Differential Cadherin-13 genotype effects in excitatory/inhibitory neuronal networks derived from iPSCs

Acknowledgements

First, I want to thank Prof. Dr. Klaus-Peter Lesch for the chance to be a part of his group at the Division of Molecular Psychiatry. Thank you for the great support and the opportunity to work in this interesting and challenging field of stem cells. I additionally want to acknowledge his encouragement to develop my own ideas and design/establish experiments by myself. I would like to thank Prof. Dr. Esther Asan and PD Dr. Frank Döring for being part of my thesis committee and the time they invested in my work and in my thesis as well as Prof. Dr. Matthias Gamer for agreeing to be the chairperson. As a doctoral student, I am also grateful to the GSLS team for all their efforts to support and ease the way for us. Thank you!

I would like to thank all people working at the laboratory. A special thanks to Johanna, Georg and Julia for all their help, regardless of whether it was work-related or not. My gratitude also goes to Rhiannon and Prof. Kittel-Schneider for their guidance during the final stages of my PhD. I wish to extend a special thanks to Antonio, my brother, who supported me with fruitful discussion and enabled me to analyze the MEA data.

However, my first and foremost thank you must go to my family for their continued support, patience, and love throughout this journey. I am more grateful to you than you will ever know.

Il mio più importante ringraziamento deve andare alla mia famiglia per il loro continuo supporto, pazienza e amore durante questo viaggio. Vi sono più grata di quanto saprete mai.

Publications

Jansch C, Ziegler GC, Forero A, Gredy S, Wäldchen S, Vitale MR, Svirin E, Zöller JEM, Waider J, Günther K, Edenhofer F, Sauer M, Wischmeyer E, Lesch KP (2021) Serotonin-specific neurons differentiated from human iPSCs form distinct subtypes with synaptic protein assembly. *J Neural Transm* 128:225-241
<https://doi.org/10.1007/s00702-021-02303-5>

Vitale MR, Zöller JEM, Jansch C, Janz A, Edenhofer F, Klopocki E, van den Hove D, Vanmierlo T, Rivero O, Nadif Kasri N, Ziegler GC, Lesch KP (2021) Generation of induced pluripotent stem cell (iPSC) lines carrying a heterozygous (UKWMPi002-A-1) and null mutant knockout (UKWMPi002-A-2) of Cadherin 13 associated with neurodevelopmental disorders using CRISPR/Cas9. *Stem Cell Res* 51:102169
<https://doi.org/10.1016/j.scr.2021.102169>

Ziegler GC, Ehlis AC, Weber H, Vitale MR, Zöller JEM, Ku HP, Schiele MA, Kürbitz LI, Romanos M, Pauli P, Kalisch R, Zwanzger P, Domschke K, Fallgatter AJ, Reif A, Lesch KP (2021) A common *CDH13* variant is associated with low agreeableness and neural responses to working memory tasks in ADHD. *Genes (Basel)* 12:1356
<https://doi.org/10.3390/genes12091356>

Ziegler GC, Radtke F, Vitale MR, Preuße A, Klopocki E, Herms S, Lesch KP (2021) Generation of multiple human iPSC lines from peripheral blood mononuclear cells of two SLC2A3 deletion and two SLC2A3 duplication carriers. *Stem Cell Res* 56:102526
<https://doi.org/10.1016/j.scr.2021.102526>

Mossink B, van Rhijn JR, Wang S, Linda K, Vitale MR, *et al.* (2021) Cadherin-13 is a critical regulator of GABAergic modulation in human stem-cell-derived neuronal networks *Molecular Psychiatry* 27, 1–18
<https://doi.org/10.1038/s41380-021-01117-x>

Vitale MR, Vitale A, Nadif Kasri N, Lesch KP (manuscript in preparation) Differential Cadherin-13 genotype effects in excitatory/inhibitory neuronal networks derived from iPSCs

Place, Date

Signature
(Maria Rosaria Vitale)